Investigating the Role of the Anti-Malarial Drug Atovaquone in Anti-Cancer Therapy

James Coates

Cancer Research UK
Medical Research Council
Oxford Institute for Radiation Oncology
Department of Oncology
St Hugh's College



A Thesis Submitted for the Degree of **Doctor of Philosophy**
University of Oxford, Trinity Term, 2019







THIS PAGE INTENTIONALLY BLANK







ABSTRACT

Radiotherapy (XRT) is used in over half of all cancer treatment regimens and can be administered alone or in tandem with chemotherapeutics to improve clinical outcomes. Sub-physiological levels of oxygen (hypoxia) is a feature of many solid tumours and can diminish the effectiveness of anti-cancer treatments. Though its detrimental impact on treatment efficacy was first realised over half a century ago, hypoxia endures as a significant barrier to improving clinical outcomes.

Historically, numerous approaches to alleviate or even exploit tumour hypoxia have been explored; however, none are in widespread clinical use today. Most strategies were predicated on therapeutic agents reaching hypoxic areas that are difficult to penetrate, yielding minimal clinical efficacy. Attempting to increase oxygen supply directly via hyperbaric chambers was similarly ineffective. An emerging alternative approach based on modulating cellular demand for oxygen was recently pioneered by our team. We theorised that reducing oxygen consumption of cells that are located in adequately perfused areas and peri-hypoxic regions might increase the concentration of unmetabolised oxygen able to diffuse across a tumour bed and into hypoxic areas.

Using a high-throughput small molecule screen, our team previously identified that the FDA-approved, anti-malarial drug Atovaquone (ATQ) reduces oxygen consumption, upregulates glycolysis, and alleviates tumour hypoxia *in vivo*. As a consequence of the alleviation of hypoxia, ATQ therapy was furthermore shown to synergise with XRT. ATQ is a ubiquinone analogue, suppressing oxidative phosphorylation via direct inhibition of Complex III subunit bc_1 of the electron transport chain (ETC). ATQ is a well-studied anti-malarial agent and our team is actively undertaking multiple clinical studies to evaluate its suitability as a clinical hypoxia modifier.

This thesis builds on our teams' previous work by exploring the broader effects of ATQ in an anti-cancer setting. The first experimental chapter (Chapter 3) probes the reversibility and tolerability of ATQ *in vitro* and *in vivo* before exploring preliminary mechanistic dependencies for how ATQ reverses hypoxia. Metabolic reprogramming towards a more glycolytic phenotype has long been implicated as a key promoter of aggressiveness and metastatic spread and so Chapter 4 probes the effects of ATQ on cancer cell migration *in vitro* and metastatic potential *in vivo*. In the last experimental chapter (Chapter 5), we reveal that ATQ potentiates the anti-cancer efficacy of platinum-class chemotherapy agents by modulating ETC-driven oxidative stress. Chapter 6 summarises the findings of the thesis as a whole and discusses future directions.

Together, the data presented in this thesis suggests that ATQ is a translationally viable and well-tolerated hypoxia modifying agent having pleotropic effects that are undoubtedly deserving of further study.

James Coates, St Hugh's College

Submitted for the degree of DPhil, University of Oxford, Michaelmas Term, 2019

THIS PAGE INTENTIONALLY BLANK

Hélène-Marie Coates (née Brosseau)

1956 – 2019

ACKNOWLEDGEMENTS

First and foremost, I would like to thank my supervisors, Professor Geoff Higgins and Professor Gillies McKenna, for allowing me to carry out my doctoral research in their laboratory. It has been a pleasure and an honour to work with them.

I am particularly thankful to Dr Thomas Ashton for his support, encouragement, and advice throughout the first years of my DPhil. A special thank you to Dr Gonzalo Rodriguez-Berriguete for his guidance in the later stages of my degree and for the many helpful discussions we had while playing darts together over the years.

Prior to undertaking my training at Oxford, I had limited experience in experimental biology and could not be more grateful for the patience and knowledge of my entire team. I would like to thank Dr Remko Prevo for his never-ending patience with me, Dr Katharine Herbert, Ms Rathi Puliyadi, and Dr Michael Skwarski for their helpful discussions, and I wish the best luck to Giovanna Granata in her DPhil and career.

This thesis would not have been possible without the collaboration of many other scientists in and outside of the department. A special thank you to Dr Simon Lord and Dr Alan McIntyre, the examiners of my thesis, for their valuable feedback on my work, to Professor Ruth Muschel for *in vivo* facilities as well as advice, and thank you to all those who challenged me scientifically and gave me the ideas that led to the results presented in this thesis.

Finally, thank you to Cancer Research UK and the Medical Research Council for their support, to Oxford MSD for awarding a Goodger & Schorstein prize, and to St Hugh's College for their support and council.

James

CONTENTS

ABSTRACT III

ACKNOWLEDGEMENTS VI

CONTENTS VII

ABBREVIATIONS, ACRONYMS, & DEFINITIONS 3

CHAPTER 1 INTRODUCTION 19

1.1 Cancer 20

1.2 Tumourigenesis 20

1.3 The Treatment of Cancer 20

1.3.1 Chemotherapy 21

Platinum-Class Agents 21

1.3.2 Radiotherapy 22

1.4 The Therapeutic Window 24

1.5 The Tumour Microenvironment 25

1.5.1 Hypoxia 26

Hypoxia and the DNA Damage Response 27

Quantitative Definition 27

Detection 28

Clinical Impact 29

1.5.2 IL-6/JAK/STAT3 Signalling Axis 29

1.6 Cellular Metabolism 30

1.6.1 Glycolysis 30

1.6.2 Electron Transport Chain & Oxidative Phosphorylation 31

1.6.3 Warburg Effect and the Inhibition of Oxidative Phosphorylation 33

1.6.4 Reactive Oxygen Species & Antioxidants 34

1.7 The Metastatic Cascade 35

1.7.1 Metabolic Effects of Hypoxia and ROS on Migration and Metastasis 37

1.8 Historical Strategies to Alleviate Tumour Hypoxia 37

1.9 Targeting Cellular Metabolism to Reverse Tumour Hypoxia 39

1.10 Atovaquone Alleviates Tumour Hypoxia by Inhibiting OXPHOS 41

1.11 Outline & Purpose of Thesis 43

CHAPTER 2 METHODS & MATERIALS 45

2.1 Tissue Culture 46

2.1.1 Maintenance 46

2.1.2 Storage & Resuscitation 47

2.1.3 Passaging 47

2.1.4 Counting 47

2.2 Colony Formation Assays 48

2.2.1 Statistical Analysis 48

2.2.2 Drug Treatment 49

2.2.3 Ultraviolet Irradiation 50

2.3 Flow Cytometry 50

2.3.1 MitoSOX 51

2.3.2 Propidium Iodide 51

2.3.3 Time Series 51

2.4 Immunofluorescence 52

2.4.1 EF5 52

2.4.1 CAIX 52

2.4.2 Analysis 53

2.5 IMMUNOHISTOCHEMISTRY 53
2.5.1 HAEMATOXYLIN & EOSIN 53
2.5.2 EF5 54
2.6 OXYGEN CONSUMPTION & GLYCOLYSIS MEASUREMENTS 54
2.7 THREE-DIMENSIONAL TISSUE CULTURE (SPHEROIDS) 55
2.7.1 SPHEROID GROWTH DELAY 56
2.8 CELLULAR MIGRATION ASSAY 57
2.9 ANIMAL STUDIES 57
2.9.1 STRAIN SELECTION 58
2.9.2 TUMOUR INDUCTION 58
2.9.3 ATOVAQUONE DELIVERY 59
2.9.4 ENDPOINTS & MEASUREMENTS 59
2.9.5 EF5 HYPOXIA STAINING 60
2.9.6 4T1 METASTATIC MODEL 60
2.9.7 ENZYMATIC DIGESTION OF TUMOURS & TARGET ORGANS 61
2.9.8 *EX VIVO* FACS 62
2.9.9 CARDIORESPIRATORY-GATED THORACIC 3.0 T MRI 62
2.9.10 CONTINUOUS EXCHANGE SATURATION TRANSFER (CEST) 9.4 T MRI 63
2.10 STATISTICAL ANALYSIS 63
2.10.1 QUANTIFICATION OF SENSITISATION 64

CHAPTER 3 ATOVAQUONE AS A HYPOXIA MODIFYING AGENT 65
3.1 INTRODUCTION 66
3.2 RESULTS 69
3.2.1 MODULATION OF OCR & ECAR BY ATOVAQUONE *IN VITRO* IS REVERSIBLE 69
3.2.2 CYTOTOXICITY OF ATOVAQUONE IS NOT DEPENDENT ON ITS ABILITY TO INHIBIT OXPHOS 70
3.2.3 ATOVAQUONE DIMINISHES CAIX EXPRESSION AND EF5 STAINING IN AVASCULAR SPHEROID MODELS 72
3.2.4 ATOVAQUONE REDUCES OCR & INDUCES CELL DEATH INDEPENDENTLY OF $pSTAT3^{Y705}$ 73
3.2.5 ATOVAQUONE REDUCES OCR & ALLEVIATES SPHEROID HYPOXIA INDEPENDENTLY OF HIF-1α 74
3.2.6 ATOVAQUONE TREATMENT IS WELL-TOLERATED *IN VITRO* & *IN VIVO* 76
3.2.7 CEST-MRI REVEALS ATOVAQUONE INDUCES EXTRACELLULAR ACIDIFICATION OF TUMOURS 78
3.3 DISCUSSION 80

CHAPTER 4 EFFECT OF ATOVAQUONE ON MIGRATION & METASTATIC POTENTIAL 84
4.1 INTRODUCTION 85
4.2 RESULTS 88
4.2.1 ATOVAQUONE DOES NOT INCREASE CHEMOTAXIS-DRIVEN CANCER CELL MIGRATION 88
4.2.2 ATOVAQUONE ABOLISHES OCR IN 4T1 CELLS AND IS SUITABLE FOR USE IN 4T1 ORTHOTOPIC METASTASIS MODELS 89
4.2.3 IMMUNOHISTOCHEMISTRY & CARDIORESPIRATORY-GATED 3T MAGNETIC RESONANCE CONFIRMS DISTANT 4T1 METASTASIS 90
4.2.4 *EX VIVO* FLOW CYTOMETRY REVEALS ATOVAQUONE THERAPY DOES NOT INCREASE LUNG METASTASIS 92
4.2.5 PRE-LOADING WITH ATOVAQUONE *IN VIVO* PRIOR TO TUMOUR INDUCTION DOES NOT INCREASE LUNG METASTASIS 94
4.2 DISCUSSION 95

CHAPTER 5 ATOVAQUONE POTENTIATES THE EFFECT OF PLATINUM AGENTS 99
5.1 INTRODUCTION 100

5.2 RESULTS 102
5.2.1 A SCREEN FOR CHEMOTHERAPIES POTENTIATED BY ATOVAQUONE-MEDIATED REVERSAL OF HYPOXIA 102
5.2.2 ATOVAQUONE INCREASES PLATINUM-MEDIATED CANCER CELL DEATH *IN VITRO* UNDER NORMOXIA 104
5.2.3 ATOVAQUONE SENSITISES CANCER CELLS TO PLATINUM AGENTS *IN VITRO* UNDER NORMOXIA INDEPENDENTLY OF pSTAT3^{Y705} 104
5.2.4 ROS-INDUCED GLUTATHIONE POOL DEPLETION UNDERPINS ATOVAQUONE-MEDIATED SENSITISATION TO PLATINUM-CLASS AGENTS 106
5.2.5 PRELOADING GLUTATHIONE USING N-ACETYL-CYSTEINE ABOLISHES ATOVAQUONE-MEDIATED PLATINUM SENSITISATION *IN VITRO* 111
5.2.6 ATOVAQUONE SAFELY POTENTIATES THE EFFICACY OF CARBOPLATIN *IN VIVO* 111
5.3 DISCUSSION 114

CHAPTER 6 GENERAL DISCUSSION 117
6.1 SUMMARY OF FINDINGS 118
6.2 SIGNIFICANCE OF FINDINGS 121
6.3 CONCLUDING REMARKS 126

REFERENCES 127

APPENDIX A TRANSFER & CONFIRMATION OF STATUS 152

APPENDIX B SUMMARY OF PUBLICATIONS 157

ABBREVIATIONS, ACRONYMS, & DEFINITIONS

The following table describes the significance of various abbreviations and acronyms used throughout the thesis. Definitions of certain key terms are also included for readability. Important and recurring acronyms are redefined throughout the text as needed.

Abbreviation	Meaning
˚C	Celsius degrees
~	Approximately
$\Delta\psi$	Potential Across the Mitochondrial Membranes (see PMF)
3D	Three-Dimensional
ABC	ATP Binding Cassette (transporters)
Acetyl-CoA	Acetyl Coenzyme A
ANOVA	Analysis of Variance
AMPK	AMP-activated Protein Kinase
APT	Amide Proton Transfer (*as in* CEST MRI)
ARCADIAN	Atovaquone in Combination with Radical Concurrent Chemoradiotherapy in Locally Advanced NSCLC
ATCC	American Type Culture Collection
ATM	Ataxia telangiectasia Mutated
ATQM	Atovaquone as Tumour HypOxia Modifier (NCT02628080)
ATR	Ataxia telangiectasia and Rad3-related protein
ADP	Adenosine-5'-diphosphate
ATP	Adenosine-5'-triphosphate
BMSU	Biomedical Services Unit (*in vivo*)
BrdU	Bromodeoxyuridine
BSA	Bovine Serum Albumin
CAIX	Carbonic Anhydrase 9
CAT	Catalase
CBDCA	Carboplatin; Cyclobutane Dicarboxylic Acid

CDDP	Cisplatin; cis-diamminedichloroplatinum (II)
cDNA	Complementary DNA
CEST	Continuous Exchange Saturation Transfer (MRI)
CFA	Colony Formation Assay
CMC	Carboxymethylcellulose
CRC	Colorectal Cancer
CRUK	Cancer Research UK
CYTB	Cytochrome C
DAHANCA	Danish Head and Neck Cancer Group Trials
DAPI	4',6-diamidino-2-phenylindole
DCE-MRI	Dynamic Contrast-Enhanced Magnetic Resonance Imaging
DDR	DNA Damage Response
DMEM	Dulbecco's Modified Eagle's Medium
DMSO	Dimethyl Sulfoxide (Non-Polar Solvent)
DNA	De-Oxyribonucleic Acid
DSB	Double-Strand Break
ECM	Extracellular Matrix
EDTA	Ethylenediaminetetraacetic Acid
EGFR	Epidermal Growth Factor Receptor
ETC	Electron Transport Chain
FACS	Fluorescence Activated Cell Sorting
FAD	Flavin Adenine Dinucleotide
$FAHD_2$	Reduced Form of FAD (see FAD)
FBS	Foetal Bovine Serum
FITC	Fluorescein Isothiocyanate
FL#	Fluorescence Channel Number #
FLuc	Firefly Luciferase

g	Earth's Gravitational Force (~9.807 m/S^2)
GI	Gastrointestinal
GAPDH	Glyceraldehyde 3-phosphate dehydrogenase
GFP	Green Fluorescent Protein
GSH	Reduced Glutathione
GLUT1	Glucose transporters 1
Gy	Gray (defined as the absorption of one joule of radiation energy per kilogram of matter)
hr	Hour
H&E	Haematoxylin & Eosin (stain)
H2AX	H2A Histone Family, Member X
HIF	Hypoxia Inducible Factor; HIF-1, -2, -3
HF	Hypoxic Fraction
Hg	Mercury
HTS	High-Throughput Screen
i.m.m.	Intramammary (injection)
i.p.	Intraperitoneal (injection)
i.v.	Intravenous
in vitro	Bench-top
in vivo	In Animals
in situ	Within the natural location where it arises
ex vivo	Animal samples excised for further processing
IL-6	Interleukin 6
IF	Immunofluorescence
IHC	Immunohistochemistry
IMRT	Intensity Modulated Radiotherapy
IR	Irradiation

JAK	Janus Kinase
k.o.	Knock-out
kb	Kilobase
kDa	Kilodalton
L-OHP	Oxaliplatin
LC	Local Control
LET	Linear Energy Transfer
M-phase	Mitotic Phase
min	Minute
MRC	Medical Research Council
MRI	Magnetic Resonance Imaging
MRN	MRE11/RAD50/NSB1
MnSOD	Manganese Superoxide Dismutase (Enzyme)
mRNA	Messenger Ribonucleic Acid
NACWO	Named Animal Care & Welfare Officer
NADH	Nicotinamide Adenine Dinucleotide
NADPH	Nicotinamide Adenine Dinucleotide Phosphate
NCI	National Cancer Institute
NF-κB	Nuclear Factor Kappa-Light-Chain-Enhancer of Activated B Cells
ng	Nanograms
NGS	Normal Goat Serum
NHEJ	Non-Homologous End Joining
NRF2	Nuclear Factor Erythroid 2-Related Factor 2
NS	Non-Specific
NSCLC	Non-Small-Cell Lung Carcinoma
NT	Non-Targeting

nt	Nucleotide
NTCP	Normal Tissue Complication Probability
NIM	Nimorazole
NIMRAD	Nimorazole and radiotherapy for head and neck cancer trial
NVS	Named Seminarian Surgeon
MYXO	Myxothiozole
OS	Overall Survival
p.o.	Oral Gavage
PARP-1	Poly [ADP-ribose] polymerase 1
PBS	Phosphate Buffered Saline
PCR	Polymerase Chain Reaction
PE	Plating Efficiency
Pen	Penicillin
PET	Positron Emission Tomography
PFA	Paraformaldehyde
PFS	Progression-Free Survival
PHD	Pro-Hydroxylases
pHe	Extracellular pH
pHi	Intracellular pH
PMF	Proton Motive Force
PI	Propidium Iodide
PI3K	Phosphoinositide 3-kinase
PPP	Pentose-Phosphate Pathway
PRX	Peroxiredoxin
PSA	Prostate Specific Antigen
PTEN	Phosphatase and Tensin Homolog
Rb	Retinoblastoma Protein

RISC	RNA-Induced Silencing Complex
RLC	RISC-loading Complex
RNAi	RNA Interference
ROS	Reactive Oxygen Species
RPMI	Roswell Park Memorial Institute
RT	Room Temperature
RT-PCR	Reverse Transcriptase PCR
s.d.	Standard Deviation
SER_{10}	Survival Enhancement Ratio at 0.10 Surviving Fraction
SF	Surviving Fraction
SSB	Single Strand Break
STAT3	Signal Transducer and Activator of Transcription 3
STR	Short Tandem Repeat
T	Tesla; Unit of Magnetic Field Strength
TCA	Trichloroacetic Acid
TCP	Tumour Control Probability
TRX	Thioredoxin
TK	Thymidine Kinase
TRAP1	TNF Receptor Associated Protein 1
TNB	Blocking Buffer (Perkinelmer)
TNBC	Triple-Negative Breast Cancer
TPZ	Tirapazamine
TW	Therapeutic Window; Therapeutic Index
Tween-20	Polyethylene Glycol Sorbitan Monolaurate
UK	United Kingdom
UVC	Ultraviolet Radiation (λ <280 Nm)
VEGF	Vascular Endothelial Growth Factor

VHL	Von Hippel–Lindau Tumour Suppressor
Wellvone	Clinical Formulation of Orally Delivered Atovaquone
WHO	(*the*) World Health Organization
XF	Agilent Seahorse XF Analyzer
XRT	Radiation Therapy
γ-H2AX	Phosphorylated-H2AX Histone
µL	Unit of 1×10^{-6} L
µM	Unit of 1×10^{-6} mol/L
µm	Unit of 1×10^{-6} m

CHAPTER 1

INTRODUCTION

1.1 Cancer

Cancer is a group of diseases involving abnormal cell growth and the potential to invade or spread to distant parts of the body [1]. As of 2018, Cancer Research UK estimates that 1 in 2 people in the United Kingdom will develop cancer within their lifetime [2]. Cancer is responsible for approximately 13% of the global deaths annually and over 7 million people die of the disease annually, making it the second leading cause of death after heart disease [1,2]. More than 360,000 people are diagnosed annually in the UK and cancer-related deaths are over 160,000 [2].

1.2 Tumourigenesis

Tumours are the result of rapid cancer cell proliferation, leading to atypical tissue architecture having marked heterogeneity [3]. Once established, Darwinian selection pressures compromise genomic integrity, perturbing homeostasis and promoting mutagenesis. Advantages conferred onto cells as a result are pleiotropic and a function of both intrinsic and extrinsic factors [4]. Over time, selection pressures maximise cellular fitness, supplanting less efficient clones in favour of those more resistant and resilient – *survival of the fittest*.

1.3 The Treatment of Cancer

Cancer can be treated by surgery, chemotherapy, radiation therapy (XRT), hormonal therapy, and/or immunotherapy. Treatment regimens depend on the location and grade of the tumour(s), the stage of the disease, and the general state of the patient i.e. performance status. To limit resistance and recurrence, treatment regimens often involve more than one modality and/or a combination of therapeutics [5]. The limiting factor in modern cancer treatment regimens is toxicity or damage to healthy cells and tissues adjacent to neoplasms.

1.3.1 Chemotherapy

Chemotherapy is the application of chemicals or drugs to kill cancer cells – its effects are generally systemic. There are several different classes of chemotherapies that can broadly be defined by how they work [6,7]: alkylating agents that damage DNA; anti-metabolites that replace or interfere with key metabolic steps or enzymatic pathways; antibiotics that impede DNA replication; inhibitors of topoisomerases preventing the unwinding of DNA; mitotic inhibitors or poisons that prevent cellular division; and corticosteroids, often used to relieve side effects from other drugs.

Platinum-Class Agents

In 1965, cancer cells exposed to a platinum-containing molecule, cisplatin, were found to arrest and undergo programmed cell death [8]. Eventually, cisplatin was approved for clinical use as an anti-cancer agent in 1979 and platinum chemotherapies are now the most common class of drug in use against cancer [9] – approximately half of all patients undergoing treatment receive a platinum-based agent [9,10]. Derivatives of cisplatin include carboplatin, tetraplatin, setraplatin, and oxaliplatin.

Platinum agents can be taken up by cells through a range of mechanisms [11]. Upon entering a cell and becoming aqueous, platinum agents become highly reactive and can bind to many intracellular biomolecules. Once inside, the *soft* nucleophile nature of platinum-complexes induces preferential binding to sulphur-containing molecules, such as the anti-oxidant glutathione (GSH). The primary mechanism of cell death induced by platinum-class agents can vary and not all platinum-based agents are readily interchangeable – it has been shown that cisplatin and carboplatin form irreparable platinum-DNA adducts while cell death caused by oxaliplatin is mediated by ribosomal damage [12].

Resistance is a major limitation in the clinical efficacy of platinum-class chemotherapies [11]. Mechanisms of resistance can be intrinsic to the tumour microenvironment or develop over time through Darwinian selection processes.

During the development of resistance, nearly every pathway relating to cell survival has been reported to be affected, making platinum resistance difficult to overcome [13]. Clinically, platinum agents are often prescribed alongside other chemotherapies to minimise chances of resistance [9].

1.3.2 Radiotherapy

XRT is used in over half of all cancer treatment regimens worldwide and can be administered alone or in tandem with other agents, such as chemotherapeutics, to improve local control, progression free survival, and overall survival [14,15]. Conventional photon XRT is also extremely cost effective, accounting for less than 5% of global cancer therapy expenditure in recent years [16].

XRT is predominantly delivered to patients daily and in small doses known as fractions to exploit more efficient DNA repair of normal cells. The dose of each fraction and the number of fractions delivered (fractionation regimen) varies according to tumour or tissue type, but also healthcare system [17]. XRT is indicated for a wide array of tumour types and can be used symptomatically for palliation in patients with incurable disease [17].

The biological effects of XRT are complex and can be difficult to predict, especially accounting for tumour heterogeneity or concomitant chemotherapies [18]. In 1975, Withers proposed a model with four main factors to describe the effects of XRT on tumours [19]. His four "R's" of radiation biology included *Repair*, *Repopulation*, *Redistribution,* and *Reoxygenation*. While the first two processes render tissue more resistant to XRT, the last two tend to make it more sensitive. More recently, Steel and colleagues proposed *intrinsic cellular Radiosensitivity* as a fifth 'R' to capture the role that certain oncogenic pathways and defects in DNA repair might play [20].

An important factor extrinsic to cancer cells that can affect radiosensitivity is oxygenation [21]. Molecular oxygen fixes XRT-induced DNA damage incurred by reactive oxygen species (ROS) as a result of the interaction of ionising radiation with water (Figure 1.2) – a concept known as the *oxygen fixation hypothesis* [19,22–24]. Experimentally, the radiation dose required to achieve the same biologic effect is approximately three times higher in the absence of oxygen than in the presence of normal levels of oxygen (OER) – OER values in tumours vary but are usually between 2 and 3 (Figure 1.3) [21,25].

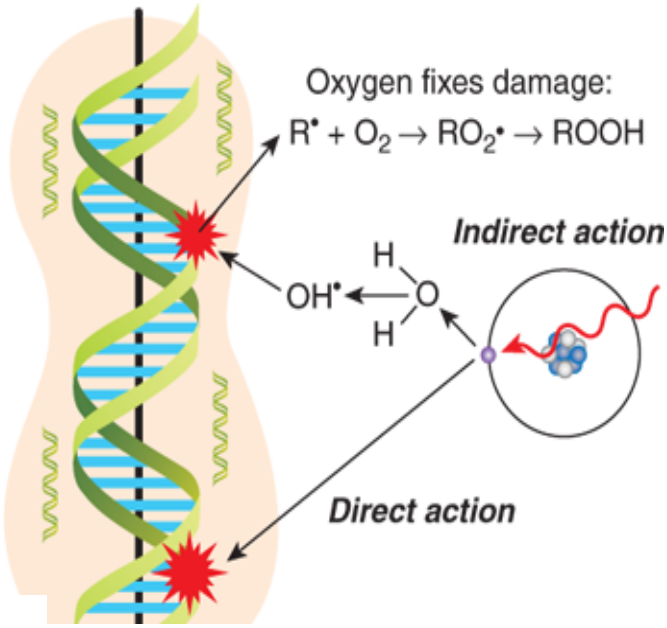


Figure 1.2 – Oxygen Fixes Radiation-induced DNA-damage and Potentiates its Efficacy. Radiation kills human cells by the formation of radicals that fix DNA damage and lead to cell death. Under hypoxia, antioxidants, especially glutathione (GSH), can donate a proton to the radical, thereby deactivating it and minimising further damage. Figure adapted from Tannock's *The Basic Science of Oncology* [26].

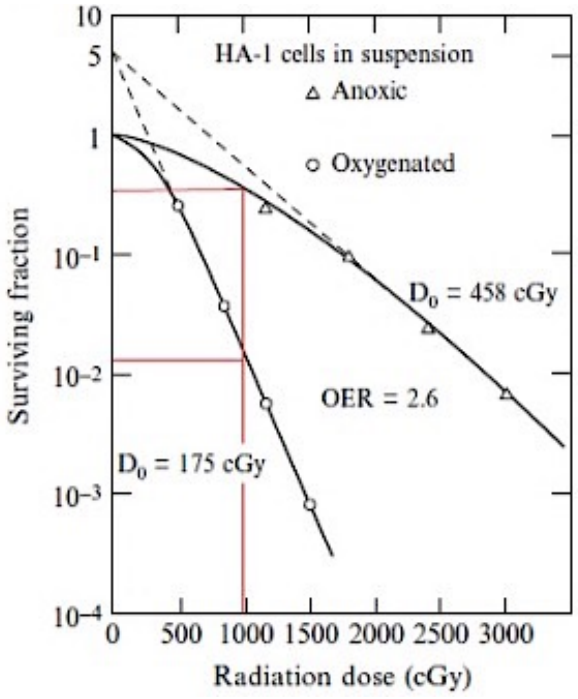


Figure 1.3 – Hypoxia Results in Resistance of Tumour Cells to Radiation. Clonogenic survival of irradiated Chinese hamster HA-1 cells is higher in hypoxia (open triangles) compared to normoxia (open circles), as determined by clonogenic assay (OER = 2.6). Figure adapted from Brown's *Tumor Hypoxia in Cancer Therapy* [27]

1.4 The Therapeutic Window

The primary dogma of radiation oncology relates the probability of achieving local control (tumour control probability, TCP) to the risk of damaging healthy tissues (normal tissue complication probability, NTCP) (Figure 1.4) [28]. This trade-off can be quantified by the therapeutic window (TW), which relates any advantage gained in treatment efficacy with its associated risk of toxicity [29–31]. Increasing the TW for a given treatment regimen, or treatment combination, theoretically translates to dose escalation without significantly affecting the rate of side effects. Whether it be for chemotherapeutic regimens or XRT, dose-limiting normal tissue side effects vary greatly across tissues types and are influenced by several factors, both intrinsic and extrinsic in nature.

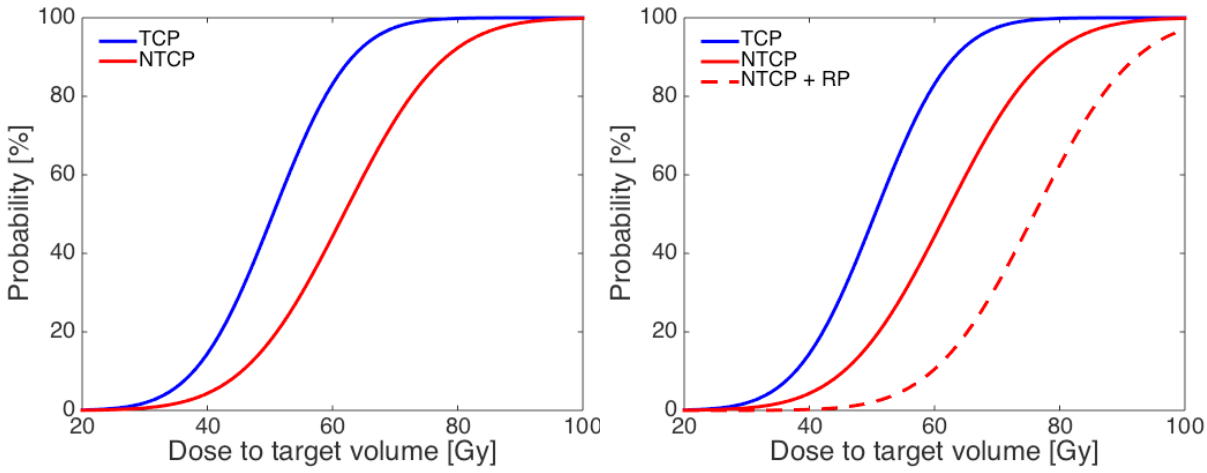


Figure 1.4 – Curves for Normal Tissue Complication Probability (NTCP) and Tumour Control Probability (TCP) without (A) and with (B) a Radio-protecting Agent (RP). Data is theoretical and is for illustration purposes only. The therapeutic window (TW) is shown by double-headed black arrows and is significantly widened with the use of RPs (case B). The TW is drawn in both cases at a dose of 60 Gy. Data and figures were generated using MATLAB®.

1.5 The Tumour Microenvironment

Intra-tumoural heterogeneity can be observed at both molecular and cellular levels in cancer. Differences in intrinsic expression found between cells in the same tumour reflect genetic, epigenetic, transcriptomic, and proteomic divergences. Common genotypic changes include mutations, gene amplifications, deletions, chromosomal rearrangements,

Responses of cancer cells are not however exclusively determined by intrinsic properties. The tumour microenvironment (TME) consists of the cells in and around tumours and is increasingly being recognised as a major determinant of clinical outcomes [32]. The TME has an important role in the response to anti-cancer therapies, for instance, it is widely recognised that vasculature is a key determinant for tumour growth and on the distribution of anti-cancer drugs [33,34]. Other factors of the TME implicated in mediating treatment outcomes include: pH, hypoxia, and stromal-tumour signalling interactions [33]. These variables can increase or diminish gene products that are directly involved in the generation of drug resistance.

1.5.1 Hypoxia

As tumours rapidly grow and proliferate, oxygen demand surpasses supply due to an invariably dysregulated, inefficient, and 'chaotic' tumour microvasculature (Figure 1.5) [27]. Sub-physiological levels of oxygen are incompatible with normal biological function but are a common feature of many solid tumours [35].

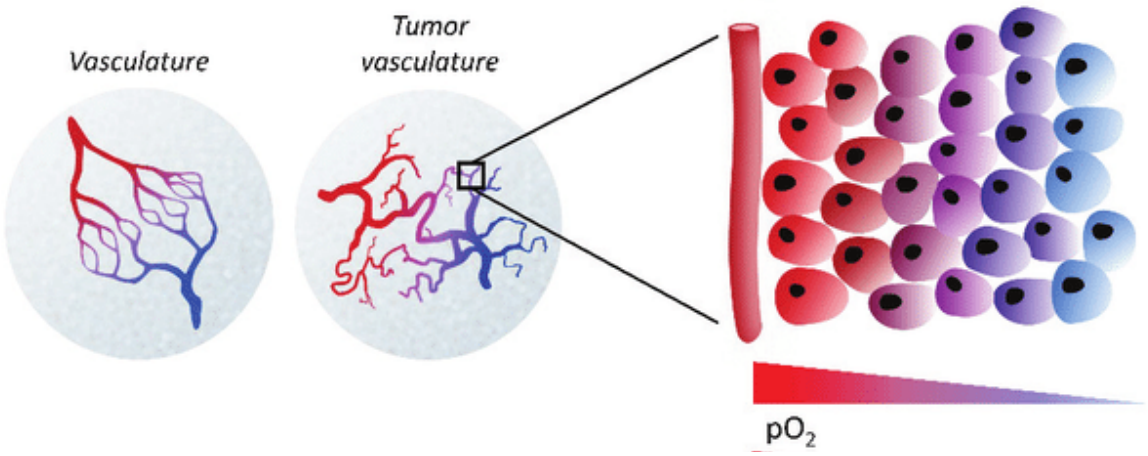


Figure 1.5 – Tortuous and Leaky Tumour Vasculature Contributes to the Pathogenesis of Hypoxia. As a tumour grows, the interior of the tumour becomes farther away from existing blood supply. The resulting hypoxic environment leads to genetic instability and is associated with cancer progression and downregulation of DNA repair mechanisms. Figure redrawn from Ramachadran *et al.* [36].

Hypoxic regions are heterogeneously distributed within a tumour and may very well be located directly adjacent to well-oxygenated tissues [37]. Perfusion-limited delivery of well oxygenated blood induces ischemic hypoxia, which is often transient and so referred to as "acute" hypoxia. Acute hypoxia occurring repetitively over time has been coined *cyclic hypoxia* due to the phenotypical differences that it induces [38]. In contrast, chronic hypoxia results from diffusion limitations, whereby the demand for oxygen surpasses the delivery albeit due to leaky vasculature or upregulated metabolism.

The master hypoxia regulator, hypoxia inducible factor 1 (HIF-1) is a heterodimeric transcriptional complex that plays an integral role in the cellular response to low oxygen but also cellular metabolism and oxygen homeostasis [39–41]. Under normal oxygen tension, a group of prolyl-4-hydroxylases (PHDs)

hydroxylate HIF-1α. The hydroxyl groups are recognised by the tumour suppressor gene, von Hippel-Lindau (VHL), which ubiquitinates HIF-1α, targeting it for proteasomal degradation. However, under hypoxic conditions, HIF-1α is not hydrolysed by PHDs and therefore not targeted for degradation. Once stabilised, HIF-1 has been shown to bind and increases transcription of > 1000 target genes, many of which have been heavily implicated in cell survival, growth, and metabolism [42].

Hypoxia and the DNA Damage Response

Gradients of hypoxia can be found throughout most solid tumours; however, cells under severe hypoxia (< 0.1 % O_2) exhibit significantly modulated DNA damage response (DDR) and is characterised by ATM- and ATR-mediated signalling, p53-dependent apoptosis, and compromised replication fork integrity [43,44]. Hypoxia-induced DDR has been posited as a key promoter of genome stability for cells under hypoxia due to the suppression of DNA repair; however, hypoxia has also been shown to lead to aberrant DNA replication, gene amplification, base substitutions, and deletions [45]. Moreover, homologous recombination (HR), a key pathway involved in repair of DSBs during S and G_2 phases, is functionally inhibited under hypoxia; however, non-homologous end-joining (NHEJ) is not [46,47]. Given the above, cells under hypoxia clearly exhibit highly modulated DDR but detailed mechanistic understanding of all downstream effectors remain elusive.

Quantitative Definition

Ambient air is 21% O_2 (150 mm Hg) but many mammalian tissues function at 2% – 9% O_2 (40 mm Hg average) [35]. As such, lower-than-normoxic levels of oxygen cannot simply define the state of severe (radiobiologically-relevant) hypoxia. Hypoxia can however be defined as critical oxygen levels below which different pathophysiological effects take place [48]. Four different parameters are described in the literature to quantify tumour hypoxia: median tumour partial pressure of oxygen (pO_2), fraction of $pO_2 \leq 2.5$ mmHg (otherwise referred to as

hypoxic fraction [HF] of 2.5), fraction of $pO_2 \leq 5$ mmHg (HF of 5), and fraction of $pO_2 \leq 10$ mmHg (HF of 10).

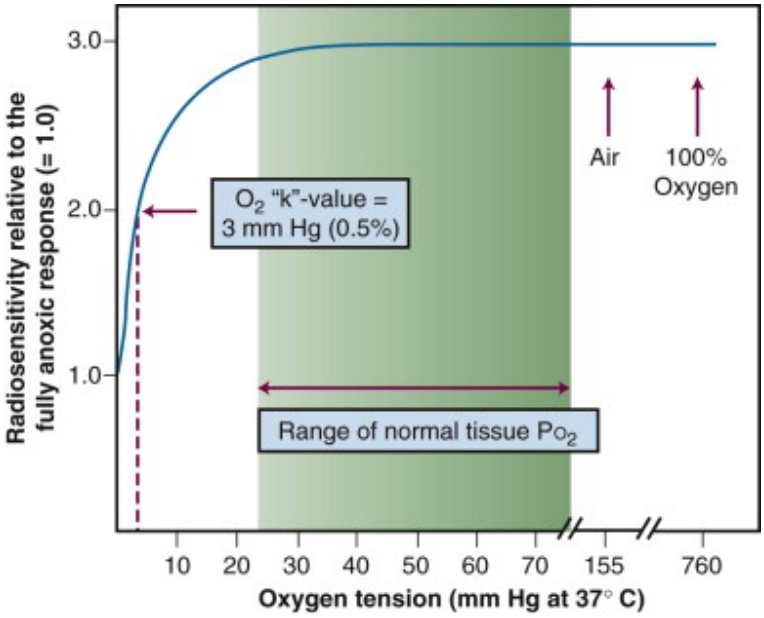


Figure 1.6 – Oxygen Sensitises Tissues to Ionising Radiation. Radiosensitisation by oxygen occurs at very low concentrations with half-maximum sensitisation ("k"-value) occurring approximately 3 mm Hg (radiobiological hypoxia). However, cells begin to elicit a pathological response under moderate hypoxia (3–15 mm Hg), which can drive selection towards aggressive phenotypes. Figure adapted from Zeman's *The Biological Basis of Radiation Oncology* [49].

Detection

Tumour hypoxia can be detected by a number of methods, some techniques more conducive to clinical use or better validated. Direct measurement of tumour oxygen levels can be obtained via electrode probe, but this is invasive and careful attention must be paid to control for contamination by atmospheric oxygen [50]. Alternatively, hypoxia can be inferred using endogenous markers, such as HIF-1α, or those downstream such as glucose transporter 1 (GLUT1) and carbonic anhydrase IX (CAIX) [51]. Notably, CAIX is one of the most well studied endogenous markers for such purposes having been shown to overlap significantly with HIF-1 staining [52]. Staining for HIF-1α can be difficult experimentally due to its short half-life under well-oxygenated conditions (5-8 min) [51].

Perhaps the most common chemical probes are nitroimidazole-based compounds, such as pimonidazole (PIMO), misonidazole (MISO), 2-

nitroimidazole (EF5), and nimorazole (NIM), which preferentially accumulate in areas of low oxygen tension [53,54]. They contain nitroheterocyclic rings whose activation is catalysed by intracellular nitroreductases to form adducts with adjacent macromolecules [55]. The ensuing covalent bonds are highly favoured and stabilised under low oxygen tension and correlate with hypoxia and HIF-1 staining [55].

Clinical Impact

Hypoxia plays a pivotal role in XRT efficacy but has also been implicated in mediating the effects of immunotherapies and hormonal therapies [48]. Impaired generation of free radicals under hypoxia can furthermore decrease the cytotoxicity of certain chemotherapy agents, such as bleomycin and doxorubicin, thereby limiting their clinical efficacy [56]. Hypoxia is associated with poor clinical outcomes in most cancers [57,58] and hypoxic tumours have a higher incidence of reoccurring locally with an increased propensity towards metastasis [33]. Six decades after the first clinical trials dedicated to reversing tumour hypoxia [59] and over one-hundred years since oxygen was implicated in mediating the effects of radiation damage [60], hypoxia endures as a barrier to improving outcomes and one of the best validated targets.

1.5.2 IL-6/JAK/STAT3 Signalling Axis

Signal transducer and activator of transcription 3 (STAT3) is a promiscuous transcription factor whose aberrant activity has been shown to play a significant role in disease progression and in modulating cellular metabolsm [61–63]. In the TME, interleukin 6 (IL-6) and Janus kinases (JAKs) interact with STAT3 through the IL-6/JAK/STAT3 signalling axis, mediating cell proliferation, survival, migration, but also immunosuppression [64]. Cytoplasmic phosphorylation of STAT3's Tyr^{705} ($STAT3^{Y705}$) by JAK proteins activates IL-6, inducing STAT3 dimerization, activation, nuclear translocation, and target gene upregulation [65]. Notably, phosphorylation of $STAT3^{Y705}$ has recently been demonstrated through gene-expression analysis to be potently inhibited by ATQ therapy [66].

Furthermore, STAT3 may also mediate tumour resistance to platinum agents [67,68] and at least one notable report suggests STAT3 activity rather than HIF-1 activity mediates resistance of triple negative breast cancer (TNBC) cells to cisplatin under hypoxia [69].

1.6 Cellular Metabolism

In contrast to most normal cells, which mainly rely on OXPHOS to produce energy for cellular processes, cancer cells in a hypoxic microenvironment depend on glycolysis as their primary energy source; however, OXPHOS still contributes to energy production in many cancers [70–72].

1.6.1 Glycolysis

Glycolysis is a universal pathway for the catabolism (breakdown) of glucose and occurs in every cell of the human body (Figure 1.7) [73]. The process converts one molecule of glucose to two molecules of pyruvic acid. The energy released in this process is conserved into the form of adenosine triphosphate (ATP) and nicotinamide adenine dinucleotide (NADH), both of which are found in all living cells [74]. Glycolysis provides energy and intermediates for critical cellular functions and consists of a sequence of ten reactions (Figure 1.7), seven of which are reversible while three are irreversible. The first five reactions use ATP and the last five yield ATP. Glycolysis occurs in the cytoplasm and yields 2x ATPs, 2x NADH molecules, and two pyruvates.

In the presence of oxygen, pyruvate dehydrogenase converts pyruvate molecules to Acetyl-CoA. Acetyl-CoA enter the mitochondria to feed the tricarboxylic acid (TCA) cycle. Through this process, one glucose molecule yields 6x NADH, 2x $FADH_2$ molecules, and 2x ATP. The 6x NADH + 2x FADH, plus the NADH produced in glycolysis, then enter the electron transport chain (ETC) to more efficiently produce ATP (Figure 1.8).

1.6.2 Electron Transport Chain & Oxidative Phosphorylation

The ETC (Figure 1.8) encompasses the cellular machinery that is at the heart of oxidative phosphorylation (OXPHOS), a system otherwise referred to as cellular respiration. OXPHOS is a highly conserved pathway amongst all eukaryotic cells whose purpose it is to generate ATP [75]. In theory, OXPHOS produces 40x ATP per glucose molecule consumed; however, experimentally acquired measurements suggest only 32 – 38x ATPs are actually generated in practice, depending on mitochondrial mutations [74].

OXPHOS relies heavily on preceding pathways of glycolysis and the TCA cycle for sourcing electron donors such as NADH, $FADH_2$, and succinate. These electron donors transfer electrons to a series of transmembrane protein complexes in the mitochondrial inner membrane, collectively forming the ETC (Figure 1.8). The electrochemical gradient across the mitochondrial membrane generated as a result induces a potential difference known as the proton motive force (PMF), powering the production ATP.

The ETC is comprised of five complexes (Figure 1.8). Complex I transports two electrons released from NADH to Coenzyme Q10 (CoQ/ubiquinone), a lipid soluble electron carrier that diffuses freely within the membrane. Complex II transports two electrons released from succinate and two electrons released from $FADH_2$ to CoQ. CoQ is therefore reduced to $CoQH_2$ (ubiquinol) by Complexes I & II and is then oxidised back to CoQ by Complex III. Complex III transports electrons released from $CoQH_2$ to the water-soluble electron carrier protein, Cytochrome C (CYTC), which diffuses freely within the intermembrane space. Complex IV transports electrons from CYTC to the ultimate electron acceptor in the chain, oxygen, a reaction that yields H_2O. The energy released by the electrons flowing through the ETC is used by Complex I, III and IV to transport protons from the mitochondrial matrix to the inner membrane space, forming a proton gradient across the inner mitochondrial membrane. Finally, the

movement of protons from the inner membrane space back into the matrix is coupled to ATP synthesis by Complex V.

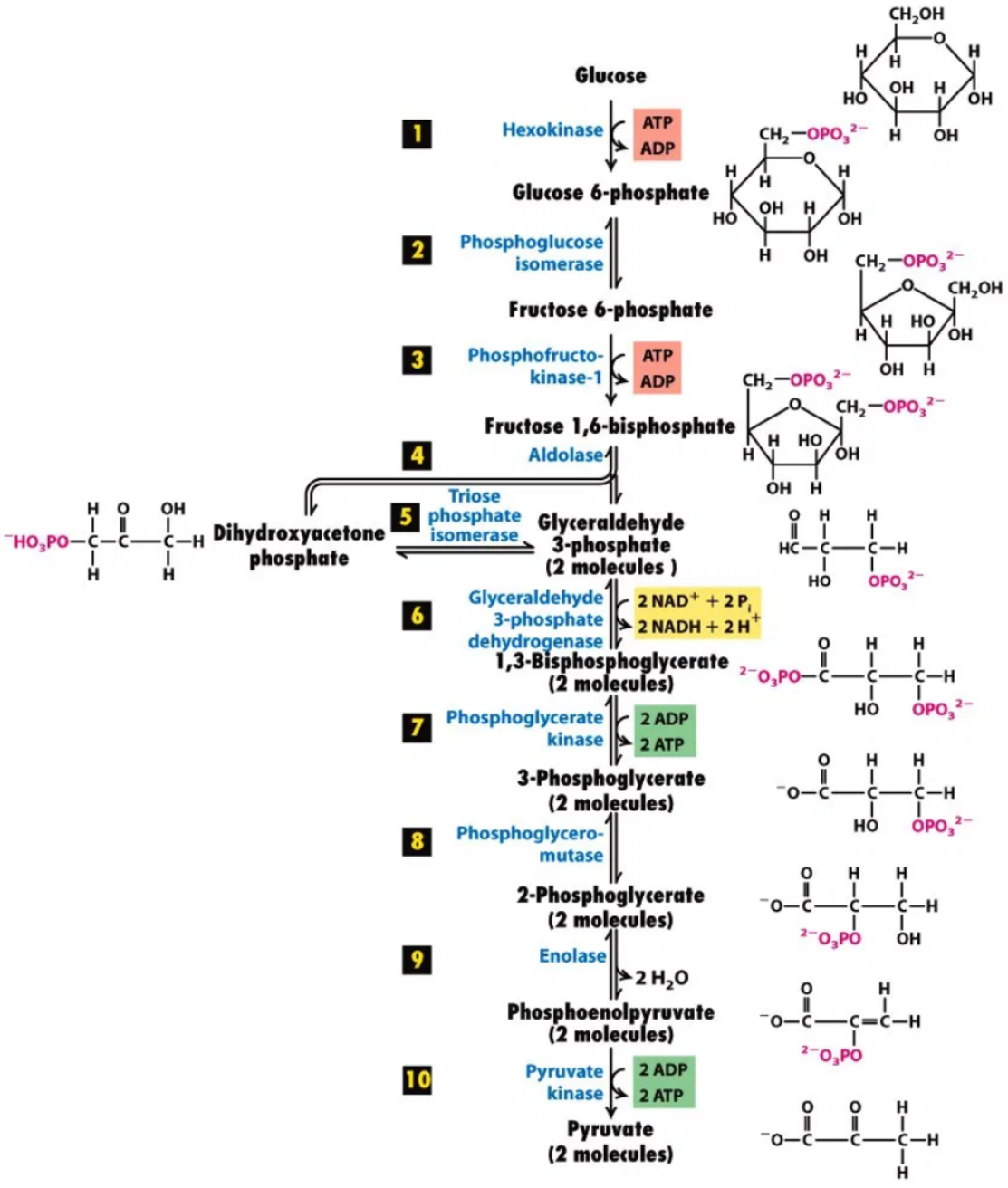


Figure 1.7 – The Glycolysis Pathway. Glycolysis is the metabolic pathway that converts glucose into pyruvate. The free energy released in this process is used to form ATP and reduced NADH. Glycolysis is a sequence of ten enzyme-catalysed reactions. It is an oxygen-independent metabolic pathway and highly conserved. The metabolism of one molecule of glucose to two molecules of pyruvate has a net yield of two molecules of ATP. Figure redrawn from Whalley et al's *Molecular Cell Biology, Sixth Ed* [76].

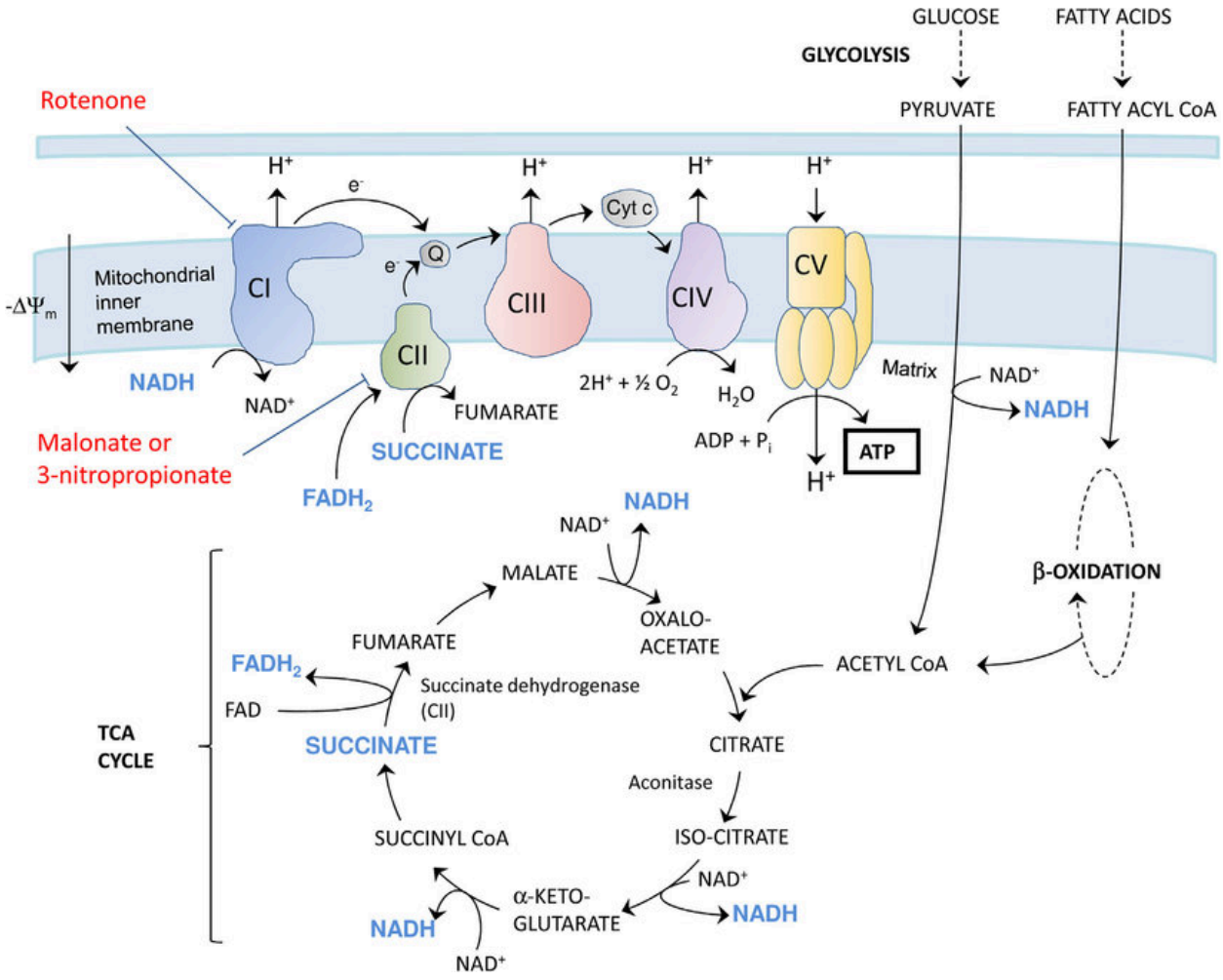


Figure 1.8 – Overview of the Tricarboxylic Acid (TCA) Cycle & Oxidative Phosphorylation. After the conversion of glucose to pyruvate and in the presence of oxygen, organisms are capable of using the tricarboxylic acid (TCA) cycle. Pyruvate must first be converted into acetyl-CoA by the pyruvate dehydrogenase complex which is an oxidative process wherein NADH and CO_2 are formed. The electron transport chain (ETC) consists of Complexes I – V and results in the generation of a cross-membrane potential gradient (proton motive force, PMF). The total number of ATP molecules obtained after complete oxidation of one glucose in glycolysis, TCA cycle, and oxidative phosphorylation is estimated to be between 30 (experimentally determined) and 38 (theoretical maximum in eukaryotes). Figure adapted from Polyzos & McMurray, 2017 [77]

1.6.3 Warburg Effect and the Inhibition of Oxidative Phosphorylation

Rather than utilising OXPHOS, cancer cells can preferentially rely on glycolysis for the generation of ATP, a phenomenon described in 1924 as the *Warburg Effect* [78]. The Warburg Effect has been shown to provide benefit to cancer cells *vis-à-vis* rapid production of ATP but also to cells intravasating into blood vessels, where they experience high levels of oxidative stress [79] –

downregulation of OXPHOS mitigates endogenously produced oxidative stress, improving chances for survival. It was initially believed that cancer cells upregulated glycolysis over OXPHOS due to mutations in mitochondrial DNA; however, it is now well-known that cancer cells often retain functional OXPHOS pathways, preferring instead a state of metabolic plasticity, shifting between glycolysis and OXPHOS in a nutrient- and environment-dependant manner [80]. Importantly, inhibition of OXPHOS, for instance by small molecules, may not necessarily induce a phenotype identical to that of the Warburg Effect as such cells would be unable to utilise OXPHOS for energy demands under any conditions. Furthermore, inhibition of OXPHOS may interfere with secondary metabolic pathways, such as glutaminolysis [81].

1.6.4 Reactive Oxygen Species & Antioxidants

The catabolism and oxidation of nutrient molecules induces ETC-driven electron flow, generating the PMF and driving ATP synthesis [74,82]. In addition to basal OXPHOS activity, incomplete reduction leads to electron leakage from the ETC and the formation of reactive oxygen species (ROS) [83,84]. Complexes I and III are the primary sites for mitochondrial ROS production, chiefly, superoxide radicals that go on to form hydrogen peroxide [83,85,86] – Complex I leakage occurs due to inadequate levels of NADH during periods of high demand [86] while leakage from Complex III has been attributed to inadequate PMF [83]. Mitochondrially generated ROS have been implicated in mediating several pro-oncogenic processes but, at low levels, are also essential for homeostatic signalling [87]. The duality of ROS as both pro-oncogenic and regulatory suggests that the mitochondria are key controllers of cell fate.

Within the mitochondria there exists an arsenal of antioxidant molecules and enzymes [88]. One of the most prominent is thiol-based glutathione (GSH), which has been shown to be involved in repairing oxidative damage [89], mediating platinum agent efficacy [90–92], and catalysing the conversion of hydrogen peroxide (H_2O_2) from superoxides ($O_2^{\bullet -}$) [93]. Once reduced,

glutathione S-transferase (GST) can convert GSH into any of a variety of molecules for further use [94]. Notably, a recent study has revealed that the deactivation of cisplatin *in vitro* is not mediated by GSH directly but instead by the enzyme glutathione S-transferase P1-1 (GST P1-1), which binds cisplatin, sequestering its activity without compromising its GSH binding ability [95].

Manganese-dependent superoxide dismutase (MnSOD), otherwise known as SOD2, is a genomically coded enzyme also responsible for maintaining mitochondrial redox homeostasis and the scavenging of superoxide radicals [96]. Increased MnSOD levels lead to an efflux of H_2O_2, which induces a shift towards glycolysis and activates signalling molecules, such as AMP-activated kinase (AMPK) [97].

Other key pathways involved in reduction and/or detoxification of reactive intermediates include: the transcription factor nuclear factor erythroid 2-related factor 2 (NRF2), which preferentially catalyses the deactivation of quinones [98,99]; thioredoxin (TRX), which reduces oxidized cysteine residues [100]; catalase (CAT), responsible for transforming hydrogen peroxide into water and diatomic oxygen [101]; and peroxiredoxin (PRX), which controls levels of intracellular peroxides [102].

1.7 The Metastatic Cascade

Metastasis is a multistep process [103]. The first step of the metastatic cascade is local invasion at the primary tumour site. This process is initiated by the activation of signalling pathways that regulate the loss of adhesion amongst tumour cells, extracellular acidification, and the degradation of the surrounding extracellular matrix (ECM) [104–106]. This facilitates tumour cell migration away from the primary tumour and into surrounding tissues. To initiate the spread to secondary sites, tumour cells must then intravasate into the blood circulation or lymphatic system and survive. Dispersal of tumour cells in the lymphatic system leads to lymph node metastasis in the first instance, while distal metastasis

usually requires tumour cells to disseminate via the blood circulation (hematogenous). The choice of a tumour cell to use either lymphatic or vascular dissemination is governed by a number of factors [107,108].

After entry into the circulation, tumour cells can disseminate widely, becoming circulating tumour cells (CTCs). CTCs have the potential to serve as prognostic markers of metastasis and survival and is discussed extensively elsewhere [109]. On reaching distal organs, surviving CTCs find their way into small capillaries or adhere to the lumen wall of larger blood vessels before extravasating and colonising.

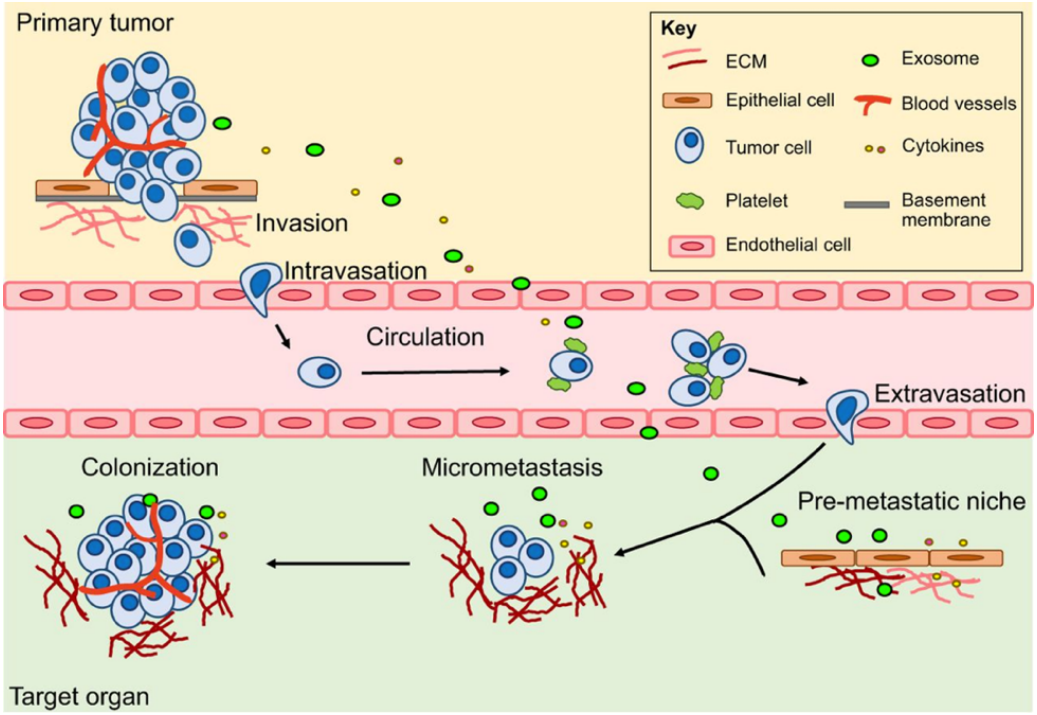


Figure 1.9 – The Metastatic Cascade. Metastasis is a multistep process. Initially, tumour cells invade locally and breakdown the local basement membrane before invading into the surrounding ECM. Intravasation then allows cells to enter the circulation. Circulating tumour cells (CTCs) need to survive shear stress while in the blood stream and evade clearance by the immune system to successfully reach distant organs. Tumour cells then attach to endothelial cells, facilitating their extravasation. After settling in the metastatic target organ, tumour cells must survive in this foreign environment and establish micrometastases. Figure adapted from Gomez-Cuadrado *et al.* [110]

1.7.1 Metabolic Effects of Hypoxia and ROS on Migration and Metastasis

Cancer cells under hypoxia can continue to proliferate but do so with highly modulated metabolic programming that is optimised for invasion [111]. A typical metabolic alteration known to promote metastasis is acidosis [80]. In patients, an inverted pH gradient across the plasma membrane of cancer cells has been observed compared to corresponding healthy tissues [112]. As opposed to normal tissues, tumours can be characterised by a more acidic extracellular pH (pHe) and a slightly alkaline intracellular pH (pHi). This results from the abnormal metabolic activity of cancer cells, including increased glycolytic flux and lactic acid release, but also reduced perfusion that limits the clearance of acidic by-products [113].

ROS produced from OXPHOS is emerging as another major promoter of tumour metastasis [72,114]. ROS leakage from ETC Complex III has been shown to play a critical role in HIF-1 stabilisation under hypoxia or as a result of re-oxygenation [115]. The activity of HIF-1 in tumours can nearly double every 24 hrs after XRT as a consequence of re-oxygenation [116,117], inducing HIF-1 and several other pro-survival factors, such as VEGF, which in turn inhibit apoptosis and provide an additional mechanism of radiation resistance [116,118]. Conversely, oxidative stress reduces CTC numbers, reflecting, at times, an opposing role, promoting and inhibiting metastatic progression [119].

1.8 Historical Strategies to Alleviate Tumour Hypoxia

As the importance of overcoming tumour hypoxia became increasingly realised, many strategies were developed and tested in combination with XRT; however, such efforts yielded only modest benefits, resulted in significant toxicity, or were impractical in the clinical setting [120]. Consequently, there are no anti-hypoxia treatments in widespread clinical use today. The development of novel and clinically applicable strategies to alleviate hypoxia is needed.

Early attempts to alleviate hypoxia involved the use of carbogen (5% CO_2 and 95% O_2) or the delivery of oxygen via hyperbaric oxygen chambers [121]. When combined with vasodilating agents, it was hoped that increased oxygen delivery would translate to more oxygen being available to diffuse throughout the tumour. Unfortunately, despite promising pre-clinical and early-phase data, such approaches did not translate into significant improvements in randomised clinical studies and raised concerns about practicality and safety [122].

The use of hypoxia-activated prodrugs was also explored to target hypoxic cells directly. Such compounds become preferentially activated and reduced to form cytotoxic species in low oxygen tension. This effect is designed to spare well-oxygenated tissues to thereby yield a larger therapeutic window. The most well-known molecule in this class is tirapazamine (TPZ), which has been shown to be 300-times more cytotoxic under hypoxia [123,124]. Unfortunately, studies using TPZ as a single agent or combined with chemoradiotherapy did not demonstrate significant efficacy. Other such bioreductive compounds have also been studied including N-oxides, quinones, and metal complexes, but similarly demonstrated modest clinical efficacy or unacceptable toxicity [125–127]. Indeed, it is possible that the use of this class of drugs is intrinsically limited since they are required to reach areas of tumours that are perfusion-restricted.

The use of pharmacological hypoxic cell radiosensitisers that promote the fixation of free radical damage acting as oxygen mimetics has also long been of interest to radiation oncology [128]. Well-known examples of such compounds are misonidazole (MISO) and nimorazole (NIM) [129]. Trials involving the former were terminated due to toxicity while the latter continues to be investigated (NIMRAD trial) [130]. Randomised clinical trials combining NIM with radical radiotherapy in head and neck cancer, namely DAHANCA 5 [131,132], demonstrated that NIM improved loco-regional control, but not overall survival. Further studies were performed using NIM establishing it as a hypoxia modifier in Denmark, but it is not widely used internationally [133,134]. As is the case with

hypoxia activated pro-drugs, hypoxic cell radiosensitisers require adequate delivery to areas of low oxygen tension within tumours, which are inherently poorly perfused and therefore difficult to reach.

1.9 Targeting Cellular Metabolism to Reverse Tumour Hypoxia

Oxygen is primarily consumed by mitochondria; however, the oxygen concentration in hypoxic regions of tumours may not be limiting for OXPHOS since ATP is generated by OXPHOS in tumour cells even within hypoxic regions [135]. As such, OXPHOS inhibition could be an effective way to reduce or even eradicate tumour hypoxia by allowing unmetabolised oxygen to diffuse from well perfused tissues into hypoxic areas (Figure 1.10). OXPHOS inhibition also appears to be efficacious in a wide range of cancer types, likely a result of the highly conserved ETC [114] and may only need to act on normoxic regions – diffusion of OXPHOS inhibitors to poorly perfused areas may therefore not be required to alleviate hypoxia.

Mathematical modelling and studies in 3D multicellular spheroids have shown that reducing OCR can alleviate hypoxia by increasing oxygen availability [136]. These models suggested that complete inhibition of oxygen consumption is not required, and that even a 30% decrease would abolish severe hypoxia. Moreover, the use of OXPHOS inhibitors to reverse hypoxia may be more amenable to *in vitro* study than other approaches, such as the normalisation of tumour vasculature.

Small molecule OCR inhibitors have previously been reported and tested, but most inhibit the HIF system, a downstream effector of hypoxia. One example is the potent BAY 87-2243, which failed clinical trials due to toxicity [137,138]. The anti-diabetic biguanide *Metformin* is another FDA-approved drug shown to reduce cellular OCR and alleviate tumour hypoxia [139–142]. Notably, a derivative of metformin, phenformin, was previously withdrawn from the market

due to adverse risk of lactic acidosis but demonstrated an ability to inhibit OCR [143].

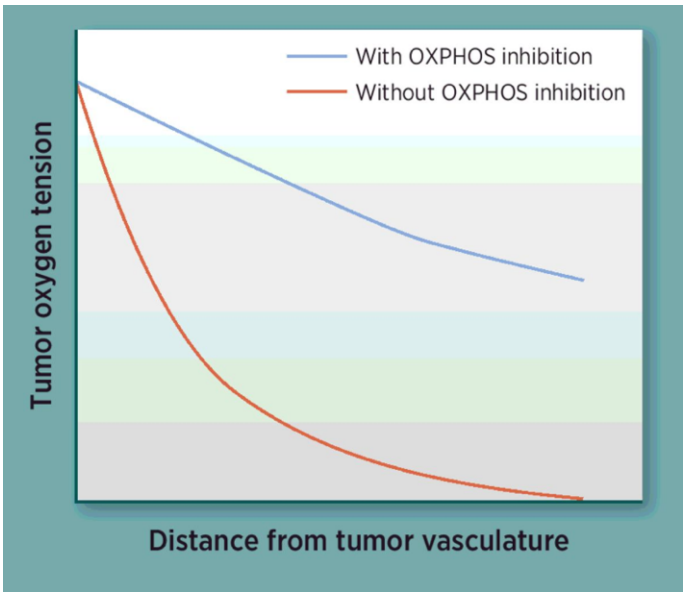


Figure 1.10 –Hypothetical Effect of OXPHOS Inhibition on Tumour Oxygen Tension. In the absence of OXPHOS inhibition, tumour oxygen tension decreases steadily with increasing distance from tumour vasculature. Both tumour areas with limited oxygen diffusion due to the pathologic tumour vasculature, and microregions distant from perfused vessels, are therefore chronically hypoxic. Under OXPHOS inhibition, we hypothesize that OXPHOS activity is greatly reduced throughout the tumour, and that the decreased cellular oxygen consumption lowers the slope of the oxygen gradient from the vessels into the tumour tissue. Figure adapted from Ashton *et al.* [72]

Some reports of the anti-cancer efficacy of metformin have been attributed to the modulation of signalling pathways [144]; however, early studies revealed that metformin inhibits mitochondrial ETC function through Complex I [141,145]. There is debate as to whether Complex I inhibition is a direct effect or not [146–148]. To further confound matters, a binding site for metformin on Complex I has yet to be reported at the time of writing [149]. In previous works, including our own, metformin-mediated OCR reduction *in vitro* was marginal compared to other well-known OXPHOS inhibitors when used at pharmacologically relevant concentrations [141,142,150,151]. In agreement with other reports [150,152–154], more efficacious OXPHOS inhibitors are therefore needed to reverse tumour hypoxia and synergise with XRT.

1.10 Atovaquone Alleviates Tumour Hypoxia by Inhibiting OXPHOS

Our team previously screened a library of 1,697 FDA-approved drugs to identify small molecules that inhibit OXPHOS and decrease OCR of cancer cells (Figure 1.11a) [151]. The Seahorse XF Analyzer was used to perform the screen, which functions using fluorophores that react with oxygen directly.

The anti-malarial drug Atovaquone (ATQ) was found to cause a reduction in OCR across a range of cell lines and at pharmacologically achievable concentrations (Figure 1.11b) [155]. ATQ also eradicates hypoxia in spheroid models and in FaDu and HCT116 xenografts (Figure 1.11c-f). When combined with XRT, ATQ caused a significant tumour growth delay (Figure 1.11g, h).

ATQ is an analogue of the electron carrier ubiquinone and decreases OCR by inhibiting the ETC at Complex III [156]. In parasite models, the IC_{50} for OXPHOS inhibition is approximately 3 nM but is significantly higher for purified human Complex III inhibition (70 to 460 nM) [157]. There is currently no evidence that ATQ accumulates in the mitochondrial; however, it is worth noting that other hydrophilic OXPHOS inhibitors, such as metformin, that have net-*positive* charge at physiological (7.4) pH have been purported to do so [158]. In contrast, the net-negative charge that ATQ carries at physiological pH and being hydrophobic might indeed promote such an effect [155]. In terms of tolerability, ATQ has been reported to have an excellent safety profile inducing only mild side effects [159]. Though it is also well absorbed by the body and can readily accumulate in tissues, it is poorly water soluble. It is eliminated hepatically with a half-life of 50–84 hr and is not significantly metabolised *in vivo* [160].

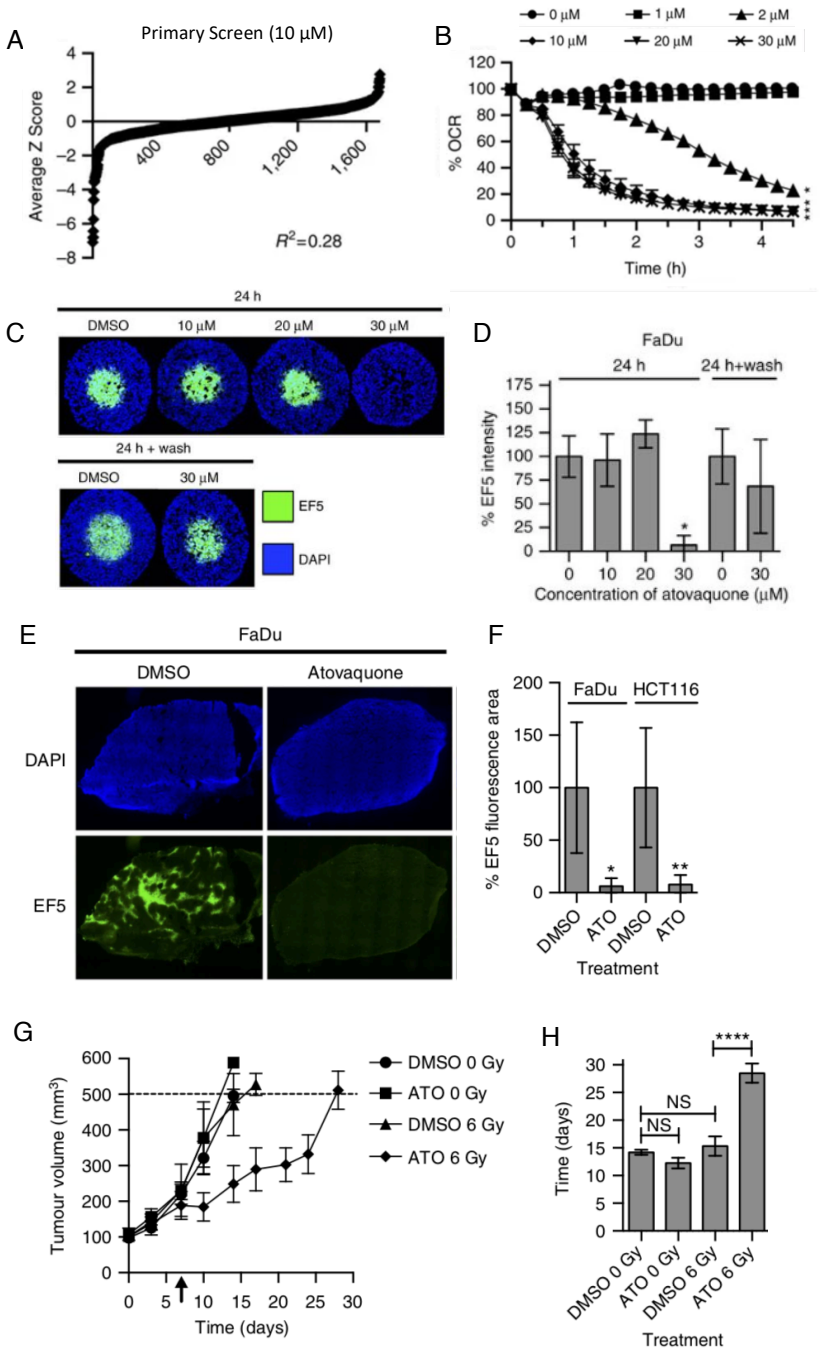


Figure 1.11 – Atovaquone Alleviates Tumour Hypoxia *in vivo* and Sensitises Tumours to Ionising Radiation **(A)** FaDu cells were incubated with a library of 1697 FDA-approved compounds for 24 hr. **(B)** The OCR of FaDu cells were measured for 4.5 hr after injection of ATQ. The % OCR post injection is shown relative to the DMSO control and normalized to the relative cell number obtained by Hoechst staining at the end of the experiment. **(C)** FaDu spheroids were treated with DMSO or ATQ either for 24 h, or for 24 h followed by recovery for 24 h in drug-free medium, as indicated. Hypoxia was assessed by staining central spheroid sections for EF5 (green), with DAPI as a nuclear counterstain (blue) and **(D)** quantified. Mice bearing FaDu xenograft tumours were treated with 50 mg/kg/day ATQ for 7 days and were injected with EF5 on day 7. **(E)** Immunostaining for EF5 with DAPI as a nuclear counterstain. **(F)** % EF5 fluorescent area relative to the DMSO-treated tumours. **(G)** Tumour growth overtime after treatment with ATQ or DMSO and 6 Gy radiotherapy (XRT) to dorsal flank FaDu tumours and **(H)** quantification thereof. Figure adapted from Ashton *et al.* [151]

1.11 Outline & Purpose of Thesis

Our laboratory group previously identified ATQ as a hypoxia modifier that synergises with XRT in animal studies [151]. The aim of this doctoral thesis is to expand on these findings exploring the broader effects of ATQ therapy to support future studies. Specifically, it aims to address the following questions:

Chapter 3 – Atovaquone as a Hypoxia Modifying Agent

Objective

Explore preliminary dependencies for how ATQ reduces OCR and probe *in vitro* & *in vivo* its tolerability and robustness as a hypoxia modifying agent

Specific Aims

- Does incubation with ATQ for prolonged periods induce cell death?
- How does ATQ affect spheroid growth over time?
- Are the effects of ATQ on oxygen consumption and ECAR reversible *in vitro*?
- To complement existing EF5 data, does ATQ diminish CAIX staining in spheroid sections?
- Can ATQ reduce OCR independently of a functional ETC?
- Does ATQ modulate metabolism and alleviate spheroid hypoxia *in vitro* independently of the master hypoxia regulator, HIF-1α?
- Does ATQ modulate metabolism *in vitro* independently of STAT3?
- Does ATQ induce cell-death independently of STAT3?
- Can higher tumour and plasma levels of ATQ safely be reached in mice?
- What higher-dose levels can be safely achieved for future animal studies?

Chapter 4 – Effect of Atovaquone on Migration & Metastatic Potential

Objective

Explore whether ATQ modulates cancer cell migration or metastatic potential

Specific Aims

- Does ATQ induce extracellular acidification *in situ* in tumour bearing mice, an effect known to precede cancer cell invasion and metastatic spread?

- Does ATQ modulate cellular chemotaxis-driven migration *in vitro*?
- Using an orthotopic model of metastasis, does ATQ modulate distant organ metastatic spread?
- Can pre-loading animals with ATQ prior to tumour induction modulate metastatic potential?

Chapter 5: Does Atovaquone potentiate the effects of chemotherapy?

Objective

Explore whether ATQ potentiates the efficacy of commonly used chemotherapies and, if so, whether the effect is dependent on ATQ's ability to reverse hypoxia

Specific Aims

- How is chemotherapy-mediated cell death modulated by ATQ therapy *in vitro*?
- Does ATQ sensitise a range of cell lines to select chemotherapies?
- Is potentiation of chemotherapeutic efficacy by ATQ dependent on hypoxia?
- Can ATQ's potentiation of chemotherapies be rescued *in vitro*?
- When combined with chemotherapies, does ATQ delay the growth of spheroids?
- When combined with chemotherapies, does ATQ delay the growth of tumours?
- Is ATQ-mediated potentiation of chemotherapeutics well-tolerable *in vivo*?

The results presented in this thesis show that ATQ is a well-tolerated and robust hypoxia modifying agent deserving of further study. We demonstrate that ATQ does not increase cellular migration or metastatic potential and that the anti-cancer effects of platinum-class chemotherapies are potentiated by ATQ, providing a novel combination for cancers treated with platinum-class agents. Taken together, our findings suggest there may be a significant clinical benefit in using ATQ or other well-tolerated OXPHOS inhibitors to increase the therapeutic window.

CHAPTER 2

METHODS & MATERIALS

2.1 Tissue Culture

2.1.1 Maintenance

All cell lines were purchased from American Type Culture Collection (ATCC), unless otherwise noted (gifts). HCT116 (colorectal), FaDu (hypopharengeal), and H1299 (lung) cell lines were selected due to their ability to form spheroids *in vitro*. 4T1 (murine mammary gland) cells were used for the orthotopic metastasis model of murine triple-negative breast cancer (TNBC) in BALB/c mice. MDA-MB-231 (breast) cells were used to explore the ability of ATQ to modulate cellular migration as they were previously optimised for use with the Xcelligence Analyzer at our institution. H460 (lung) cells were used for *in vivo* experiments with ATQ and carboplatin due to many previously published studies detailing non-toxic dosing regimens in identical models (flank xenografts in BALB/c nu/nu mice).

Isogenic DLD-1 (colorectal) cell mutants for $STAT3^{Y705}$ ($STAT3^{Y705F/Y705F}$) and 143B cybrids (143B-CYTB) harbouring a cytochrome bc_1 mutation were generous gifts from Prof David Frank at Harvard, gifted in addition to mitochondrial DNA deficient 143B (143B-ρ) cells generated using Ethidium Bromide by their team. $HCT116^{HIF\text{-}1\alpha,\ -/-}$ isogenics for studying the ATQ's dependency on HIF-1α were a generous gift from Prof Adrian Harris at the University of Oxford and maintained in DMEM medium supplemented with 10% FBS.

HCT116, FaDu, and H1299 cells were maintained in Dulbecco's modified Eagle's medium (DMEM, Sigma) high-glucose supplemented with 10% foetal bovine serum (FBS) and 100 U penicillin + 100 µg/mL streptomycin. The HCT116 and DLD1 isogenics as well as the 4T1 H460 cell lines were maintained in Roswell Park Memorial Institute (RPMI-1640, Sigma) media supplemented with 10% FBS and 100 U penicillin + 100 µg/mL streptomycin. MRC5 cells were maintained in minimum essential medium

(MEM, Sigma) supplemented with 10% FBS and 100 U penicillin + 100 µg/mL streptomycin. The 143B, 143B-ρ, and 143B-CYTB cells were maintained in high-glucose DMEM with 0.015 mg/mL 5-bromo-2'-deoxyuridine (BrDu), 100 U penicillin, 100 µg/mL streptomycin, 2 mM Glutamine, 50 pg/mL uridine, 100 µg/mL pyruvate, and 10 % FBS.

All cell lines were authenticated by LGC standards (ATCC) by short tandem repeat (STR) profiling and tested for mycoplasma using MycoAlert (Lonza).

2.1.2 Storage & Resuscitation

Cells were kept in cryovials stored in vapour phase liquid nitrogen. Cells were thawed in a water bath at 37° C. Cells were immediately diluted in 10 mL of media in a 50 mL falcon tube and centrifuged at 240 g for 5 min. The media was removed, and the cells were re-suspended in 5 mL of media and seeded in a T25 flask.

2.1.3 Passaging

The media was removed from the flasks. Cells were washed in 5 – 10 mL of 1x phosphate buffered saline (1x PBS) and 1 – 2 mL of trypsin-ethylenediaminetetraacetic acid (EDTA) was added to the flask. Cells were then returned to the 37° C incubator for 5 - 10 min. Medium was added after cells had lifted, and the cell suspension was diluted appropriately in medium. Typically, the cells were passaged at 1:10, 1:15 or 1:20 and returned to the incubator. Cell lines were passaged for a maximum of 21 d and were passaged when cells reached 60 – 80 % confluency. Cells were cultured in incubators at 37° C supplied with 5 % CO_2.

2.1.4 Counting

The cells were trypsinised as described above. A 50 µL cell suspension was diluted 1:10 in DMEM in a microcentrifuge tube and counted using the Scepter 2.0 (Millipore) hand-held automated cell counter, or a 10 µL cell

suspension without dilution was counted using a microfluidics-based LUNA II (Logos Biosystems) automated cell counter.

2.2 Colony Formation Assays

The cells could attach for 4 hr and then treated as indicated in each experiment for up to 24 hr. After completion of treatment, cells were cultured for approximately 2 weeks, stained with crystal violet, and then counted using a GelCount colony counter (Oxford Optronix). Plated cell numbers for DMSO controls are shown in Table 2.1. Experimental plating numbers are as described for each experiment and vary depending on plate-type used (6-, 12-, or 24-well).The colony forming assay (CFA) was developed over 60 years ago by Puck and Marcus [161] and remains a gold-standard technique to measure relative deactivation or inhibition of proliferative capacity [162]. For CFAs, cells were allowed to attach for 4 hr and then treated as indicated for 24 hr. After completion of treatment, cells were cultured for approximately 2 weeks, fixed and stained with crystal violet in methanol (MeOH), and then counted using a GelCount colony counter (Oxford Optronix). Plated cell numbers for DMSO controls are shown in Table 2.1. Experimental plating numbers are as described for each experiment and vary depending on plate-type used (6-, 12-, or 24-well).

2.2.1 Statistical Analysis

CFA survival data was curve fitted using GraphPad Prism by non-linear regression of the linear quadratic (LQ) model (Equation 2.1):

$$SF = e^{-\alpha D - \beta D^2} \quad \text{(Eq 2.1)}$$

where SF denotes surviving fraction, D (Gy) is radiation dose and α (Gy^{-1}) and β (Gy^{-2}) are parameters to fit. Each treatment condition had $N = 6$ technical replicates and no fewer than three experimental repeats.

Table 2.1 – Plated cell numbers for colony formation assay (CFA) controls (untreated) for 6-well tissue culture plates

Cell Line	CFA Plating Numbers
FaDu	200
H460	200
143B^{wt}	200
143B-ρ	400
143B-CYTB	800
4T1^{wt}	200
4T1-eGFP-FLuc	200
HCT116	200
H1299	200
MRC5	800
DLD1^{wt}	200
DLD1 STAT3^{Y705F}	400
DLD1 STAT3$^{Y705F/Y705F}$	400

2.2.2 Drug Treatment

Single agent drug treatments were performed for 24 hr by adding 20x concentration to each well (6-well or 96-well plates) and then washed off by medium change. When multiple drugs were used sequentially to explore combinatorial effects, incubation time is as described per drug per experiment but does not exceed 24 hr in total e.g. 1-hour pre-treatment with a first compound and 23 hr combination treatment by adding a second compound, both at concentrations that are 20x. As described above, medium was changed at 24 hr to wash off the drug(s) – colonies could form for up to two weeks before fixing, staining, and counting.

2.2.3 Ultraviolet Irradiation

FaDu cells for UVC irradiation experiments were grown in DMEM as described and then plated according to cell numbers listed in Table 2.2. Cells were allowed to attach for 4 hours and then pre-treated with either DMSO or ATQ at 30 μM for 2 hours. Shortly before irradiation, medium was removed and kept separate because UVC radiation is rapidly attenuated by aqueous solutions, such as medium. UVC irradiation was performed using a CL-1000 ultraviolet cross-linker equipped with 254 nm tubes (UVP).

Table 2.2 – Plated cell numbers for UVC CFA Experiments

Treatment	DMSO Cell Numbers	Atovaquone 30 μM Cell Numbers
Control	200	400
0.5 J/m^2	200	400
1 J/m^2	200	400
2 J/m^2	400	800
5 J/m^2	800	1600

2.3 Flow Cytometry

Flow cytometry for all experiments was performed using a FACSCalibur (Becton Dickinson). The cytometer settings were set at a flow rate of 150 - 250 events per second and the working voltage varied between 200 V and 400 V. Histogram plots were produced using open source Flowing Software 2.5.1 and at least 10,000 events recorded per condition. At least three experimental repeats were performed for each experiment.

In general, single parameter histograms were then recorded with at least 1 x 10^5 cells per treatment condition by normalising reference population to a fluorescence intensity of 10^1, permitting positive cell populations to then be identified in the range of 10^2 - 10^5. If distinct cell populations could not be identified prior to gating on fluorescence channel histograms, then

experiments were repeated or adjusted by modulating the channel voltage by up to +/- 10% relative to previous experimental conditions.

2.3.1 MitoSOX

Measurement of mitochondrial superoxide was performed using the fluorescent dye MitoSOX. The reagent was stored at –80°C and dissolved in DMSO to a stock concentration of 2.5 mM.

Cells were counted and plated as described but at a density of 0.5 × 10^6 cells per well. Cells were then allowed to attach for 4 hours prior to being incubated with 5 μM MitoSOX for 30 mins (to allow proton motive gradient-dependant uptake). Either DMSO or ATQ 30 μm was then added for 2 hours prior to medium removal, a 37°C-prewarmed PBS wash, and trypsinisation. Samples were then centrifuged at 200 x g for 5 minutes, the supernatant was discarded, and then resuspended in 200 μL ice-cold PBS. Samples run on channel FL3 and analysis performed via geometric mean due to the cumulative fluorescent nature of the probe.

2.3.2 Propidium Iodide

Medium was removed but retained for centrifugation. Cells were washed with 1x PBS, lifted in trypsin-EDTA, re-suspended in fresh pre-warmed medium, transferred to FACS tubes, and spun down at 200 x g for 5 min. Cell pellets were washed with 1 mL of ice-cold 1x PBS and resuspended in 200 μL of 50 μg/mL propidium iodide (Sigma) in FACS-ready tubes. Samples were kept on ice and away from light, gently vortexed, and then immediately analysed via flow cytometry on channel FL3.

2.3.3 Time Series

Cells were treated as indicated in each experiment for up to 24 hours and then left to recover after drug-free medium change. At each timepoint (24, 48, 72, or 96-hours), propidium iodide (PI) analysis via flow cytometry was performed as described above.

2.4 Immunofluorescence

All samples for immunofluorescence were prepared and mounted using VectaShield medium (Vector Laboratories). Fluorescence microscopy (Nikon 90i, Nikon) was performed shortly thereafter. Every treatment condition included at least N = 8 spheroids and each experiment was repeated at least in triplicate.

2.4.1 EF5

Spheroid hypoxia was quantified by EF5 staining using an α-EF5 antibody probe, both of which were generous gifts from Dr Cameron Koch at the University of Pennsylvania. A 10 mM stock of EF5 concentrate prepared from powder was made up in an antibody carrier specific by the manufacturer. Each spheroid was incubated with 200 μM EF5 for 6 hr before fixation in 4% paraformaldehyde for 24 hr, incubation in 30% sucrose for 24 hr, and then addition of OCT (VWR, TissueTek) for cryosectioning. Spheroid sections were incubated for 45 min in TNB blocking reagent (Perkin Elmer), washed for 5 min in 1x PBS, 0.3% Tween 20, and then incubated overnight with 70 ml of undiluted 75 mg mL x 1 α-EF_5 antibody. Three washes of 45 min were then performed using 1x PBS, 0.3% Tween 20 (PBST) before incubating with DAPI at 1 μg/mL for 10 minutes. Samples were washed 3 x 5 mins in PBST, mounted, and then imaged.

2.4.1 CAIX

Spheroids were treated, fixed, and embedded as described. Sections were cut via cryostatic sectioning at 10 μm and maintained at -20 °C until ready to stain. A hydrophobic barrier around spheroid sections was drawn using a pat pen. Sections were blocked in 10% Goat Serum / 1% BSA / 0.1% Triton in PBST for 1.5 hr at RT and then washed for 10 min in PBST.

Probing was performed with primary antibody (ab184006: Raised in Rabbit, Reactive with Human & Mouse) diluted in 1% BSA in PBST (α-CAIX, 1:500) o/n at 4 °C or for 2 hr at RT. Samples were washed 2 x 5 min in PBST. Secondary antibody was then diluted in 1% BSA in PBST and incubated for 1 hr at RT (Goat α-Rabbit-Alexa488, 1:500 from Molecular Probes). Washing was done 3 x 5 min in PBST. Finally, samples were Incubated with 0.5 µg/mL DAPI for 10 minutes. and Washed 2 x 5 min with PBST.

2.4.2 Analysis

Quantification of immunofluorescent probes used in spheroid experiments as described below was were done by first delineating spheroid sections according to the DAPI signal. Average signal intensities were then measured for each spheroid on each section and the integrated intensity was recorded. Spheroid area was used to normalise each spheroid to allow comparisons between treatment groups.

2.5 Immunohistochemistry

2.5.1 Haematoxylin & Eosin

Tumours and lungs were harvested from BALB/c mice bearing intramammary 4T1-eGFP-FLuc primary tumours. Tissues samples were fixed in formalin and embedded in paraffin blocks before cross-sections of 5 µm in thickness were taken and mounted. Slides were rehydrated in 100% alcohol twice for 5 min, then in 95% alcohol for 2 min and 70% alcohol for 2 min. Sections were washed in PBS and were stained using Harris haematoxylin (Sigma, Gillingham, UK) for 1 min. After that, sections were washed in running tap water for 5 min. Subsequently, sections were differentiated in 1% acid alcohol for 30 sec following washing in running tap water for another 5 min. Sections were counterstained in eosin solution (Sigma, Gillingham, UK) for 1 min. Finally, sections were dehydrated using 90% alcohol followed by 2 changes

of 100% alcohol, 5 min each and finally washed in xylene for 5 min. Sections were covered with cover slips using mounting medium (Vector Laboratories, Peterborough, UK). Scoring was kindly performed by Prof Ruth Muschel, pathologist (University of Oxford).

2.5.2 EF5

Spheroid hypoxia was quantified by EF5 staining, using an anti-EF5 antibody (both reagents obtained from University of Pennsylvania). Two hundred micromolar EF5 was added to the spheroids for 6 hr before fixation in 4% paraformaldehyde for 24 h, incubation in 30% sucrose for 2.5 h, and then addition of OCT (VWR, TissueTek) for cryosectioning. Spheroid sections were incubated for 40 min in TNB blocking reagent (Perkin Elmer), washed for 5 min in 1 x PBS, 0.3% Tween 20, and then incubated overnight with 70 ml of undiluted 75 µg / mL anti-EF5 antibody. Three washes of 45 min were then performed using 1 x PBS, 0.3% Tween 20 before addition of DAPI vectorshield mounting medium (Vector Laboratories) and fluorescence microscopy (Nikon 90i, Nikon). Spheroid diameter was derived from the spheroid cross-sectional area measured by the Gelcount Colony Counter (Oxford Optronix) or Axiovert200M (Carl Zeiss MicroImaging GmbH).

2.6 Oxygen Consumption & Glycolysis Measurements

Cells were lifted and counted as described then plated in 96-well XF Cell Culture plates at a density of 1 x 10^5 cell per well. Cells were then allowed to attach overnight. Drugging was performed as indicated in each experiment and then cells were further incubated for 24 hr. XF Hydration Cartridges (Agilent) were prepared prior to running the assay and allowed to equilibrate to 37 C in a non-CO_2 incubator to compensate for daily fluctuations. When ready, the medium was removed and replaced with drug- and FBS- free XF Assay Medium (Agilent) containing 5 mM glucose, 5 mM sodium pyruvate and 4 mM L-glutamine. After calibrating for atmospheric pressure and

temperature, cellular oxygen consumption and extracellular acidification measurements were recorded in parallel and in triplicate (3 x 30 min intervals) using an automated XF96 Analyzer (Seahorse Biosciences, Agilent). Kinetics experiments, measurements were collected every 15 minutes following injections. The cells were then fixed in ice-cold methanol for 5 min and incubated in 1x PBS with 4 µg/mL Hoechst 33258 (Sigma) for 1 hr before measuring fluorescence using a POLARstar Omega plate reader (BMG Labtech) to obtain the relative cell number per well.

The cells were grown for 24 hr in DMEM containing 5 mM glucose and 4 mM L- glutamine, and then measurements of the OCR were taken in XF assay medium (Seahorse Biosciences) containing 5 mM glucose, 5 mM sodium pyruvate and 4 mM L-glutamine using an XF96 Analyzer (Seahorse Biosciences). For the kinetics experiments, measurements were collected every 15 min following injection of ATQ. For the experiments with uridine and pyrimidine synthesis inhibitors, the cells were incubated with the compounds for 2 or 24 hr as indicated, the medium was replaced with the assay medium also containing the compounds, and then measurements were made. The OCR measurements were corrected for cell number using Hoechst staining, as described above.

2.7 Three-dimensional Tissue Culture (Spheroids)

FaDu, H1299, or HCT116 cells were passaged, maintained, lifted, and counted as described above. Cells were plated in Ultra Low Attachment U-bottom plates (Corning, #9009) at a density of 1 x 10^5 cells per well, each containing 200 µL of low-glucose DMEM medium (Sigma) and supplemented with 10% FBS and 200 µM pyruvate (Sigma). Plates were then incubated for at least 72 hr and enveloped in highly porous bread bags to minimise the influence of convective thermal gradients. PBS plates were placed at all sides

of spheroid plates while incubating during this time to mitigate edge effects associated with evaporation.

Three-dimensional spheroid formation was inspected manually and confirmed using microscopy-based optical density gradient analysis. After 72 hr, spheroid diameter was recorded daily and derived from cross-sectional area measurements acquired with a GelCount Colony Counter (Oxford Optronix). Once spheroids reached 550 - 650 μM in diameter, they were treated for 24 hr as indicated in each experiment with at least N = 8 spheroids per condition. In the case of EF5 staining, spheroids were incubated for an additional 6 hr with 200 μM EF5 and then carefully collected, PFA fixed, cryoprotected, cryostatically sectioned, mounted, and analysed as described in Section 2.5.

2.7.1 Spheroid Growth Delay

FaDu, H1299, or HCT116 cells were seeded to generate spheroids, as described above. Once platted, plates were symmetrically divided into sections of $N = 16 – 32$ spheroids per intended treatment condition to control for thermal incubator gradients and CO_2 fluxes during the extensive follow-up period (30 days). Spheroid plates were placed in also porous bread bags (Lakeland, #43208-2503) to further reduce incubator gradients and homogenise spheroid sizes across each experiment.

Once spheroids reached 550 – 650 μm in diameter, half the medium of each well (100 μL) was removed and replaced with 2x ATQ 30 μM or concentration volume-matched control solvent (DMSO) since ATQ 30 μM has been demonstrated to alleviate spheroid hypoxia without aberrant toxicity. Each plate contained a DMSO control and each ATQ-treated plate contained DMSO and ATQ controls to account for plate-to-plate variations.

After 24 hr, spheroids were concomitantly treated with either control solvent or a select chemotherapeutic agent. Chemotherapies were added at

16x concentration to each well to minimise perturbations to the spheroids. ATQ was not re-added. Plates were then incubated for a further 24 hr.

Drugs were then washed off via serial medium change (3x). Spheroids were observed and diameter measurements were recorded thrice a week using a high-throughput amenable 96-well plate BrightField microscope (Celligo, Nexelcom). Half the volume of medium of each spheroid well was changed thrice weekly to maintain growth, or regrowth.

2.8 Cellular Migration Assay

Real-time cell reattachment and chemotaxis was measured using the xCELLigence RTCA DP device (Acea Biosciences) according to the manufacturer's protocol. Briefly, 20,000 cells per well were added to electrode-containing microtiter plates (E-plate) for reattachment. MDA-MB-231/MCF-7 (40,000 cells/well) and FaDu/H1299/HCT116 (20,000 cells/well) were added to each CIM-plate 16 for migration. CIM-plates are similar to a Boyden chamber, containing an upper and a lower chamber separated by a polyethylene terephthalate membrane with 8-mm pore size. The membrane has gold electrodes on the bottom of the upper chamber to detect cells moving into the lower chamber. The chemoattractant used was 5% FBS. Reattachment and migration rates were quantitatively recorded as Cell Index – a change in electrical impedance of the current flowing through the electrodes. Impedance was recorded every 1 - 5 min for 2 hr for reattachment and every 15 mins for 24 hrs for chemotaxis. Raw data were exported to Microsoft Excel. Graphs shown are averages of three independent repeats with three wells per condition of each experimental run.

2.9 Animal Studies

The project licence covering the animal studies in this work (PPL30/2922) was approved by the Oxford University Animal Welfare and Ethical Review Body

(AWERB), and granted by the UK Home Office Animals in Science Regulation Unit (ASRU) under the Animals (Scientific Procedures) Act 1986 [ASPA]) and in accordance with the guidelines for the welfare and use of animals in cancer research.

2.9.1 Strain Selection

Xenograft models employed anthymic BALB/c nude female mice (Charles River) at age 55 – 70 d while allograft models used BALB/c female mice aged 50 – 75 d (Charles River).

2.9.2 Tumour Induction

Cells were freshly thawed, lifted, and counted as described. Final cell numbers for inoculation varied by cell type and model (Table 2.3). Cells were made ready for injection by suspension in 200 µL of equal parts Phenol-red Free MatriGel (BD Biosciences) and PBS. Prior to injection, cell suspensions and syringes were kept on ice to minimise *in situ* solidification of the MatriGel and to preserve cellular viability while injecting. Mice were anaesthetised using a gaseous 1:1 mix of isoflurane and oxygen prior to and throughout injections.

Table 2.3 – Cell Numbers and Injection Routes for in vivo Experiments

Model Strain Cell Line	Cell Number Volume Injected	Injection Route
Heterotopic Xenograft BALB/c nu/nu H460	1×10^6 200 µL	s.c. (Right Dorsal Flank)
Heterotopic Xenograft BALB/c nu/nu FaDu	1×10^6 200 µL	s.c. (Right Dorsal Flank)
Orthotopic Allograft BALB/c 4T1-eGFP-FLuc	1×10^5 50 µL	i.m.m. (Lower Right Inguinal Mammary Fat Pad)

2.9.3 Atovaquone Delivery

Once the tumours had reached the desired volume of between 50 – 100 mm^3 (according to experiment), ATQ in the form of Wellvone™ was administered via oral gavage (p.o.) at 100 mg/kg per day in 0.1% carboxymethylcellulose – ATQ in the form of Wellvone™ was selected for use to better reflect the clinical administration of the compound, which comes as an oral suspension rather than solution due to ATQ's insolubility in water at standard conditions. Calculations were performed assuming that a 20 g mouse would consume 5 mL water per day, as was indicated to be standard by BMSU staff at our institution. Mice were given this dose for 10 days because ATQ takes 1 – 2 weeks to reach a steady-state plasma concentration in patients [163].

2.9.4 Endpoints & Measurements

Animals were randomly assigned to each treatment group the day on which their tumours reached critical size (50 – 100 mm^3, depending on experiment) using a random number generator (Microsoft Excel), but the experiment was not blinded. A sample size of N = 6 – 12 mice per group was used yielding 90% power (s.d. 1⁄4, 30%, alpha 1⁄4, 0.05) to detect a 70% decrease, based on our previous experience and published data. A two-tailed test was performed for this determination. Use of 6 – 12 animals per treatment group allowed us to overcome the problem of differences in variance between groups being statistically compared.

Tumour size was measured with callipers and done every other day with two independent operators using the formula $V = (a \times b^2) / 2$, where a and b are the largest and the smallest perpendicular diameters, respectively. Measurements were averaged for each animal on each day of measurement. Once tumours were found to have reached between 500 – 1000 mm^3, animals were injected with EF5 to eventually confirm presence and abolishment of hypoxia and then culled using a UK Home Office *Schedule 1* method [164]. Schedule 1 consists of several possible methods to sacrifice experimental

animal. In this work, pentobarbital (100 mg/kg i.p.) overdose followed by exsanguination and observation of *rigor mortis* (post-mortem rigidity) was typically employed.

2.9.5 EF5 Hypoxia Staining

To assess hypoxia by immunostaining, mice were injected intraperitoneally with the nitroimidazole hypoxic cell marker EF5 (10 μL/g of body weight of a 10 mM solution in 0.9% saline; kindly provided by Dr Cameron Koch, University of Pennsylvania, PA) at 4 hours before Schedule 1 death, followed by tumour or organ harvesting.

2.9.6 4T1 Metastatic Model

The 4T1 mammary carcinoma is a transplantable tumour cell line that is highly tumourigenic and invasive [165] and, unlike most tumour models, can spontaneously metastasise from the primary tumour in the mammary gland (fat pad) to multiple distant sites including lymph nodes, blood, liver, lung, brain, and bone (Figure 2.2). Mice were obtained from the Charles River Laboratories/NIH (Wilmington, MA, USA). The mice were housed in a ventilated barrier rack (Lab Products Company, USA) in a temperature-controlled facility on a 12 hr photoperiod.

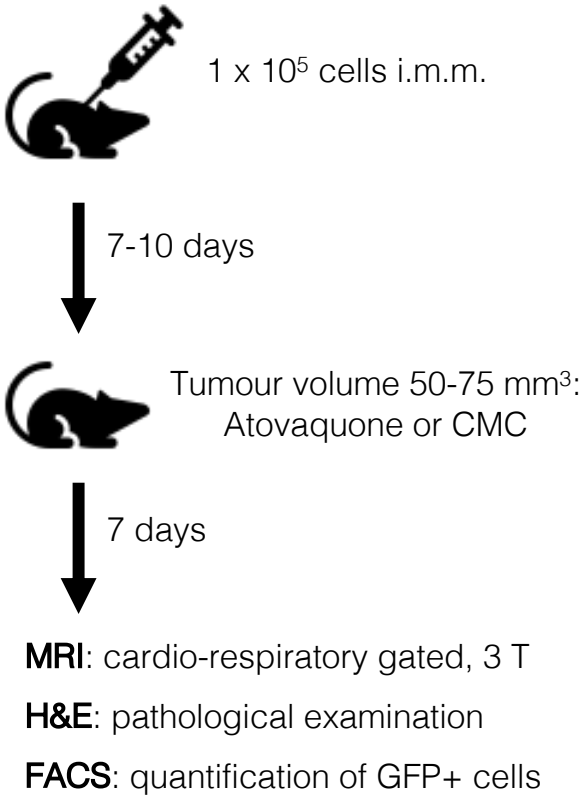


Figure 2.2 – 4T1 Spontaneous Metastasis Model. Six- to eight-week-old, female BALB/c mice (15 – 25 g) were injected s.c. with 4T1-eGFP-FLuc cells (1×10^5 cells/50 µL PBS/mouse) into the fourth mammary fat pad (lower right inguinal) under isoflurane anaesthesia. Tumour growth was monitored by measuring the tumour volume, as [length × (width)^2]/2. After tumours were established (50–75 mm^3) on day 7 - 10, mice were divided into groups (8 mice/group) and subjected to CMC control or ATQ treatments. Once tumour burden reached 1000 mm^3 (7 – 14 days later), animals underwent MRI imaging before Schedule 1 sacrifice. Lungs, liver, spleen, and primary tumours were excised and either processed for FACS, or fixed and embedded for IHC analysis.

2.9.7 Enzymatic Digestion of Tumours & Target Organs

Tumours, lungs, and livers were excised, and surface blood was removed by rinsing in Hanks' Buffered Salt Solution (HBSS). The tumours and organs were minced with scissors in 2.5 mL HBSS, then cells and fragments were added to 2.5 mL filter-sterilised enzyme cocktail. All enzymes were purchased from Sigma (St Louis, MO, USA). Primary tumours were digested in collagenase type I (10 mg/ml) for 1 hr at 37 °C on a platform rocker. The lungs were digested in 10 mg/ml collagenase type IV to which 30 units elastase had been added directly before use. Lung samples were placed at 4 °C for 75 min on a platform rocker. Livers were digested in a mixture of 10 mg/mL collagenase

type I and 10 mg/mL hyaluronidase for 20 – 30 min at 37 °C on a platform rocker. Spleens were dissociated by mechanical disruption and sieving through 70-µm cell strainers from BD Biosciences (Bedford, MA, USA).

2.9.8 *Ex vivo* FACS

Cells were prepared as described above to obtain single cell suspensions. Cells were incubated for 30 min with the provided blocking agent to decrease non-specific binding of immunoglobulins. Cells were examined with a Beckman-Coulter XL/MCL Flow Cytometer (Beckman-Coulter, Hialeah, FL, USA). Thresholding on forward angle light scatter was first used with signals from low angle forward light scatter (FS) and orthogonal light scatter (SS) prior to fluorescent channel 1 (FL1) logarithmic amplification. The optical filters were set to collect approximately 525 nm (FL1, fluorescein), approximately 575 nm PE (FL2, PE), approximately 670 nm (FL3, PC5) and > 740 nm (FL4, PC7). Data files were analysed, and median fluorescence intensities were determined with FlowJo software (Tree Star, Inc., Ashland, OR, USA).

2.9.9 Cardiorespiratory-gated Thoracic 3.0 T MRI

BALB/c mice with established 4T1 primary tumours suspected of global metastatic disease were anesthetized with 2% to 3% isoflurane in a mixture of 30% oxygen and 70% nitrogen. Respiration and rectal temperature were monitored and maintained at 40 to 60 breaths/min and 37 °C, respectively.

MRI was performed under the guidance and direction of our institutions' imaging team, directed by Dr Sean Smart, using a protocol optimised for thoracic metastases imaging published elsewhere [166]. Briefly, using a 3.0 T (Varian) system, scans were performed volumetrically with automatic and immediate reacquisition of data corrupted by respiration motion and operated such that the scan automatically adapted to any instantaneous changes in respiration rate. Images were processed by the imaging core and then qualitatively analysed by a pathologist (Prof Ruth Muschel).

2.9.10 Continuous Exchange Saturation Transfer (CEST) 9.4 T MRI

Continuous Exchange Saturation Transfer (CEST) MRI experiments were performed alongside Dr Kevin Ray from Professor Nicola Sibson's group at our institution [167]. The primary readout of CEST MRI is amide proton transfer (APT) [168]. In tumour regions, the concentration of proteins able to readily exchange protons is elevated compared to surrounding tissues, and subsequently, the increased intracellular exchanges lead to increased APT levels. APT has been demonstrated to correlate with tumour grade [169] and necrosis [170], but has recently been extended to quantify pH by measuring proteins levels in tumours samples [167].

Imaging used a 9.4 T Varian Inova spectrometer (Agilent Technologies). Mice with established subcutaneous FaDu tumours were placed in a supine position and insulation was used to prevent excessive heat loss and provide a small amount of immobilisation. Animals (N = 4 – 5 per group) were euthanised with an overdose of pentobarbital and replaced in the MRI, with their temperature continually maintained at 37 °C to minimize variations in relaxation times owing to reduced thermal regulation post-mortem and segmentation was done by Professor Sibson's group.

2.10 Statistical Analysis

The significance of differences between means was measured by two-tailed t-test or one-way ANOVA with Bonferroni post-test for multiple comparisons using the GraphPad Prism program version 8.0 (GraphPad Software, USA). Measurements on time-course plots and bar charts are expressed as mean ± s.d. unless, otherwise indicated. Significance was determined according to two-tail p-values where *$p<$ 0.05; **$p<$ 0.01; ***$p<$ 0.001; ****$p<$ 0.0001 was considered statistically significant.

2.10.1 Quantification of Sensitisation

The sensitisation enhancement ratio (SER), alternatively referred to as the dose modification ratio (DMR) [171], was used to quantify the effectiveness of combination treatments (Equation 2.2):

$$SER_{10} = \frac{D_{10}}{D_{10,ATO}} \quad \text{(Eq 2.2)}$$

where SER_{10} presents the SER at 10% survival, D_{10} is the dose required to achieve 10% survival without ATQ, and $D_{10,ATQ}$ is the dose of an agent needed to achieve 10% survival when used in combination with ATQ. In general, SER values vary according to whether a sensitiser increases the required dose of an agent to achieve the same efficacy (antagonism; SER < 1), does not affect it (additivity; SER ≈ 1), or lowers it (supra-additivity, or synergism; SER > 1). As the SER factor grows larger, synergistic effects are increasingly pronounced.

CHAPTER 3

ATOVAQUONE AS A HYPOXIA MODIFYING AGENT

3.1 Introduction

Tumour hypoxia is an important impediment to effective cancer therapy and exists to some degree in most solid tumours [27]. It occurs due to inadequate oxygen delivery by abnormal vasculature coupled with demands of rapidly proliferating cancer cells. Oxygenation throughout a tumour is dynamic and can change over time making the development of anti-hypoxia therapies challenging. Clinically, some chemotherapeutic drugs have been shown to be less effective under low oxygen tension, limiting their efficacy. Hypoxia has also been recently shown to be a potent barrier to effective immunotherapy treatment [120,172]. In the case of XRT, cell death occurs primarily due to indirect ionisations forming ROS that go onto damage DNA. Oxygen is therefore a key mediator of XRT efficacy and hypoxic tumours are therefore radiation resistant. Given the long-standing recognition of hypoxia as an important barrier to anti-cancer treatment, many approaches to reverse tumour hypoxia have been tried; however, none are currently in widespread clinical use [173].

Early studies attempting to reverse hypoxia delivered oxygen directly to patients [121,122]. When combined with vasodilating agents, increased oxygen supply was theorised to translate to more oxygen available to diffuse throughout a tumour. Unfortunately, despite promising pre-clinical and early-phase data, such approaches did not translate into significant improvements in randomised clinical studies, while simultaneously raising concerns about practicality and safety [122]. Hypoxia-activated pro-drugs were developed to target hypoxic cells preferentially. Such compounds become activated and reduced to form cytotoxic species in low oxygen tension – an effect designed to spare well-oxygenated tissues to thereby yield a larger therapeutic window. Unfortunately, clinical studies did not demonstrate significant efficacy. The use of hypoxic cell radiosensitisers promoting the fixation of free radical

damage by acting as oxygen mimetics was also of interest to the field [129]. As is the case with hypoxia-activated pro-drugs, hypoxic cell radiosensitisers require adequate build-up in areas of low oxygen tension [135], which are inherently poorly perfused and therefore difficult to reach.

Attempting to increase the supply of oxygen to tumour cells has historically been as ineffective as attempting to deliver drugs to hypoxic regions directly – since oxygen is unable to reach hypoxic areas, it is unsurprising that small molecule pro-drugs or oxygen-mimetics are unable to either. These efforts may not have been in vain, however, by helping to delineate desirable characteristics of candidate hypoxia modifiers, such as: 1) good tolerability, 2) robustness stability for study *in vitro* study i.e. stable, 3) functionally independent independence from oxygen tension, 4) inactivity in well-oxygenated tissues, and 5) efficacy at active at pharmacologically achievable concentrations. A possible alternative strategy to alleviate tumour hypoxia is to reduce cellular oxygen consumption rate (OCR) in well perfused cells, or those at the peri-hypoxic interface, in order to allow unmetabolised oxygen to diffuse into hypoxic areas [72]. Reduction of OCR in 3D spheroid models causes a decrease in the volume of the central region of hypoxia by increasing the availability of oxygen [174]. Mathematical modelling indicates that a decrease of 30% or more in OCR could abolish radiobiologically relevant tumour hypoxia [175,176].

Our group previously completed a high-throughput screen (HTS) of FDA-approved drugs to identify compounds that inhibit cellular OCR and are well-tolerated. We identified that the anti-malarial drug Atovaquone (ATQ) safely reduces cancer cell oxygen consumption *in vitro* and alleviates tumour hypoxia *in vivo* [151] and synergise with XRT in xenograft models. ATQ inhibits oxidative phosphorylation (OXPHOS) through the direct inhibition of the electron transport chain (ETC), namely, Complex III subunit bc_1. Our

group is now currently undertaking clinical safety studies to evaluate the suitability of ATQ as a clinical hypoxia modifier.

This chapter presents a wide range of experimental findings that describe the broader the effects of ATQ in the context of hypoxia modification. We present data on the cytotoxicity of ATQ and its tolerability in spheroid models, probe what role HIF-1α and $pSTAT3^{Y705}$ have in mediating the reversal of spheroid hypoxia, evaluate ATQ's tolerability *in vivo*, and demonstrate preliminary evidence that ATQ induces extracellular acidification in xenograft models (in collaboration with Professor Nicola Sibson's group from our institution).

3.2 Results

3.2.1 Modulation of OCR & ECAR by Atovaquone *in vitro* is Reversible

ATQ-mediated alleviation of tumour hypoxia is dependent on ETC inhibition. As such, we theorised that it should be a reversible process.

To test this, FaDu cells were incubated with either DMSO or ATQ for 2, 4, or 8 hr and a dose-response was performed concurrently using 10, 20, or 30 μM ATQ while volumetrically corrected for DMSO content across all treatments and controls (Figure 3.1). As demonstrated previously, 2 hr incubation with 10 – 30 μM ATQ was enough to reduce FaDu cell OCR and increase ECAR. Notably, no statistical difference in ECAR was found for any recovery treatment groups relative to DMSO control, which indicates that the upregulation of ECAR induced by ATQ therapy at up to 30 μM for up to 8 hr is reversible. In terms of OCR, no statistical difference was observed between DMSO control and any ATQ recovery group indicating that FaDu OCR inhibition by ATQ is reversible.

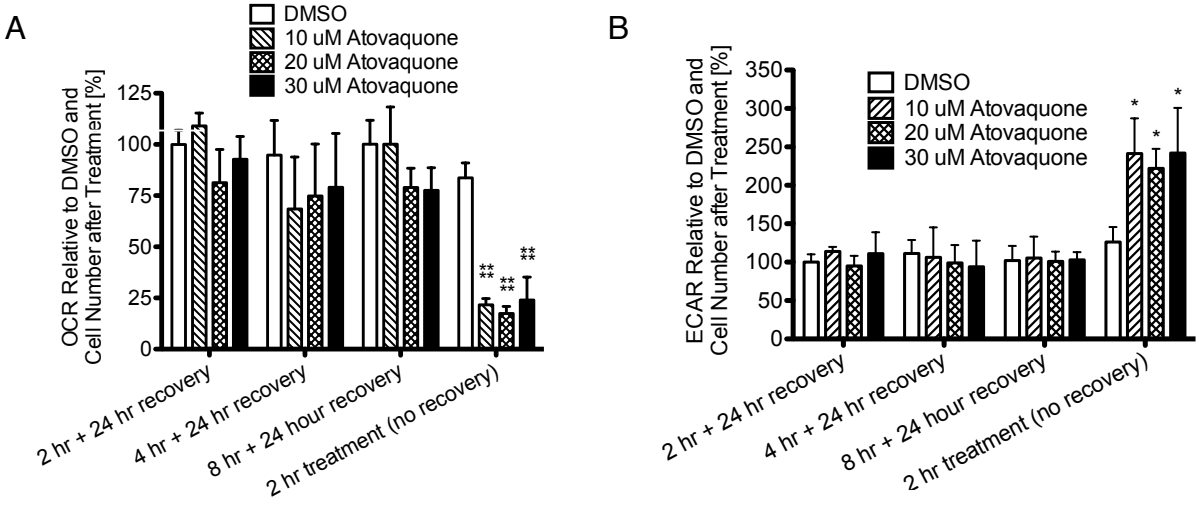


Figure 3.1 – Metabolic Effects of Atovaquone Treatment are Reversible *in vitro*. **(A)** Oxygen consumption rate (OCR) and **(B)** extra cellular (ECAR) measurements of FaDu cells were recorded after treatment with ATQ 30 μM for 2 – 8 hr and/or recovery for 24 hr by medium wash-off. Measurements were acquired using a SeaHorse XF Analyzer and completed in triplicate. Data represents mean and error bars are s.d. Data is representative of three independent repeats.

3.2.2 Cytotoxicity of Atovaquone is not Dependent on its Ability to Inhibit OXPHOS

ATQ has been shown to directly bind to subunit bc_1 of ETC Complex III [156], but whether this binding mediates cytotoxicity has not been explored. We probed this effect by acquiring 143B cells in three variations: wild-type with tyrosine kinase (TK) deficiency ($143B^{wt,TK-}$), ρ-converted *cybrids* harbouring a cytochrome b loss-of-function mutation ($143B^{CYTB}$), and the isogenic cell lines to $143B^{CYTB}$ ($143B^{iso}$). Using the SeaHorse XF Analyzer, we analysed what effect ATQ has on the above cell lines.

A time-course analysis revealed ATQ at 2, 10, and 30 μM reduced cellular OCR in $143B^{iso}$ and $143B^{wt,TK-}$ cells (Figure 3.2a-b). We then tested the efficacy of other well-known Complex III inhibitors, Myxothiazol (MYXO) and Antimycin A (ANTA), alongside ATQ in the 143B lines. After 24 hr incubation, we found that both $143B^{iso}$ and $143B^{wt,TK-}$ cells to be similarly modulated by each agent (Figure 3.2c-d). Comparatively, the OCR and ECAR of $143B^{CYTB}$ cells was unaffected by ATQ, MYXO, or ANTA treatment (Figure 3.2e). We probed further by incubating 143B variants with a range of ATQ doses for 72 hr and recording cell viability via Hoechst staining (Figure 3.2f). No difference in IC_{50} values was noted. Proliferation after ATQ treatment was then assessed using $143B^{iso}$ and $143B^{CYTB}$ cells via Hoechst staining (Figure 3.2g).

Taken together, results from these experiments indicates that ATQ suppresses proliferation and increases cell death in 143B osteosarcoma cells in a manner which is independent of its ability to inhibit OXPHOS via reduction of mitochondrial activity, inhibition of ETC Complex III, or by downregulation of thymidine synthesis.

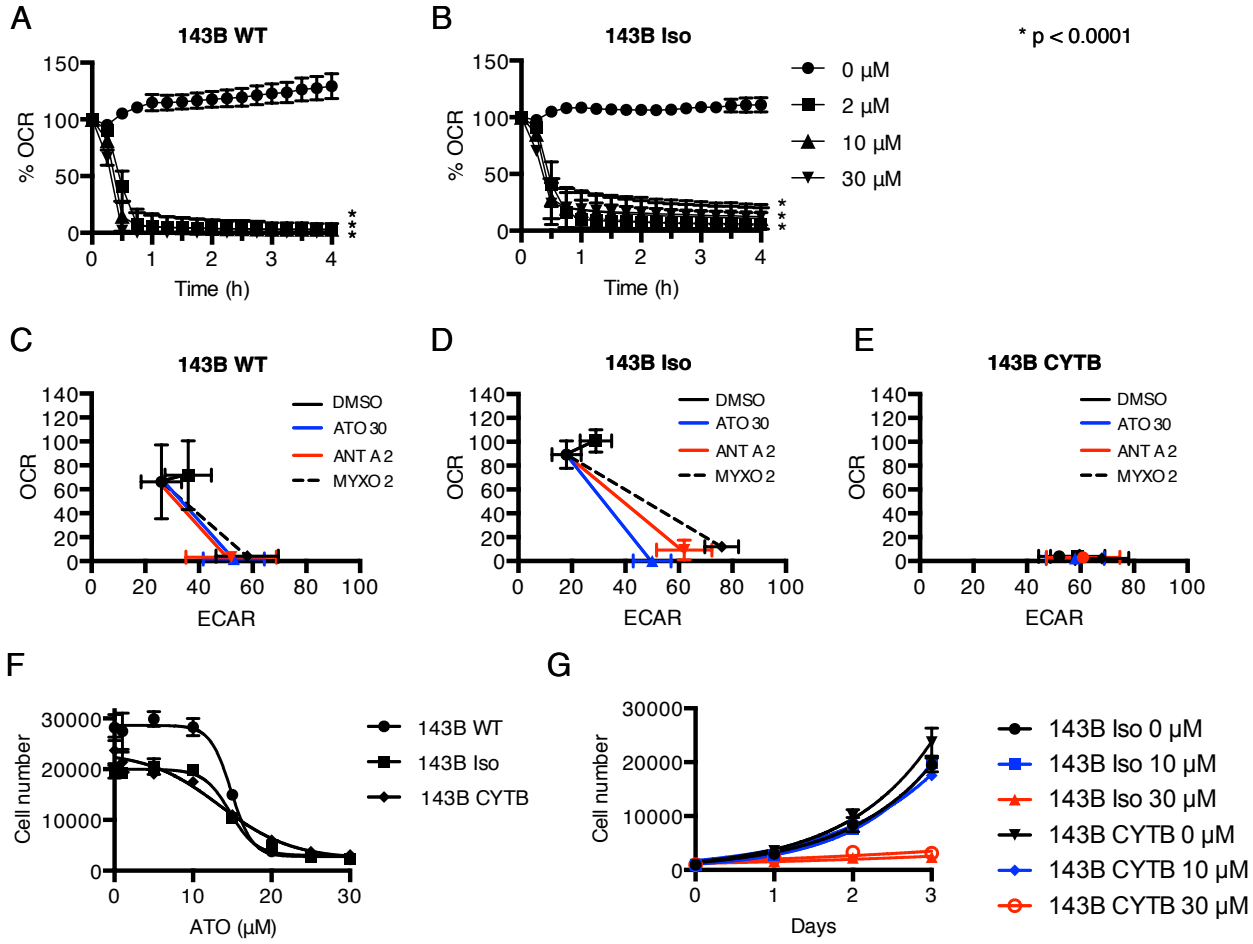


Figure 3.2 – The Cytotoxic Effects of Atovaquone are Independent of its Ability to Inhibit Oxygen Consumption **(A)** 143B wild-type thymidine kinase (TK) negative cells ($143B^{wt,TK-}$) and **(B)** 143B isogenic ($143B^{iso}$) cells were plated and allowed to attach overnight before treatment with 0 – 30 µM ATQ and recording oxygen consumption rate (OCR). **(C)** 143B-wt and **(D)** $143B^{iso}$ variants were plated and allowed to attach overnight before 24 hr incubation with ATQ 30 µM, Myxothiazol (MYXO) 2 µM, or Antimycin A 2 µM, following OCR and extracellular acidification rate (ECAR) measurements. **(E)** As in (C-D), but using 143B isogenics with loss-of-function mutations in cytochrome b ($143B^{CYTB}$).

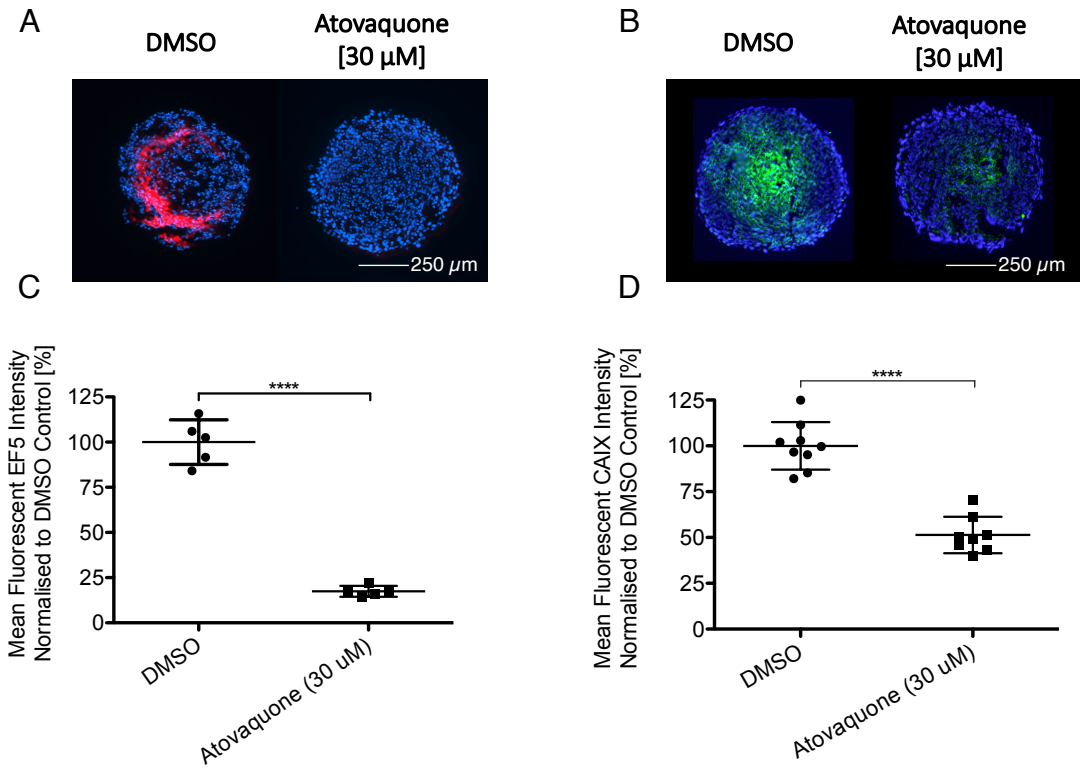


Figure 3.3 – Atovaquone Alleviates Spheroid Hypoxia According to EF5 and CAIX Immunofluorescence Staining. FaDu spheroids were treated with DMSO or Atovaquone (ATQ) either for 24 h. Hypoxia was assessed by staining central spheroid sections for **(A)** EF5 (red, Cy3) or **(B)** CAIX (green, FITC), with DAPI as a nuclear counterstain (blue). Mean fluorescence intensity relative to DMSO controls is shown for **(C)** EF5 and **(D)** CAIX. At least $N = 5$ spheroids were used per treatment condition and data is representative of three biological repeats.

3.2.3 Atovaquone Diminishes CAIX Expression and EF5 Staining in Avascular Spheroid Models

Our group previously demonstrated a reduction in EF5 staining using 30 µM ATQ in spheroids. To corroborate those findings and to rule out an interaction between ATQ and nitroreductases, which are responsible for EF5 adduct formation, we treated FaDu spheroids (500 – 600 µm in diameter) with DMSO or ATQ 30 µM for 24 hrs, fixed in 5% PFA_{aq} for 24 hr, cryoprotected in 10% $sucrose_{aq}$ for 24 hr, embedded in OCT, and then cryostatically sectioned before staining adjacent 5 µm slices with anti-EF5 (Figure 3.3a) or anti-CAIX antibodies (Figure 3.3b). By using EF5 as a hypoxia marker, we reproduced previous results indicating a significant downregulation in mean EF5 fluorescent fluorescence EF5 intensity, which indicates the reversal of hypoxia

relative to paired DMSO-control spheroids (Figure 3.3c). Parallel adjacent staining for CAIX similarly yielded a reduction in mean fluorescent fluorescence intensity; however, the signal was not abolished (Figure 3.3d). Importantly, the half-life of CAIX expression is approximately 38 hrs [177], which may therefore necessitate a longer exposure time for the signal to be entirely eliminated. Alternative staining targets, such as HIF-1, that have shorter half-lives could be used [53].

3.2.4 Atovaquone Reduces OCR & Induces Cell Death Independently of pSTAT3^{Y705}

Constitutive STAT3 expression has been shown to play a significant role in disease progression and in modulating cellular metabolism [61–63]. Cytoplasmic phosphorylation of STAT3^{Y705} induces dimerization and translocation for target gene upregulation. ATQ has recently been shown to inhibit STAT3^{Y705} phosphorylation [66]. As such, we sought to explore whether ATQ reduces OCR independently of pSTAT3^{Y705} and whether pSTAT3^{Y705} mediates the cytotoxicity of ATQ *in vitro*. To accomplish this, we obtained parental (wildtype) DLD-1 cells alongside a DLD-1 cell line having homozygous knock-in of STAT3$^{Y705F/Y705F}$ (mutants), preventing Tyr^{705} phosphorylation and therefore pSTAT3 dimerization [178,179]. STAT3^{Y705} is not generally phosphorylated *in vitro* and so IL-6 stimulation was used where indicated.

We confirmed via Western blotting that the mutant cells do not express pSTAT3^{Y705} with or without IL-6 stimulation (Figure 3.4a). We then tested the ability of ATQ to reduce OCR in a dose dependent manner without IL-6 stimulation (Figure 3.4b) and with IL-6 stimulation (Figure 3.4c). These results indicate that ATQ can reduce OCR significantly after 24 hr incubation in both cell lines, independent of pSTAT3^{Y705} expression. To probe whether a difference in sensitivity to ATQ exists between the cell lines, we treated cells with 0, 10, or 30 μM ATQ and recorded cell number over the course of 72 hr

(Figure 3.4d). No difference in cell number was recorded between the isogenics, indicating the cytotoxic effects of ATQ are independent of STAT3^{Y705} phosphorylation.

3.2.5 Atovaquone Reduces OCR & Alleviates Spheroid Hypoxia Independently of HIF-1α

HIF-1α is considered a key player in maintaining oxygen homeostasis, modulating cellular metabolism, and controlling hypoxia-induced responses, having pleiotropic effects cell-wide [41,180]. We sought to determine whether HIF-1α is involved in the mechanism by which ATQ reduces cellular OCR or whether it is involved in how ATQ alleviates spheroid hypoxia. We acquired HCT116 isogenic cell lines for HIF-1α, HCT116$^{HIF\text{-}1+/+}$ and HCT116 $^{HIF\text{-}1-/-}$, and tested the ability for ATQ to reduce OCR using the SeaHorse XF analyser (Figure 3.5a). We found that ATQ significantly reduces cellular OCR *in vitro* under normoxic conditions independently of HIF-1α status after 24 hr incubation.

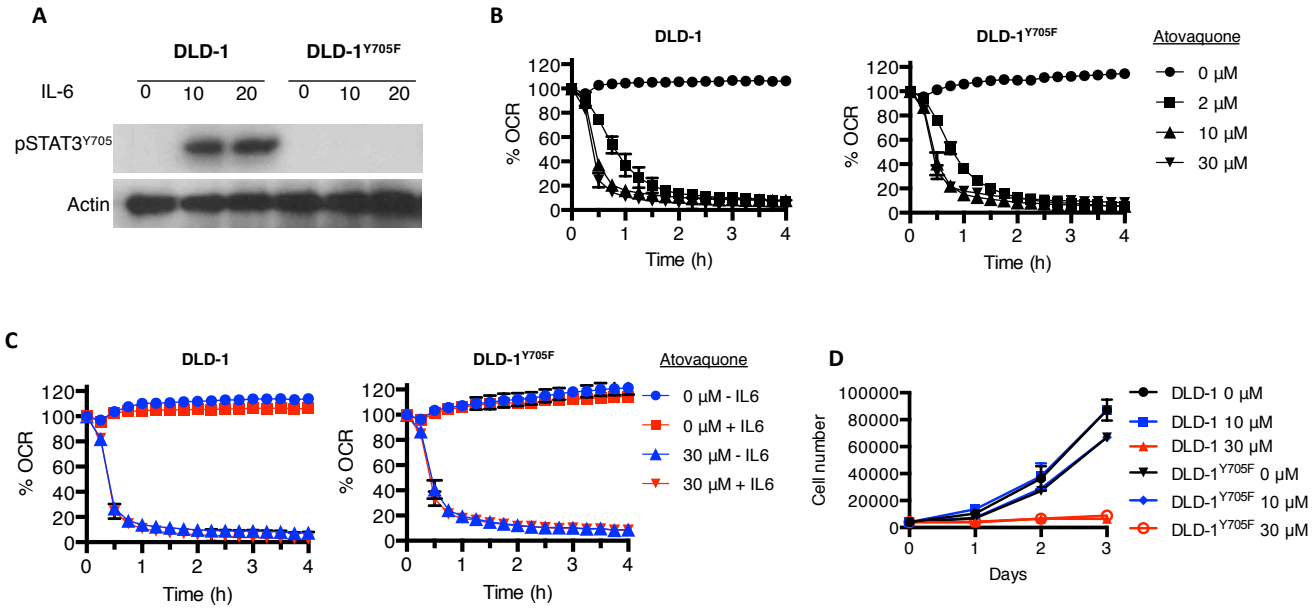


Figure 3.4 – Atovaquone Reduces Oxygen Consumption Rate (OCR) and Reduces Proliferation Independently of STAT3^{Y705}. (A) Western blot using DLD-1 isogenics for pSTAT3^{Y705} with and without IL-6 stimulation [ng/mL] for 2 hr **(B)** pSTAT3^{Y705} isogenic were plated (2x10^4), allowed to attach overnight, and then treated for 24 hr with ATQ or DMSO before XF analysis to record OCR. **(C)** as in (B) but using IL-6 to stimulate STAT3 phosphorylation. **(D)** Brightfield microscopy following proliferation of isogenic DLD-1 wild-type and mutants after DMSO or ATQ treatment, with and without IL-6. All values are presented as representative mean (of 3 repeats) ± s.d.

To further probe any effect that HIF-1α may have in mediating the ability for ATQ to reduce OCR under hypoxic, rather than normoxic, conditions i.e. alleviate spheroid hypoxia, we formed generated a 3D spheroids spheroid model using HCT116$^{HIF\text{-}1+/+}$ or HCT116 $^{HIF\text{-}1-/-}$ cell lines, and treated them with ATQ or DMSO. We then probed for regions of hypoxia by staining for EF5 adducts in cryostatically acquired sections. A dramatic reduction in EF5 staining was observed for both cell lines following ATQ treatment (Figure 3.5b). DMSO control spheroid sections showed significant levels of EF5 staining, indicative of hypoxia and confirming that the isogenic pair can respectively form hypoxic spheroids. Taken together, these findings support a HIF-independent mechanism.

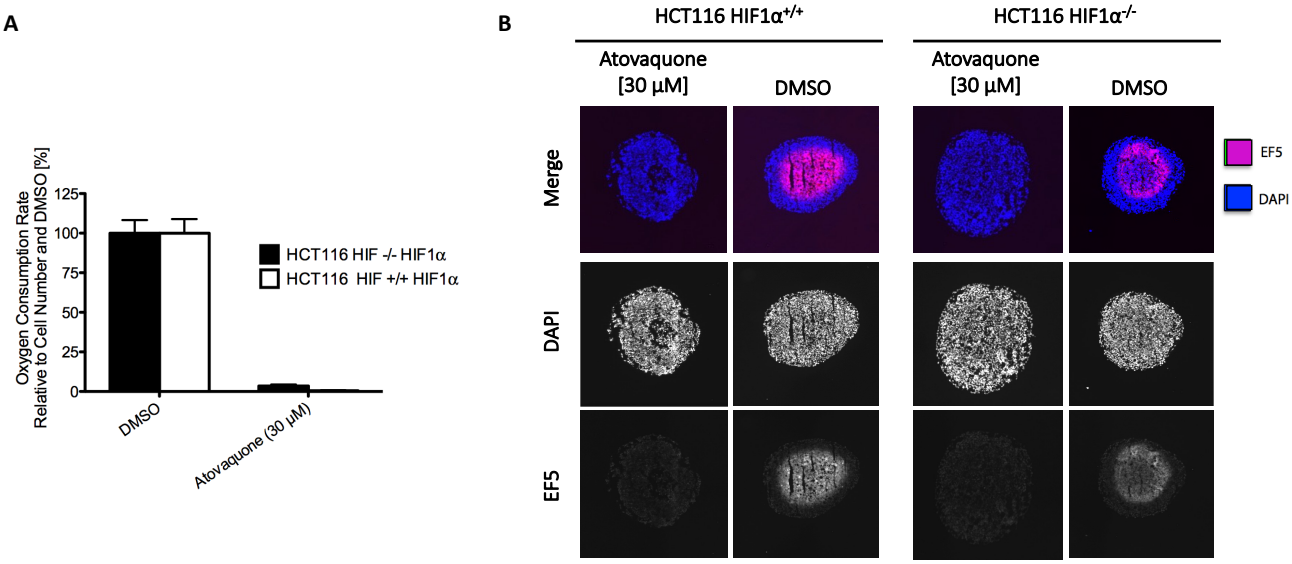


Figure 3.5 – Atovaquone Reduces Oxygen Consumption Rate (OCR) and Alleviates Spheroid Hypoxia Independently of HIF-1α. (A) HCT116 cells isogenic for HIF-1α (wildtype or -/-) were plated (2x10^4), allowed to attach overnight, and then treated for 24 hr with ATQ or DMSO before XF analysis for OCR. **(B)** Cells from each isogenic were plated (1x10^4) in U-bottom plates to generate spheroids. Once 550-650 μm in diameter, spheroids were treated with DMSO or Atovaquone (ATQ) for 24 h. Spheroids were then fixed, embedded, and sectioned. Hypoxia was assessed by staining central spheroid sections for EF5 (red, Cy3) with DAPI as a nuclear counterstain (blue). All values are presented as representative mean (of 3 repeats) ± s.d.

To further probe any effect that HIF-1α may have in mediating the ability of ATQ to reduce OCR under hypoxic conditions, we formed spheroids using HCT116$^{HIF\text{-}1+/+}$ or HCT116 $^{HIF\text{-}1-/-}$ cell lines. We then stained for EF5 adducts in cryostatically acquired sections and observed a dramatic reduction in EF5 staining for both cell lines (Figure 3.5b). Taken together, these findings support a HIF-independent mechanism.

3.2.6 Atovaquone Treatment is Well-Tolerated *in vitro* & *in vivo*

Previously, our group reported *in vitro* toxicity using ATQ at up to 30 μM for 24 hr, or less, across a variety of cell lines. In order to probe its candidacy for use in future spheroid growth delay experiments, we explored what effect long-term ATQ incubation has on spheroid models in order to probe its candidacy for use in future spheroid growth delay experiments. FaDu spheroids remained intact for the duration of observation after treatment with 30 μM ATQ and continuous incubation; however, growth stagnated (Figure 3.6a).

Our team also demonstrated previously that ATQ can be used to alleviate hypoxia in xenografts using tumour-bearing immunocompromised mice for up to 7 d at a dose of 50 mg/kg/day. No detectable changes in weight or behaviour were observed, but to expand on these findings we evaluated the tolerability of longer treatment windows to facilitate subsequent *in vivo* experiments. We tested the effect of 30 days administration of 50 mg/kg/day p.o. ATQ using BALB/c nu/nu mice (Figure 3.6b). No significant changes in bodyweight were observed and behaviour was unremarkable. We then recorded mouse bodyweight (b.w.) over time after treatment with 0, 100, or 200 mg/kg/day ATQ for 7 days (Figure 3.6c), which similarly had no significant influence. The ability to achieve adequate levels of ATQ was then confirmed by HPLC demonstrating concentrations in plasma and tumour significantly

above those shown previously to alleviate tumour hypoxia and without influence on b.w. (Figure 3.6d).

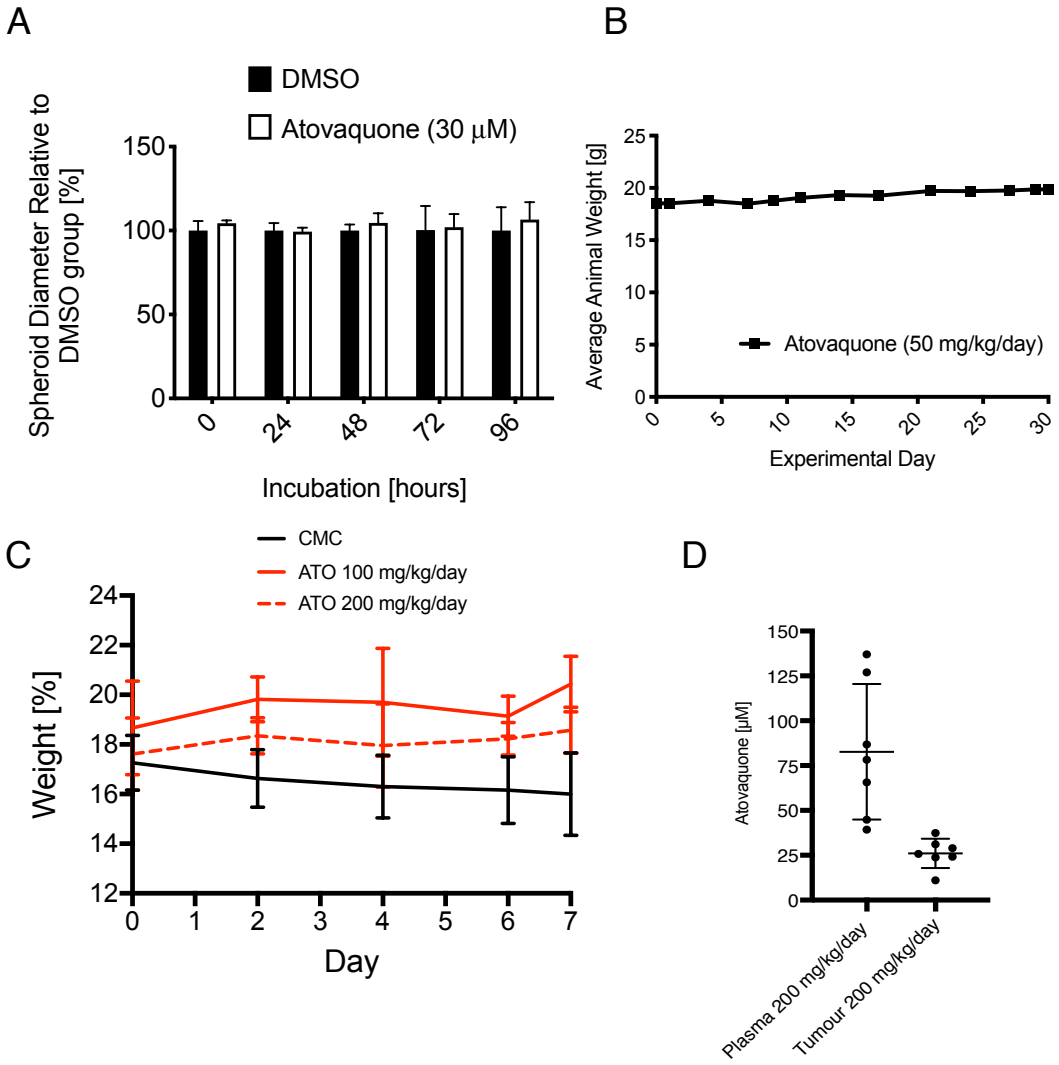


Figure 3.6 – Atovaquone Treatment is Well-Tolerated *in vitro* & *in vivo*. **(A)** FaDu spheroids were generated after plating 2 x 105 cells and incubating in ultra-low attachment plates for 72 – 96 hr. Spheroids were then treated with DMSO or 30 μM ATQ continuous and spheroid diameter was recorded daily using BrightField microscopy. **(B)** Non-tumour bearing BALB/c nu/nu mice were treated with 50 mg/kg/day ATQ gavage (p.o.) for up to 30 days and weights recorded to evaluate long-term tolerability. **(C)** As in (B) but treated for 7 days with 0, 100, or 200 mg/kg/day ATQ p.o. **(D)** HPLC analysis of plasma and tumours extracted from high-dose treated subjects in (C). At least $N = 6$ mice were included per group.

3.2.7 CEST-MRI Reveals Atovaquone Induces Extracellular Acidification of Tumours

Given the ability for ATQ to increase ECAR in vitro, we probed whether ATQ induces extracellular acidification as indicated by CEST-MRI imaging APTR* to record proton (^{1}H) exchange rates between bulk (water) with chemical species and tissues. To control for signal contributions originating from protein concentration differences, we used Coomasie staining in parallel with EF5 hypoxia quantification of cryogenically embedded tumour sections. Representative sections of tumours from mice in the DMSO control or ATQ-treated groups are shown in Figure 3.7a were stained for DAPI (cell nuclei), EF5 (hypoxia) and Coomassie (protein concentration). The alleviation of tumour hypoxia in the ATQ-treated tumour is evident as a reduction in the intensity of the fluorescent signal in the image. The relative fluorescence intensity over all animals showed the significant effect of ATQ in reducing tumour hypoxia (Figure 3.7b). Importantly, no concomitant alteration in cytoplasmic protein concentration was observed (Figure 3.7c).

The histogram of APTR* measurements from ATQ treated tumours was significantly different from the histogram of APTR* measured from control animals, with the median APTR* being lower in ATQ-treated animals (Figure 3.7e). The spatial heterogeneity of the APTR* maps in tumours is shown in Figure 3.7f for two representative animals, clearly showing a higher APTR* in control animals compared with ATQ treated. Crucially, because no significant change in protein concentration was measured between the two groups, it is likely that this difference is a result of a change in tumour pH associated with the reduction in tumour hypoxia. The size of this pH change was estimated as -0.07 pH units (Figure 3.7g), reducing tumour pH from 7.14 ± 0.01 to 7.07 ± 0.01.

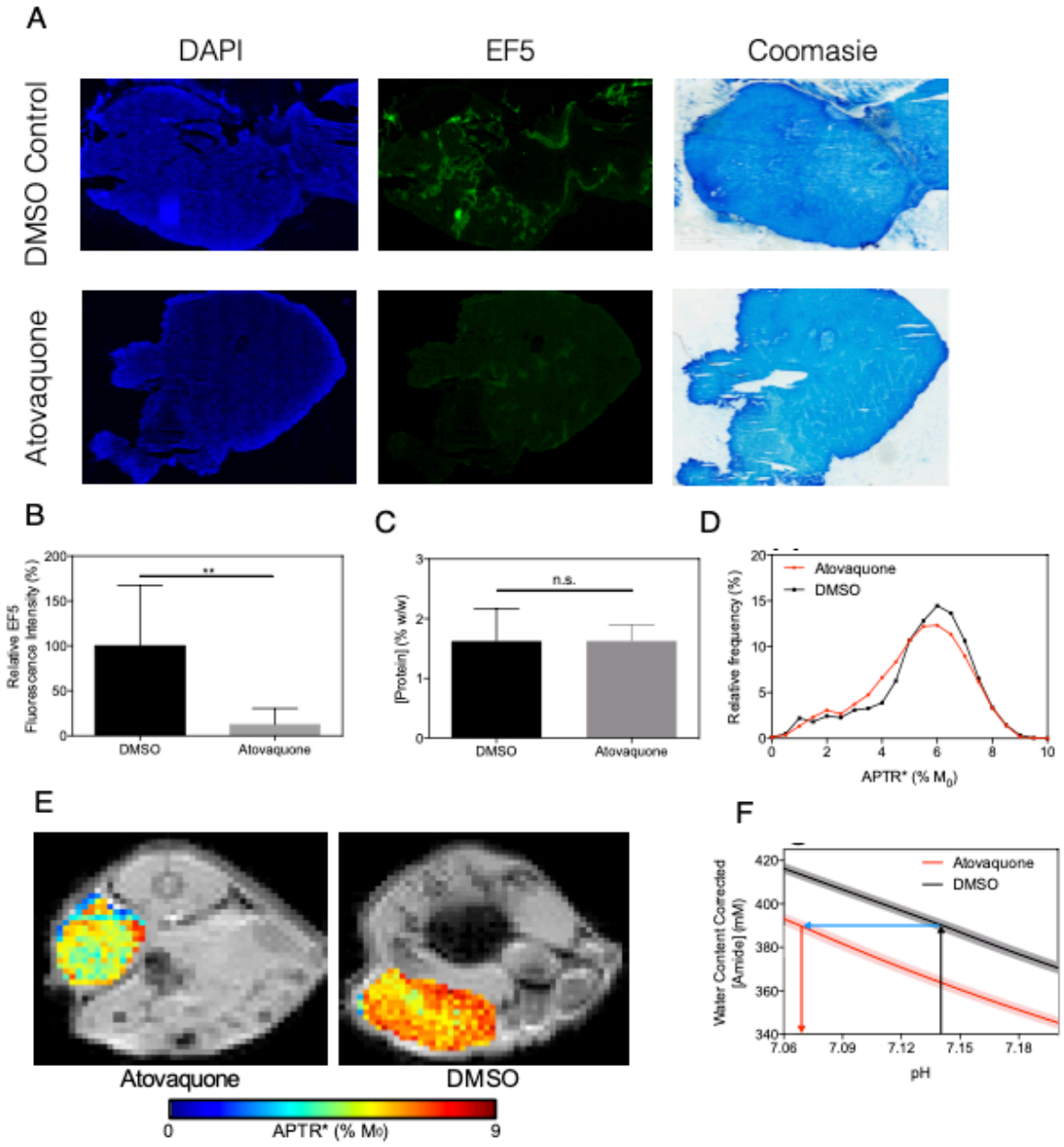


Figure 3.7 – Atovaquone Alleviates Tumour Hypoxia and Increases Extracellular Acidity According to CEST-MRI **(A)** Representative tissue sections from tumours in the DMSO or Atovaquone 50 mg/kg/day treatment groups (7 days treatment, p.o.) stained for DAPI, EF5, and Coomassie show reduction in tumour hypoxia due to Atovaquone with no concomitant alteration of protein concentration, alongside quantifications thereof **(B, C)**. **(D)** Histogram of APTR* values measured from tumours on mice treated with Atovaquone to decrease tumour hypoxia vs. DMSO – the median APTR* was significantly lower in Atovaquone-treated animals ($p < 0.001$, Mann–Whitney test). **(E)** The heterogeneity of APTR* values within single tumours is shown in representative animals from each group to demonstrate the necessity of the histogram analysis. **(F)** isoAPTR* analysis measured a tumour pH reduction of 0.07 pH units, consistent with the decrease in tumour pH expected with a reduction of tumour hypoxia. Experimental data representative of two independent repeats.

3.3 Discussion

This chapter explored the broader effects of ATQ as a hypoxia modifier. We found ATQ to be well tolerated in animal experiments at high doses or for up to one month. The effects of ATQ on cellular OCR and ECAR *in vitro* at pharmacologically relevant concentrations were found to be readily reversible, supporting the conclusion that ATQ-induced OXPHOS inhibition occurs due to direct ETC disruption. Experiments using 143B isogenic cybrids demonstrated that the cytotoxicity of ATQ is not mediated by its ability to inhibit OXPHOS, however. We confirmed that ATQ can alleviate spheroid hypoxia by staining spheroid sections with the hypoxia marker EF5 in addition to CAIX, which is upregulated by cancer cells under hypoxia. Importantly, CAIX staining demonstrates that ATQ is not unexpectedly attenuating the formation of EF5 adducts, such as by inhibiting nitroreductases required for the formation of EF5 adducts [181].

In collaboration with an imaging group at our institution (Dr Nicola Sibson), we performed *in vivo* CEST MRI to determine whether ATQ induces a decrease in tumour cell pHe, and, if so, whether such changes could be quantified non-invasively. We prepared the tumour bearing mice, designed the experiment, and processed the samples for biochemical analysis while the imaging core performed the imaging. A previous publication can be found detailing CEST MRI theory, methods, and the same results but in more detail [167]. Expectedly, alkalosis of control tumour pHi was identified and agrees with previous reports demonstrating acidic tumour pHe. Importantly, a shift in pHi of ATQ-treated tumours was recorded to values seen in normal tissues (more acidic) and might be a marker for ATQ-mediated alleviation of tumour hypoxia. In the future, techniques such as CEST MRI might be used clinically for patients receiving ATQ, or other hypoxia modifiers, in order to differentiate responders from non-responders. In the next chapter, we probe the impact of

ATQ-induced extracellular acidification on cellular migration *in vitro* and metastatic potential *in vivo*.

ATQ has been recently shown to be an excellent pSTAT3^{Y705} inhibitor [66]. We used OCR and ECAR measurements, cytotoxicity assays, and proliferation studies to demonstrate that ATQ can reduce OCR independently of STAT3^{Y705} phosphorylation. We then generated spheroids using HCT116 cells that were isogenic for HIF-1α to demonstrate that ATQ alleviates spheroid hypoxia independently of HIF-1α.

Further work is needed to validate *in vivo* that ATQ-induced OXPHOS inhibition leads to reduced oxygen consumption, which directly increases the level of unmetabolised oxygen throughout a tumour bed; however, doing so is likely to be challenging. Several techniques have been developed to measure tumour oxygenation *in situ*, chiefly, oxygen probe monitoring. However, caution is warranted when using direct measurements due to the risk of oxygenating tissues that come into contact with the equipment and kit. Imaging techniques such as DCE-MRI could be employed to evaluate oxygenation levels non-invasively but are often laborious and limit clinical relevance. To validate the mechanism *in vivo*, cell lines for tumour induction would need to form hypoxic tumours *in vivo* and be rigorously validated. Some cell lines, including 143B cybrids that have a dysfunctional ETC, are unable to form hypoxic spheroids nor tumours *in vivo*.

The dose-limiting toxicity for XRT is damage to healthy tissues [31]. As such, we are actively assessing the effect of ATQ on non-transformed murine intestinal crypt cells after abdominal XRT. We intend to probe whether ATQ therapy radiosensitises normal gut epithelial cells by evaluating apoptosis of the intestine, frequency of loss of villus tip, and villus length. Given the quiescent nature of differentiated normal cells compared to cancer cells, we

do not expect ATQ to significantly induce radiosensitisation, though this remains a key pre-clinical experiment.

Some studies have described cyclical hypoxia in tumours, characterised by periods of hypoxia followed by periods of reoxygenation, to lead to excessive ROS production and promote increased resistance to XRT [182]. Cyclical hypoxia is thought to occur because of changes in vessel perfusion and fluctuations in the flux of red blood cells within perfused vessels; however, the contribution of tumour cells undergoing or exposed to cycling hypoxia to clinical outcomes remains unclear besides increasing the risk of metastasis [183,184]. These studies highlight potential issues with reoxygenating tumours, though literature overwhelmingly suggests the benefits of eradicating hypoxia outweigh the risks [45,185].

Hypoxia has readily been reversed in a number of animal models pre-clinically, but this has not translated to hypoxic human tumours [186]. The factors which cause human tumours and not *in vivo* models to be refractory to anti-hypoxia strategies for the most part remain unknown, but is most likely to be the result of the complexity and heterogeneity of the tumour microenvironment. Furthermore, beyond transient hypoxia induced in preclinical models, there is little information on the relative significant of the types of hypoxia to clinical outcomes [187]. As such, it is unclear if only one or more could similarly lead to radiobiological hypoxia yet have rather different pathophysiology. This could important because different hypoxia sub-types might be predicted to require different diagnostic and therapeutic approaches. Even more challenging, no agreement exists for the best way to measure hypoxia.

In terms of clinical tolerability, one case report [188] describes that in its clinical formulation (Wellvone™) of a patient that consumed more than 100-fold the maximally prescribed daily dose of ATQ (for treating malaria) and

presented with only Grade 1 gastrointestinal (GI) toxicity. To understand how ATQ can be used safely in humans, our team is conducting a Phase 0 proof-of-principle clinical trial known as ATQM (Atovaquone as a Tumour hypOxia Modifier, NCT02628080). The study is investigating the effect of ATQ on tumour hypoxia in patients with resectable non-small cell lung cancer (NSCLC) in a standard window-of-opportunity design. If demonstrated to reduce tumour hypoxia in patients, larger clinical trials will be conducted to determine whether this well-tolerated and inexpensive agent improves clinical outcomes. Importantly, the ATQM study also aims to validate research techniques for investigating tumour hypoxia in the clinical setting, including: [^{18}F]-MISO positron emission tomography (PET), perfusion CT, DCE-DWI MRI, serology, immunohistochemistry, and metagene analysis. This will allow a detailed study on the efficacy of ATQ but also may allow the identification of a biomarker to allow future studies with ATQ to stratify responders from non-responders.

Overall, it is important to recognise that to realise the full potential of any anti-hypoxia strategy, robust clinically validated hypoxia biomarkers must be developed to identify patients who may benefit from such treatment. Otherwise, the translation of safe and effective hypoxia modifiers may be limited.

CHAPTER 4

EFFECT OF ATOVAQUONE ON MIGRATION & METASTATIC POTENTIAL

4.1 Introduction

Cancer cells have a range of metabolic circuitry to respond to signals from the microenvironment. Their metabolism is modulated in response to nutrient depletion, for example, shifting between catabolic and anabolic states, and then relayed to adjacent cells and cascaded onwards [111]. The unifying, sum-total effect of all such cues underpins cancer cell behaviour and can culminate in driving invasion and disease progression.

The ECM is a principal component of many healthy tissues, providing a three-dimensional network of macromolecules, such as collagen and glycoproteins, for structural support and the facilitation of biochemical signalling [189]. Reorganisation of the ECM is central to normal tissue expansion, regeneration, and wound healing; however, ECM remodelling is also important in tumourigenesis and its progression [189]. It is a requisite step for tumour growth, promoting cancer cell intravasation into the blood stream, and eventually colonisation of distant organs. Metabolically, several key players involved in ECM remodelling rely upon increased glycolytic metabolism for rapid proliferation. Though remodelling and cellular metabolism are coincident in many biological contexts, oncological and others, the mechanistic links between these processes in each step of the metastatic cascade are not entirely well elucidated.

Tumour cells are known to not generally couple glycolysis to OXPHOS, even under normal conditions of oxygen and glucose availability (Figure 4.1) [78]. Instead, they convert pyruvate to lactate through aerobic glycolysis, to yield ATP more rapidly. This is known as the *Warburg effect* and, although inefficient, allows for periods of increased biosynthetic demand. The Warburg effect has been implicated in driving invasion through extracellular acidification and ECM degradation.

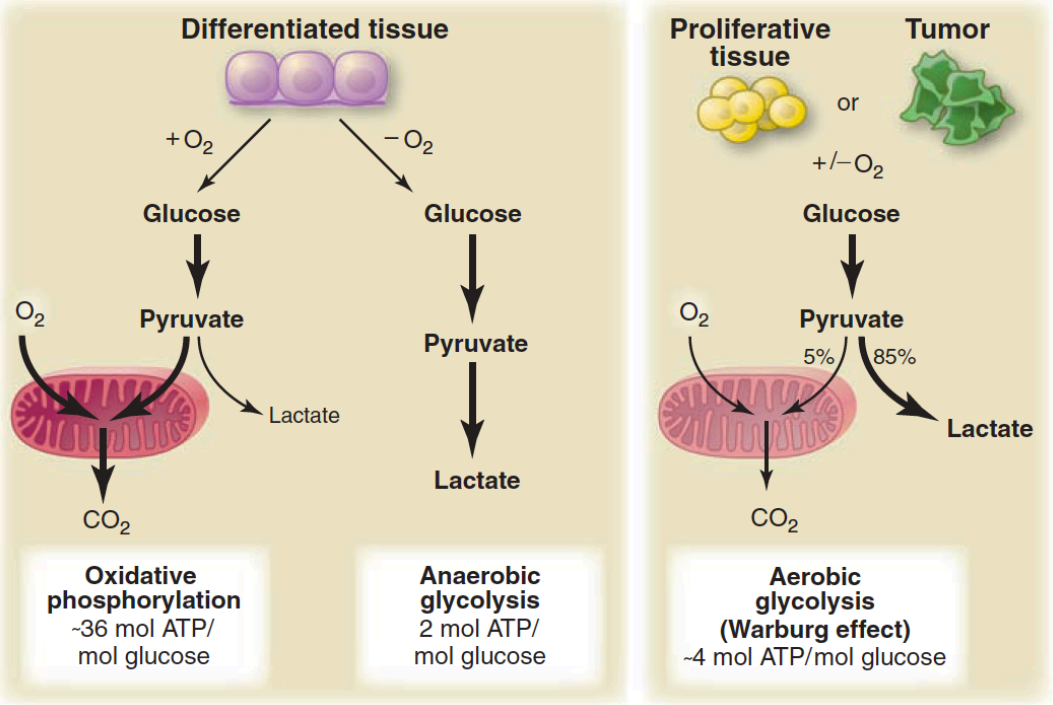


Figure 4.1 – Major metabolic pathways comparing differentiated cells to tumour cells. In normal tissues, cells can use OXPHOS which generates approx. 36 ATP or anaerobic glycolysis which yields 2 ATP. For the same 1 glucose molecule, OXPHOS produces 18 times more ATP. Normal tissues only use this less efficient pathway in the absence of oxygen. Though the Warburg Effect dictates cancer cells prefer fermentation as a main source of energy rather than the more efficient mitochondrial pathway of OXPHOS, it is now widely recognised that cancer cells often display metabolic plasticity depending on environmental cues and accessible nutrients. Figure adapted from Vander Heiden *et al.* [190]

At the time of Warburg's work, metastasis was the major cause of cancer-associated deaths globally and this remains true today. His work therefore spawned much interest and led to a readily interpretable mechanistic model linking metabolism to metastasis by implicating ECM degradation as the pivotal junction. Identifying the metabolic underpinnings of the regulatory mechanisms controlling whether tumour cells become "directed walkers" has given much insight to-date; however, we now know that metabolism of cancer cells is rather more complex.

Cancer cells do have functional mitochondria but use glycolytic or oxidative metabolic programmes to obtain energy when confronted with different scenarios [191]. It has been suggested that the functional

heterogeneity of cancer cells might require them to use different types of metabolism depending on their environment [104,192]. In the case of intravasated cells, for example, the high concentration of oxygen in the blood stream might induce a phenotypical switch upregulating OXPHOS that is supported by increased levels of oxygen albeit in the form of ROS [193]. Targeting cancer cell metabolism has been of interest for tumour types that predominantly rely on OXPHOS to cope with their energetic demands, as compared to differentiated tumour cells, but cancer cells can revert to glycolysis under certain conditions [194]. TME cues that affect metabolism such as hypoxia, together, provide opportunities and driving forces for cancer cells to migrate, invade, and colonise distant organs.

Our team demonstrated that ATQ reliably inhibits cellular OCR in a variety of cell lines; however, we also showed that ATQ upregulates glycolysis as indicated by ECAR [151]. As such, we theorised that the alleviation of tumour hypoxia would reduce metastatic potential; however, we also considered the possibility that ATQ might instead increase metastatic potential given the link between metabolism and metastatic spread. This chapter explores what effect ATQ has on cancer cell migration, before investigating how ATQ treatment modulates metastatic potential. The xCELLigence assay is used to probe whether ATQ modulates chemotaxis-driven migration *in vitro*, although does not replicate the complex signalling cascades involved in spontaneous metastatic spread, such as cues from the TME. Hence, a 4T1 spontaneously metastasising orthotopic model of murine breast cancer was used to investigate ATQ's influence *in vivo* as a model that closely mimics the progression and spread of human breast cancer [195]. These experiments tested what effect ATQ has on established tumours, but we also tested whether pre-loading animals with ATQ prior to inoculation significantly modulates metastatic potential with the intention to study the metastatic potential of tumours that had never been hypoxic.

4.2 Results

4.2.1 Atovaquone Does Not Increase Chemotaxis-driven Cancer Cell Migration

ATQ therapy inhibits OCR and cells correspondingly upregulate glycolysis within 1 – 2 hr of exposure, likely to homeostatically maintain intracellular ATP pools. Among other effects, increased glycolysis has been associated with increased cellular migration which we assessed over 18 hr using an automated xCELLigence device (Figure 4.2a-b).

MDA-MB-231 or H1299 cells were seeded in serum-free medium in the upper chamber and allowed to migrate through a semipermeable membrane toward the lower chamber containing medium with serum at 10% FBA serving as a chemoattractant (Figure 4.2c-d). Neither cell line demonstrated an increase in cell index, the dimensionless impedance measurement proportional to migration, or motility. Intriguingly, a non-statistically significant reduction in cell index was observed in the case of both cell lines and appeared to increase throughout the course of the assay.

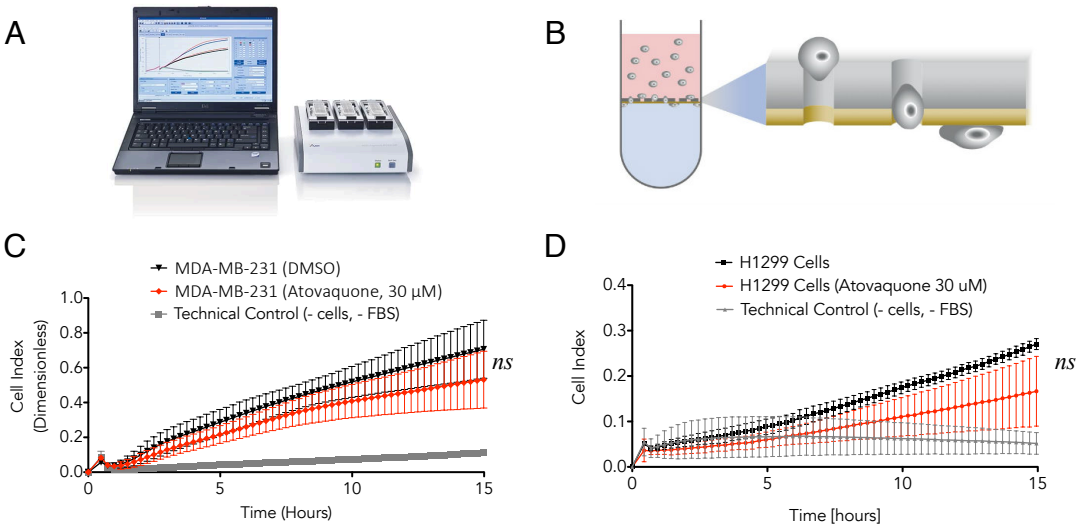


Figure 4.2 – Atovaquone Does Not Increase Chemotaxis-Driven Cell Migration. **(A) The** xCELLigence migration observation system (Roche) records impedance measurements as cells migrate across **(B)** a gold electrode towards a chemoattractant (in this case, foetal bovine serum [FBS]). Cell motility was examined in **(C)** MDA-MB-231 and **(C)** H1299 cells over 15 hr using the according to the manufacturer's protocol. Cells were maintained in serum-free medium for 24 hr prior to the assay. Between-group comparisons were performed using the independent *t*-test with *ns* = not significant (DMSO vs ATQ). Data representative of three independent repeats.

4.2.2 Atovaquone Abolishes OCR in 4T1 Cells and is Suitable for use in 4T1 Orthotopic Metastasis Models

We sought to explore whether ATQ therapy has the potential to modulate cellular invasion and therefore metastatic potential *in vivo*. We chose to use an orthotopic 4T1 model to study such an effect because it induces spontaneous metastasis that closely mimic those of human triple-negative breast cancer (TNBC) and allows hypoxic primary tumours to form before ATQ treatment. We first characterised whether the 4T1 cell line is susceptible to OCR inhibition by ATQ therapy using the SeaHorse XF Analyzer (Figure 4.3a-b). Reflecting previous results using human-derived cell lines, ATQ therapy significantly downregulated cellular OCR within 1 – 2 hr and was sensitive to ATQ therapy at 10 – 30 µM.

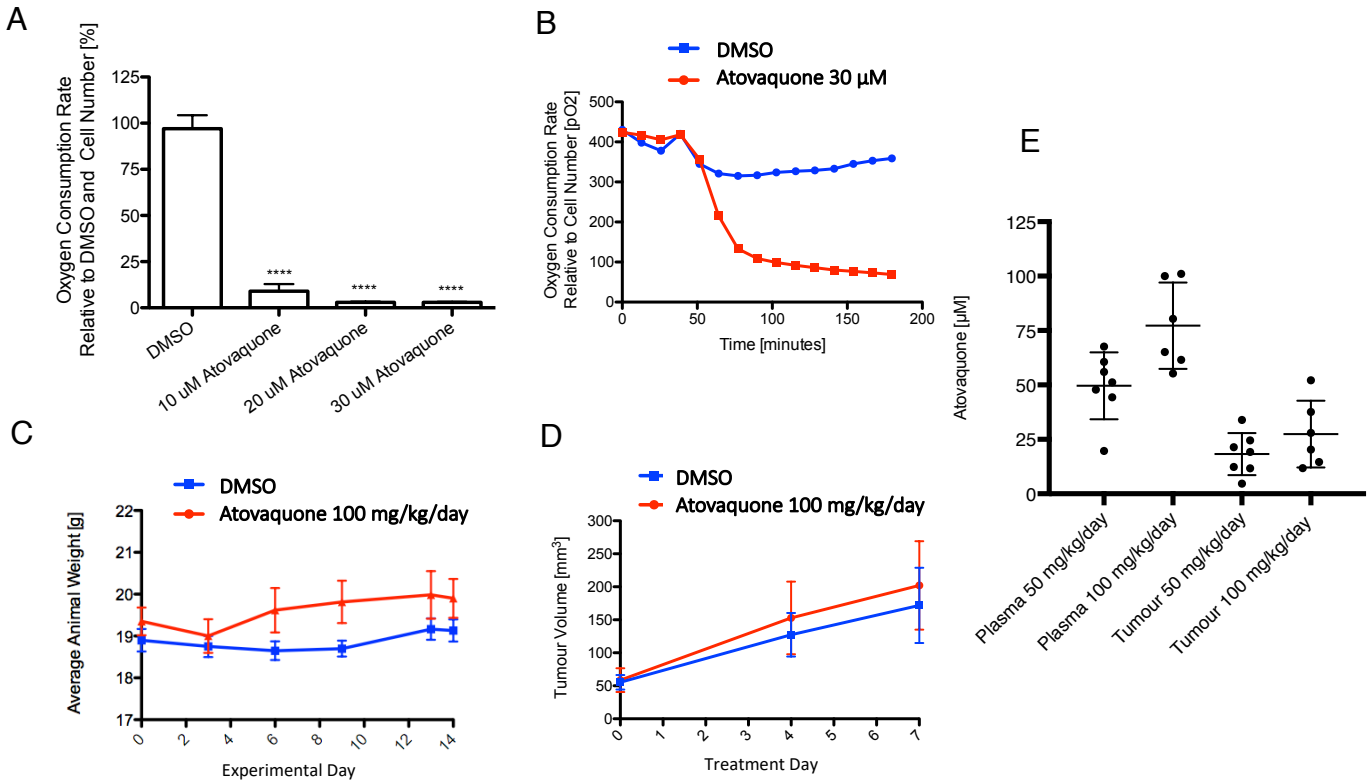


Figure 4.3 – The Orthotopic 4T1 Spontaneous Metastasis Model is Conducive to *in vivo* Study Using Atovaquone **(A)** Oxygen consumption rate (OCR) of murine 4T1 cells after exposure to 0 – 30 µM Atovaquone (ATQ) for 24 hr. All values normalised to DMSO & corrected for cell number via Hoechst staining. **(B)** Time course of OCR measurements of 4T1 cells exposed to ATQ 30 µM or DMSO. To validate the model *in vivo*, BALB/c mice were inoculated with 1 x 10^5 4T1 cells i.m.m. and treated via oral gavage (p.o.) ATQ 100 mg/kg/day or CMC control for 7 days once tumours reached 50 mm^3. **(C)** Subject weights were recorded weights in addition to **(D)** tumour volumes. **(E)** A second *in vivo* experiment as in was performed but using two dose levels of ATQ for 7 days and processing plasma and tumour samples via HPLC to quantify ATQ levels. SeaHorse data representative of 3 biological repeats and *in vivo* data representative of two independent repeats.

4.2.3 Immunohistochemistry & Cardiorespiratory-gated 3T Magnetic Resonance Confirms Distant 4T1 Metastasis

We used a combination of imaging and IHC to validate whether the spontaneously metastasising 4T1 model produces distant (liver, lung) metastasis and whether it is suitable to study the effects of ATQ on metastatic potential.

BALB/c mice were injected with 1 x 10^5 4T1 cells which were transduced with eGFP and FLuc (4T1-eGFP-FLuc) s.c. into the lower right inguinal mammary fat pad (i.m.m.) of $N = 10$ subjects each via 50 µL insulin syringes, to maximise precision. Once tumours reached 100 mm^3, subjects were randomly allocated to either ATQ (100 mg/kg/day p.o.) or CMC Control (200 µL/day p.o.) groups. In this instance, the higher dose of ATQ was chosen due to successful tolerability experiments but also to further increase steady-state levels to those seen clinically [160]. At the time of randomisation, comparison of tumour burden between groups revealed no significant differences in weight (Figure 4.3d) or primary tumour initiation (Figure 4.3e). After 7 days treatment, subjects underwent thoracic imaging to validate the 4T1 model (Figure 4.4).

Magnetic resonance image acquisition of the lungs and thoracic cavity of each subject was gated to breathing rate and heart rate (cardiorespiratory gating) to minimise perturbations and maximise resolution. Subjects were anesthetised prior to imaging and their temperatures were monitored throughout acquisition. Imaging revealed spontaneous nodules in various compartments of the lungs (Figure 4.4a-d) and suspected splenomegaly (Figure 4.4e), all of which are consistent with metastatic spread. Once imaging was complete, subjects were sacrificed via Schedule 1, lungs inflated, and fixed via PFA for IHC staining analysis.

Figure 4.4 –The 4T1 Spontaneous Metastasis Model Induces Distant Metastasis BALB/c mice were inoculated i.m.m. with 1 x 10^5 cells and then imaged 14 days later using 3 T cardiorespiratory-gated magnetic resonance imaging (MRI). **(A)** Control animal, **(B-D)** subjects with suspect lung nodules, or **(E)** splenomegaly. Samples were confirmed to have lung metastasis using **(F)** H&E staining after Schedule 1 death. Experiment consisted of $N = 6$ animals per treatment condition.

Lungs were fixed and embedded in paraffin for H&E staining to corroborate magnetic resonance observations of distant metastatic spread to the lungs, an expected progression of the 4T1 model. BrightField microscopy of lung sections revealed the presence of suspected metastatic nodules in both ATQ and control groups (Figure 4.4f), which were confirmed by consultation with a pathologist (Prof Ruth Muschel, Oxford) having expertise in preclinical metastatic models.

4.2.4 *Ex Vivo* Flow Cytometry Reveals Atovaquone Therapy Does Not Increase Lung Metastasis

Having confirmed the suitability of the 4T1 model for studying the modulation of metastatic potential by ATQ therapy, we repeated the experiment using *N* = 24 subjects (Figure 4.5a-c). Tumour induction was performed as before and ATQ or CMC control therapy was given similarly for 7 days prior to Schedule 1 death; however, in this case, tumours, spleens, livers, and/or lungs of each subject were extracted immediately post-mortem and processed *ex vivo* for flow cytometry quantification of enhanced GFP-positive cells. This allowed us to control for differences in lung mass between subjects and was accomplished by digesting, filtering, and sifting samples until a single-cell suspension remained for evaluation.

Gating on FL3, primary tumour samples and healthy lung tissues were used to benchmark upper and lower limits of GFP-positive cell count. We found between 30 – 50% of tumours were GFP-positive but admittedly sampled only a single tumour for each treatment group. No increase in GFP cell number was found comparing the lungs of CMC control vs. ATQ treatment groups, indicating that ATQ does not significantly modulate metastatic potential in this model.

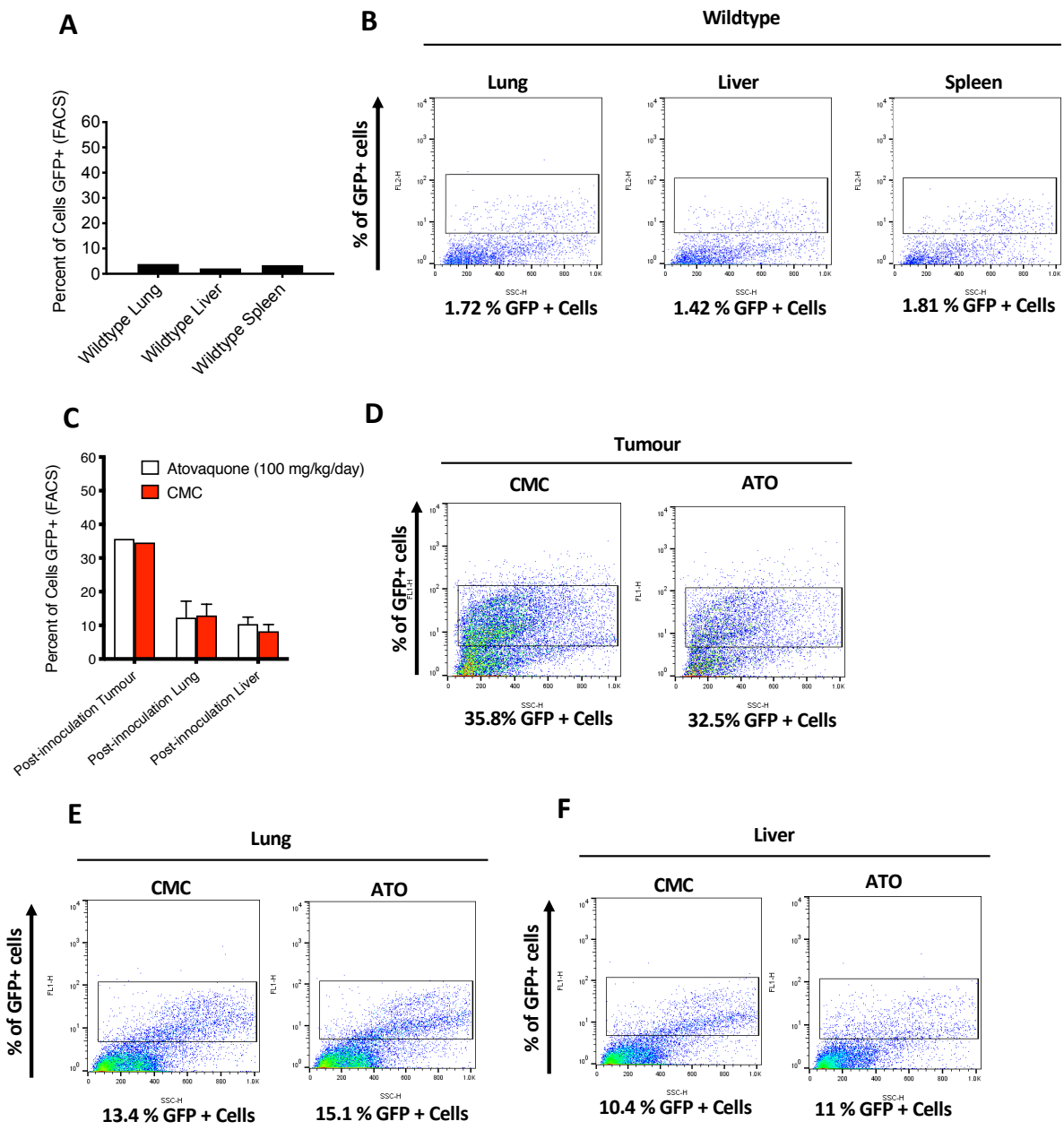


Figure 4.5 – Quantification of primary tumour and distant metastatic cells from mice with established tumours treated with Atovaquone. Cells were gated from lung, tumour, or liver of recipient mice inoculated i.m.m. with 1 x 10^5 4T1-eGFP-FLuc cells. Treatment (CMC or ATQ 100 mg/kg/day) began once primary i.m.m. tumours reached 50 mm^3. After 14 days, mice were culled via Schedule 1 and samples processed then analysed by FACS. **(A)** The average ± standard deviation of $N = 6$ samples from non-tumour bearing wildtype BALB/c mice for reference with representative gating shown in **(B)**. **(C)** summary values for tumour and target organ GFP values with **(D-F)** associated gating.

4.2.5 Pre-loading with Atovaquone *in vivo* Prior to Tumour Induction Does Not Increase Lung Metastasis

We performed another *in vivo* experiment using the 4T1 model to explore what effect pre-loading subjects with ATQ has on metastatic potential (Figure 4.6). BALB/c mice were treated for 7 d prior to tumour induction, randomised, and then ATQ or control treatments were continued for another 7 days. We identified no change in GFP-positive cell number for either group.

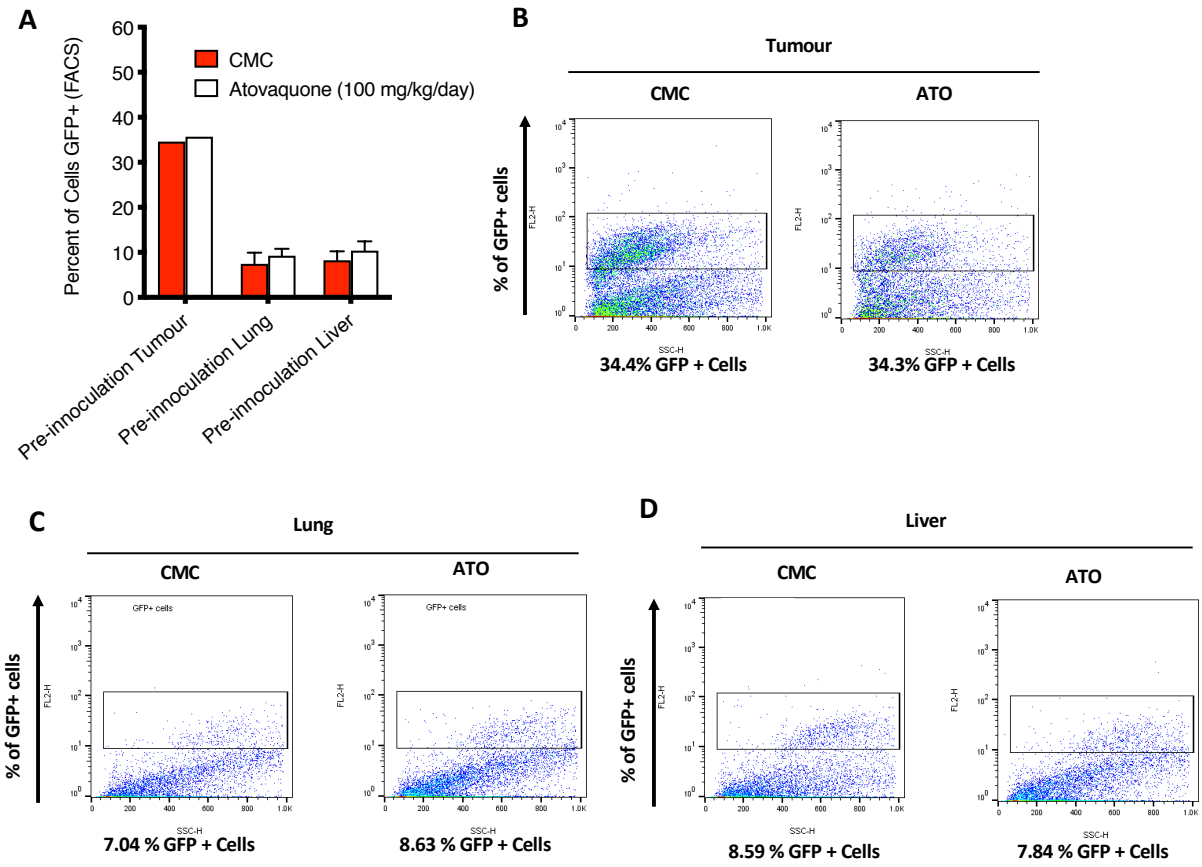


Figure 4.6 – Quantification of Primary Tumour and Distant Metastatic Cells from Mice Primed with Atovaquone Prior to Inoculation Cells were gated from lung, tumour, or liver of recipient mice inoculated i.m.m. with 1 x 10^5 4T1-eGFP-FLuc cells. Treatment began 7 days prior to primary tumour induction and continued for 14 d. Mice were culled via Schedule 1 and samples processed then analysed by FACS. **(A)** The average ± standard deviation of $N = 6$ samples with **(B-D)** associated gating.

4.2 Discussion

Metastatic spread is responsible for most cancer-related deaths [196]. The reversal of tumour hypoxia has been shown to reduce metastatic potential in several animal models and, in the clinic, tumours evaluated using meta-gene signatures found to have increased hypoxic fractions have similarly been shown to be more aggressive [57]. Though ATQ has been shown to alleviate tumour hypoxia, our team has demonstrated that ATQ reliably upregulates glycolysis, as evidenced by increased ECAR [151]. Increased glycolysis is considered a hallmark of ECM degradation [32,189], which itself is a key step of the metastatic cascade. We therefore sought to determine whether ATQ significantly modulates cellular migration *in vitro*, or metastatic potential *in vivo*, as part of evaluating its translational viability.

We firstly presented a series of *in vitro* experiments using xCELLigence technology. xCELLigence assays are based on chemotaxis-driven migration measurements across ultra-sensitive electrodes measuring impedance. We demonstrated that ATQ does not significantly increase migration using this method and did so using a variety of cell lines. As is the case with many *in vitro* experiments, xCELLigence assays are only able to replicate certain aspects of cellular migration that occurs *in vivo*. Importantly, the assays do not consider the heterogeneity, variability, and diversity of the TME. To generate more clinically relevant data, we then proceeded to test the ability of ATQ to modulate spontaneous metastatic potential *in vivo.*

There exist many animal models in literature to test metastatic potential of tumours in mice [197]. One of the most common uses tail vain injection of cells into the blood stream and then quantifying distant tumour burden via imaging or post-mortem. In our case, we wanted to replicate what effect reoxygenation might have on hypoxic tumours, thereby requiring untreated tumour-bearing mice at the time of ATQ delivery. In addition, a tail-vein

injection-based model for evaluating metastatic potential would not be suitable. We therefore opted to use a BALB/c mammary gland-derived 4T1 orthotopic model for this purpose as it readily spontaneously metastasises. Tumour growth and metastatic spread of 4T1 cells very closely mimic human breast cancer.

After characterising 4T1 cells by demonstrating they are not resistant to ATQ therapy, we evaluated whether BALB/c mice could tolerate ATQ therapy without changes in weight or tumour volume. With assistance from the NVS and NACWO at our institution, we firstly confirmed that s.c. injected 4T1 cells into the lower right inguinal mammary fat pad spontaneously metastasise to the lungs in our hands. This was accomplished using immunohistochemistry H&E staining and then independent, expert pathologist review. We then repeated the experiment using cardiorespiratory-gated 3 T MRI to visualise lung metastases with concurrent *ex vivo* flow cytometry of lungs, liver, spleen, and tumours, but did not record any increase in the 4T1 cells in treated vs. untreated groups.

We also tested whether pre-loading mice with ATQ might modulate metastatic potential more significantly than treating established, hypoxic tumours. On the one hand, we theorised that tumours having never been hypoxic may have reduce metastatic potential. The cytotoxicity of ATQ and its high concentration in plasma could also theoretically reduce metastatic potential *in vivo*. On the other, upregulation of ECAR could become more pronounced and therefore lead to increased extracellular acidity. We then performed FACS but found no significant differences in GFP+ cells in the lungs of any treatment group, albeit control, ATQ, pre- or post-inoculation. This may indicate that ATQ does not modulate cellular migration, possibly due to the trade-off between OXPHOS inhibition and glycolytic upregulation; however, the precise mechanism remains unclear and may involve other players that are modulated by ATQ.

Though there exists a link between glycolytic potential, extracellular acidity, ECM degradation, and intravasation, we found no evidence to indicate that ATQ increases metastatic potential. Counter-intuitively, we found that ATQ induces a slight downregulation of cellular migration via xCELLigence chemoattraction experiments. To confound matters further, OCR is considered an indicator of OXPHOS activity, which itself has been linked to tumourgenicity and metastatic potential [198]. As such, it is possible that the reduction in OCR induced by ATQ may positively outweigh the negative impact on ECM degradation that upregulating ECAR is thought to induce. Further experiments are needed to fully explore this balance and may include testing of other chemically variant OXPHOS inhibitors to rule-out off-target effects.

Some have suggested that metabolic profiles of invasive cells may depend on which target organ they colonise [199]. CTCs from a murine breast cancer model showed increased levels of peroxisome proliferator-activated receptor gamma coactivator 1 alpha (PGC-1α) relative to primary tumours having enhanced OXPHOS [200]. Conversely, PGC-1α has been shown to repress metastasis in a murine model of prostate cancer [201]. Another study using models of breast cancer demonstrated that some cells reaching target organs can readily use OXPHOS and glycolysis but those found in the liver used exclusively glycolysis [202]. Furthermore, the same study reported that metastatic cells found in the lungs relied on glutamine uptake to meet their bioenergetic demands.

One variable that contributes to metastatic progression is local nutrient availability and composition. In the case of lungs, for instance, higher levels of pyruvate may promote TCA-mediated ATP generation [203]. It is possible that colonisation of different tissues may however depend on other minor metabolic pathways compared to glycolysis or the TCA. For instance, murine

breast cancer cells have been demonstrated to rely heavily on proline when metastasising to the lungs *in vivo* [204] though brain metastasis observed using the same model were found to have upregulated gluconeogenesis and glutaminolysis.

CHAPTER 5

ATOVAQUONE POTENTIATES THE EFFECT OF PLATINUM AGENTS

5.1 Introduction

Delivery of chemotherapies to hypoxic regions, their cellular uptake, and therefore clinical efficacy, can be greatly affected by hypoxia [33]. Some chemotherapeutic drugs require oxygen to generate free radicals which significantly contribute to their cytotoxicity [58]. Hypoxia can similarly induce cellular adaptations that compromise the effectiveness of some chemotherapies [205]. Increased extracellular acidity due to HIF-mediated upregulation of glycolysis might reduce the efficacy of compounds having activity at higher pKa values, such as vinblastine and paclitaxel, for instance [206]. Moreover, in response to nutrient deprivation, the rate of proliferation of cancer cells decreases; and yet, many chemotherapeutic drugs are more effective against proliferating cells [120]. Hypoxia can also induce post-translational and transcriptional changes that promote cell survival or angiogenesis, modulate metabolism, expression of transporters, and increase growth factor expression [207].

Our group previously demonstrated the efficacy of ATQ in reversing tumour hypoxia *in vivo*; however, what role, if any, ATQ might have in modulating the effectiveness of chemotherapies was unknown. To this end, we explored whether ATQ-mediated reversal of hypoxia could increase the effectiveness of several commonly used chemotherapies, motivated by the potential future clinical use of ATQ with concurrent chemotherapies. In the first instance, we probed ATQ's ability to chemosensitise *in vitro* in a manner relevant to hypoxia modification – we developed a three-dimensional *spheroid growth delay* assay in which spheroid hypoxia is alleviated using ATQ before treating spheroids concomitantly with a chemotherapy. By following the growth of spheroids for up to a month, we found ATQ to potentiate the spheroid growth-limiting effects of carboplatin, a second-generation platinum-class chemotherapy derivative of cisplatin.

Platinum agents are used to treat a multitude of cancers [9]. Classically, they have been viewed as DNA damaging agents since early studies noted they form intra-strand DNA adducts. More recent studies, however, have expanded platinum agent interactions to include binding to a variety of cellular components [11], such as: cytosolic proteins, mitochondrial proteins, and mitochondrial DNA. Importantly, not all platinum agents are created equal – mechanistically, cisplatin and carboplatin demonstrate distinct mechanisms of action, as well as resistance, compared to the third-generation platinum derivative, oxaliplatin [208]. We therefore limited the work presented in this chapter to cisplatin and carboplatin.

Despite their initial effectiveness, resistance to single-agent cisplatin or carboplatin eventually occurs and represents a significant clinical challenge. To limit resistance, they are frequently commonly used in combination with other non-platinum drugs [9]. Mechanisms of platinum resistance are variable [11,209], but include changes in cellular uptake and efflux, increased biotransformation, detoxification in the liver, increased DNA repair, and anti-apoptotic mechanisms. Extrinsic limitations in drug delivery owing to the TME also play a key role in limiting the efficacy of platinum agents. Therefore, effective strategies to improve platinum-therapy efficacy would have direct and expansive clinical relevance.

This chapter firstly present the results of a spheroid screen and then explores the effectiveness and tolerability of ATQ-platinum combination therapy *in vitro* and *in vivo*. We probe whether ATQ-induced re-oxygenation mediates the sensitising effects and propose a mechanism of action. We conclude by demonstrating that ATQ and carboplatin combine to increase tumour growth delay *in* vivo, without aberrant toxicity.

5.2 Results

5.2.1 A Screen for Chemotherapies Potentiated by Atovaquone-mediated Reversal of Hypoxia

Given the link between hypoxia and chemoresistance, we explored whether ATQ-mediated reversal of spheroid hypoxia could potentiate the effectiveness of chemotherapies. To accomplish this, we developed a *spheroid growth delay* assay that reflects the clinical context in which ATQ might be used and as an antecedent to *in vivo* tumour growth delay studies. The assay follows the growth of spheroids to evaluate the effectiveness of anti-hypoxia therapies in combination treatment.

FaDu spheroids were generated and pre-treated with ATQ or DMSO prior to co-incubation with one of 2DG, carboplatin, etoposide, or 5FU (Figure 5.1a). Dose ranges and treatment schedules were selected based on previously published literature, which spanned the range of plasma concentrations reported in pharmacokinetic and pharmacodynamic studies [160,210,211]. ATQ was found to potentiate the effect of carboplatin by delaying spheroid growth. No other combinations were found to be supra-additive. This effect was reproduced in H1299 spheroids (Figure 5.1b).

We repeated the experiment with FaDu spheroids but using a dose-range of 0 - 50 μM carboplatin and longer incubation times (Figure 5.1c). We observed a dose-dependent level of potentiation, notably limiting the growth (increase in diameter over time) of spheroids entirely at 50 μM carboplatin. Spheroid diameter doubling times indicate dose-dependent sensitisation (Figure 5.1d). Microscopy images of spheroids can be seen in Figure 5.1e.

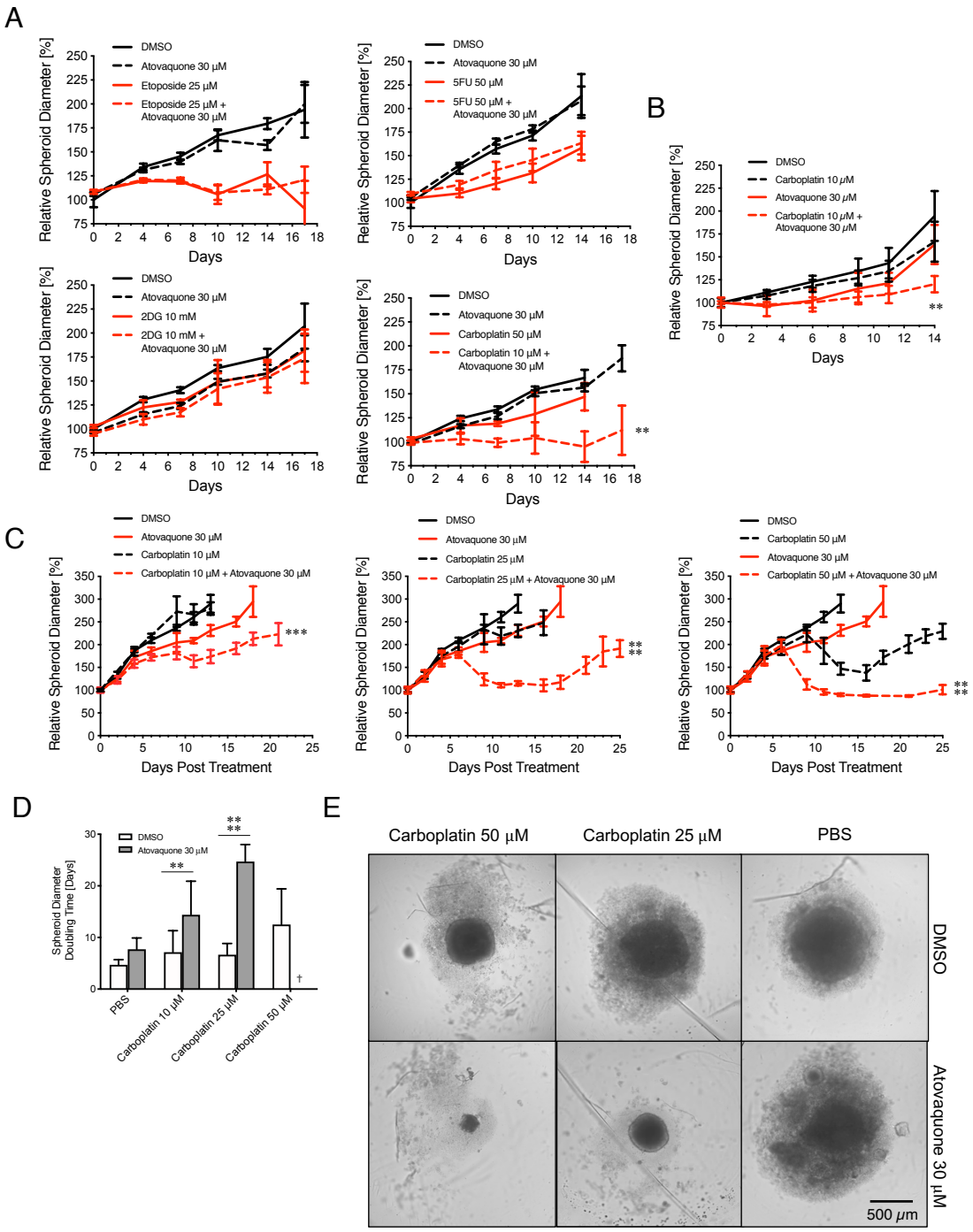


Figure 5.1 – Atovaquone Potentiates the Delay the Growth of Spheroids when Combined with Carboplatin, but not other Chemotherapies **(A)** FaDu cells were plated (2 x 10^4/well) to form spheroids 550 – 650 µm in diameter and treated for 12 hr with ATQ or DMSO then co-incubated for a further 12 hr with a chemotherapeutic agent, as indicated. Once treatment was complete, medium was changed (3x) microscopy used to assess spheroid diameter over 14 - 18 days. **(B)** As in (A) but using H1299 cells. **(C)** FaDu spheroids were grown and treated with 30 µM ATQ or DMSO for 24 hr but then co-incubated with 0 - 50 µM carboplatin for a further 24 hr prior to medium change and microscopy. **(D)** Quantification of spheroid diameter doubling time from (C). At least *N* = 16 spheroids used for each treatment condition. **(E)** Day 17 microscopy of (C). Error bars represent s.d. and † = spheroid growth was stunted and did not double within the observation window.

5.2.2 Atovaquone Increases Platinum-mediated Cancer Cell Death *in vitro* Under Normoxia

To explore what effect ATQ has when combined with platinum-class chemotherapy agents under normoxia, CFAs were performed using six cell-lines treated with carboplatin (Figure 5.2a) or cisplatin (Figure 5.2b). The combination resulted in potent and reproducible chemosensitisation across all cell lines tested, suggesting a mechanism for chemosensitisation that is independent of ATQ's ability to alleviate spheroid hypoxia.

To further probe the striking sensitisation observed under normoxia, time-course PI-exclusion experiments were completed using carboplatin (Figure 5.2c) or cisplatin (Figure 5.2d). Cells were treated as indicated then analysed 24, 48, 72, or 96 hrs after drug-wash off and medium change. PI-positive fractions were significantly higher in combination treated groups at 48 hrs, increasing at 72 hrs and 96 hrs.

5.2.3 Atovaquone Sensitises Cancer Cells to Platinum Agents *in vitro* under Normoxia Independently of pSTAT3^{Y705}

We explored the role of pSTAT3^{Y705} in mediating ATQ-platinum sensitisation given a recent report showing that ATQ is a potent inhibitor of STAT3^{Y705} phosphorylation [212]. We completed CFAs using DLD-1 cells wild-type and STAT3$^{Y705F/\ Y705F}$ mutants (Figure 5.3a). These experiments demonstrated no observable differences in ATQ-mediated colony reduction using cisplatin or carboplatin. We then evaluated the sensitivity of the isogenic pair to ATQ by generating a dose-response curve for inhibition of cellular proliferation (Figure 5.3b). No statistical difference between the isogenic pairs was observed. To further exclude any involvement of STAT3, we used STATTIC, a potent and specific small molecule inhibitor of STAT3 dimerization [213], in combination with carboplatin, but no sensitisation was observed (Figure 5.3c). Consequently, ATQ may be a potent and safe inhibitor of pSTAT3^{Y705} but appears not to mediate platinum chemosensitisation nor the ability of ATQ to interrupt the ETC and reduce cellular OCR.

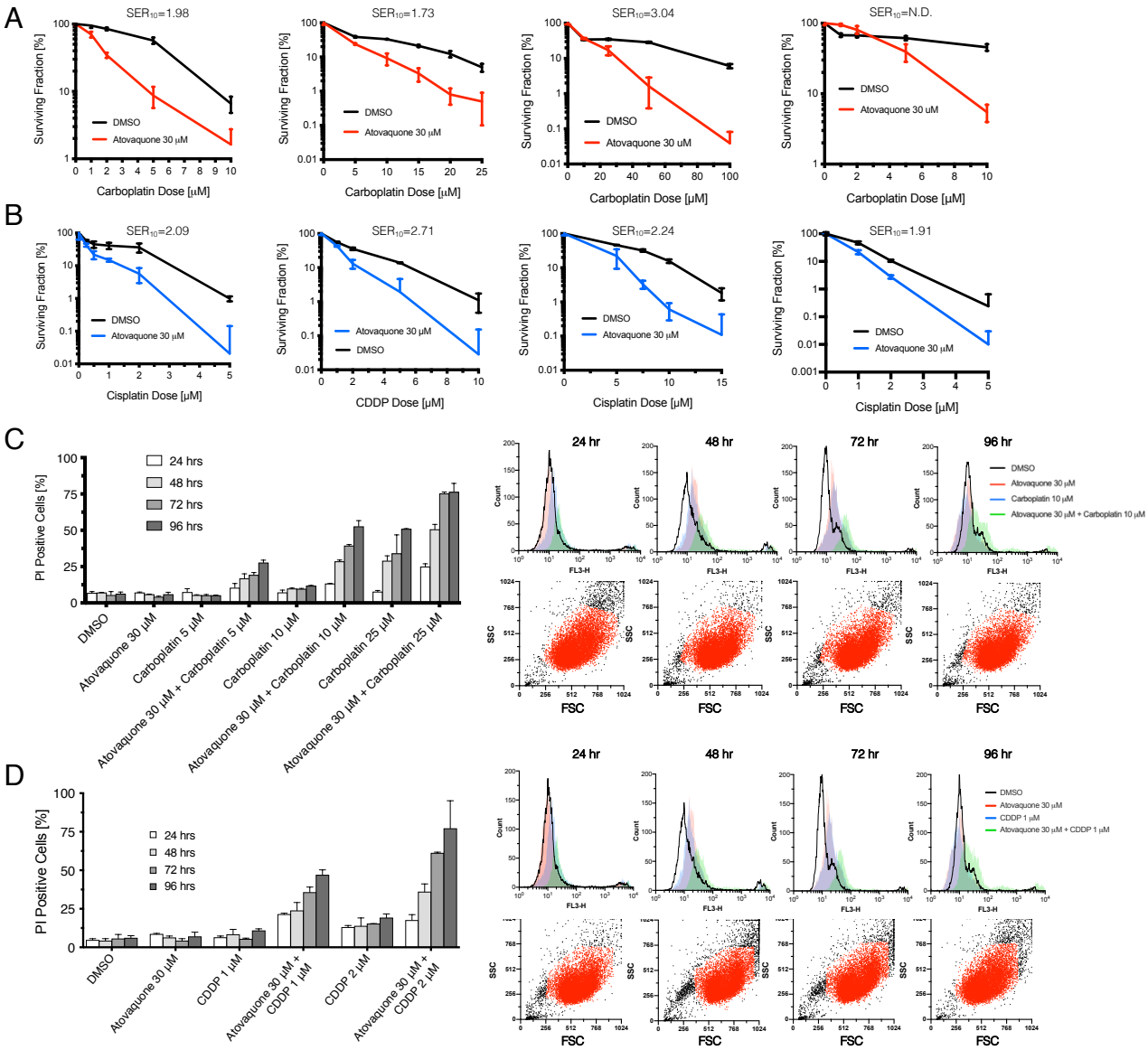


Figure 5.2 – Atovaquone Sensitises Cancer Cells to Platinum-mediated Cell Death Under Normoxic Conditions. **(A, B)** Colony forming assays (CFAs) were performed using (left to right) FaDu, HCT116, DLD1, or H460 cell lines using a 2 hr preincubation with 30 μM ATQ or DMSO and then 24 hr concomitant incubation with carboplatin or cisplatin. Sensitising effects were quantified using SER_{10} and are as indicated. Time-course PI-exclusion cytometry using 1 x 10^5 H460 allowed to attach overnight. Cells were then treated with **(C)** carboplatin or **(D)** cisplatin as in (A, B) then lifted and stained with 50 μg/mL PI and processed by flow cytometry at 24, 48, 72, or 96 hr after treatment.

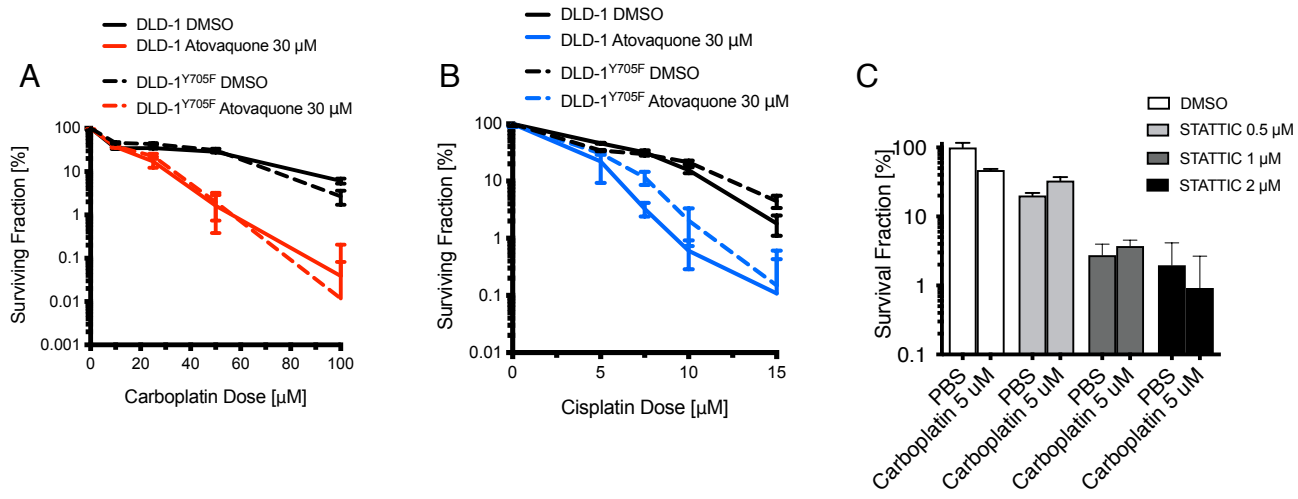


Figure 5.3 – Atovaquone Sensitises Cancer Cells to Platinum-mediated Cell Death Independently of pSTAT3^{Y705} **(A)** Wild-type and pSTAT3^{Y705} mutant DLD-1 cells (as indicated) were plated for colony forming assays (CFAs) and allowed to attach overnight before stimulation with 20 ng/mL IL-6 and 2 hr preincubation with ATQ or DMSO followed by 24 hr concomitant incubation with carrying doses of **(A)** carboplatin or **(B)** cisplatin. **(C)** CFAs were completed using FaDu cells treated for 2 hr with the STAT3 inhibitor STATTIC or DMSO before concomitant incubation with carboplatin for 24 hrs. After treatment, medium of CFA experiments was washed off and cells were allowed to form colonies for 12-14 days before crystal violet staining and quantification via BrightField microscopy. Data shown is representative of $N = 3$ repeats.

5.2.4 ROS-induced Glutathione Pool Depletion Underpins Atovaquone-mediated Sensitisation to Platinum-class Agents

Cellular resistance to platinum-class agents has been shown to be partly mediated by intracellular GSH pools, which have been hypothesized to interact with platinum-bearing molecules to form irreversible thiol complexes that render them ineffective as cytotoxic agents [214]. A very recent publication [95], however, suggests that the enzyme GST P1-1 instead is responsible for platinum agent sequestration and deactivation but this remains to be validated. It has also been shown that inhibition of ETC Complexes I, II, or III can upregulate mitochondrially-generated superoxide production leading to intracellular oxidization and, consequently, GSH pool depletion [214]. As such, we theorised that oxidative stress may be increased by ATQ and further increased after concomitant exposure to platinum-class chemotherapies, thereby mediating the observed synergy.

We explored ATQ-induced superoxide production in H460 and FaDu cells using MitoSOX, a fluorescent indicator specific for mitochondrial superoxide. No increase in superoxide production was observed using ATQ at up to 10 μM, but a striking increase was recorded at 30 μM (Figure 5.4a-b). We are actively confirming these results using MitoPY1, a hydrogen peroxide probe that is chemically dissimilar to MitoSOX.

Using the lowest dose of ATQ found to reliably increase superoxide production (30 μM) and the highest dose that did not increase the generation of ROS (10 μM), we next probed proliferative capacity using resazurin. Resazurin is a reliable redox indicator of proliferation and growth as it does not interfere with ETC reactions, unlike tetrazolium reagents such as MTT [215]. At 4 hr post-treatment, no decrease in relative fluorescence was recorded using 10 μM ATQ alone; however, 30 μM ATQ significantly reduced redox potential (Figure 5.4c). We then sought to evaluate intracellular glutathione (GSH) levels at 0, 4, and 24 hr post-ATQ treatment (Figure 5.4d). GSH is an abundant intracellular anti-oxidant, known to mediate platinum-agent effects when used as a single agent. A significant decrease in GSH was observed using 30 μM ATQ, but not 10 μM ATQ, at 4 hr and 24 hr. No decrease was observed at 0 hr post-treatment.

To link GSH depletion with ATQ-induced ROS production at 30 μM ATQ but not 10 μM, we quantified PI-positive cell fraction over 24 – 96 hrs using both dose levels of ATQ (Figure 5.5a). A positive two-way dose-dependency was observed and increased dramatically over time after combination treatment with 30 μM ATQ, but not 10 μM ATQ. Sensitisation was further probed in H460 and FaDu cells using both dose levels in a colony forming assay (Figure 5.5e-f). Reliably, ATQ 30 μM but not 10 μM sensitised cells to cisplatin or carboplatin treatment.

Having shown that ATQ treatment at 30 μM, but not 10 μM, induces superoxide production, depletes intracellular GSH pools, and sensitises cancer cells to platinum-mediated cell death, we acquired the specific inhibitor of GSH synthesis, buthionine sulfoximine (BSO), to validate GSH pool depletion and platinum-agent synergy (Figure 5.5d-e). Using BSO, the effects of cisplatin or carboplatin were potentiated suggesting GSH pool depletion as a potential mechanism by which ATQ might sensitise cells to platinum agents.

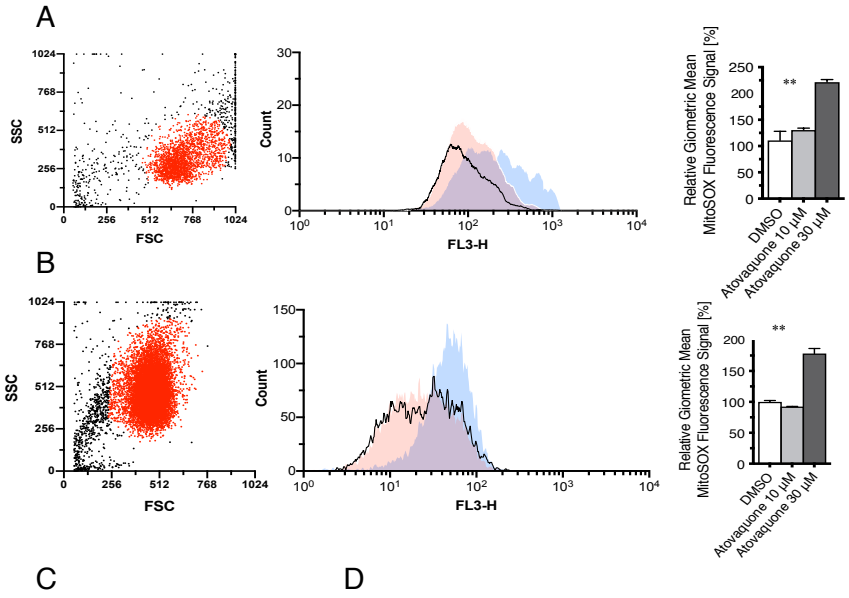


Figure 5.4 – Atovaquone Induces Oxidative Stress and Depletes GSH Pools in in a Dose-Dependent Manner. Gating histograms showing MitoSOX red fluorescence after 0 – 30 µM ATQ treatment for 2 hr in **(A)** FaDu and **(B)** H460 cells. **(C)** H460 cells were plated and allowed to attach overnight, then underwent resazurin (AlarmarBlue) staining after 4 hr post-treatment, as indicated. All values are presented as *N* = 3 group mean ± s.d. Flow cytometry was performed on three separate clonal cell lines per group on three separate occasions. **(D)** H460 cells were plated and allowed to attach overnight, then assayed for GSH levels using a colorimetric assay and processed at 0 – 24 hr post carboplatin treatment. Histograms are from representative runs

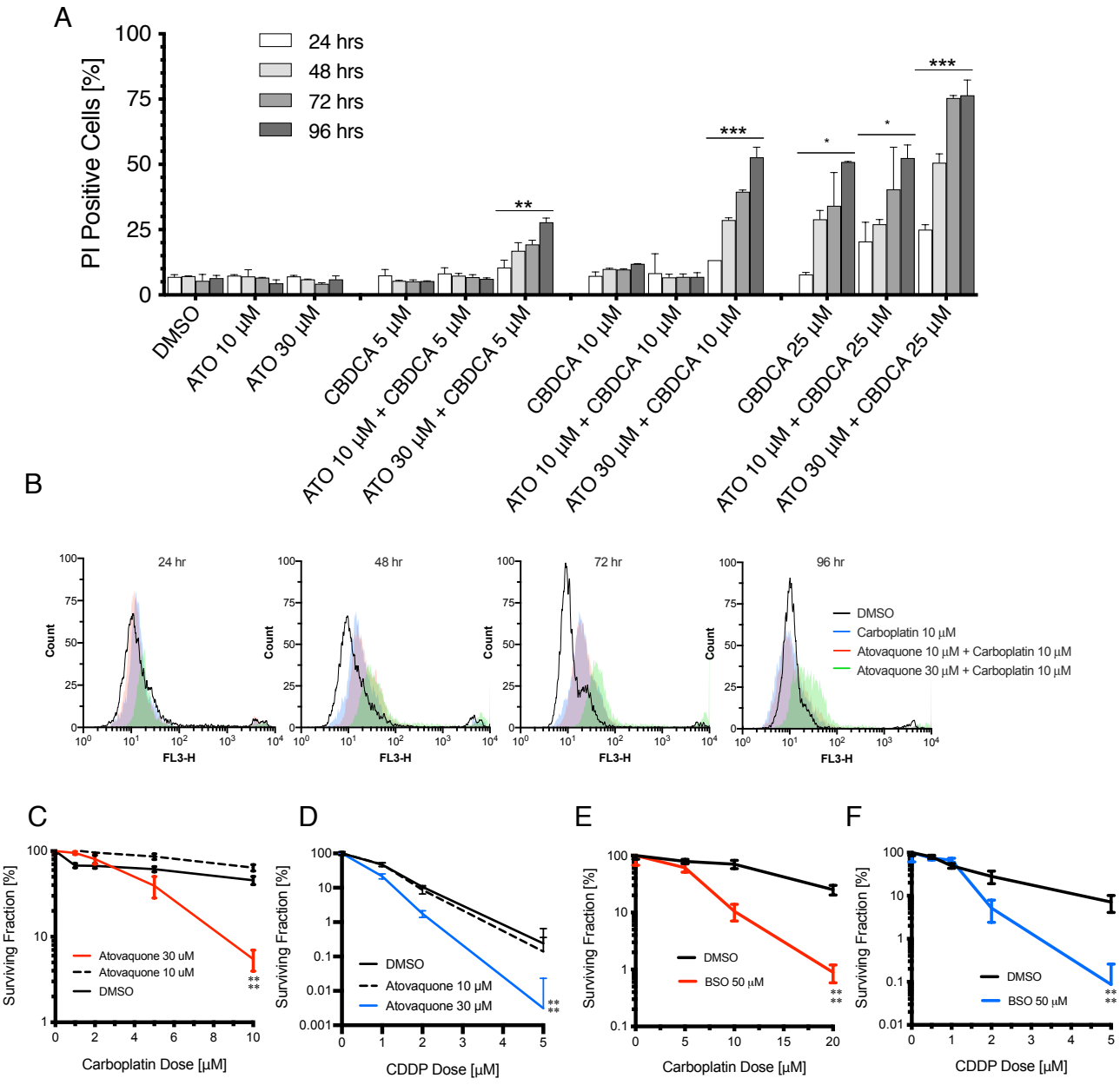


Figure 5.5 – ROS-induced GSH Pool Depletion Mediates Atovaquone-Platinum Sensitisation. **(A)** Time-course PI-exclusion assay using 2 x 10^5 H460 cells plated and allowed to attach overnight before 2 hr preincubation with 0 – 30 µM ATQ or DMSO followed by 24 hr concomitant incubation with carboplatin (labelled as CBDCA). Cells were then lifted, stained with 50 µg/mL PI, and processed by flow cytometry at 24, 48, 72, or 96 hr after treatment. **(B)** Histograms of PI-exclusive as in (A) for 10 µM carboplatin. H460 cells were plated for colony forming assays (CFAs) and pre-treated for 2 hr with 0 – 30 µM ATQ or DMSO followed by 24 hr concomitant incubation with varying doses of carboplatin. **(C)** carboplatin or **(D)** cisplatin. H460 cells were plated for CFAs and pre-treated for 2 hr with the specific glutathione (GSH) inhibitor butathione (BSO) followed by 24 hr concomitant incubation with varying doses of **(E)** carboplatin or **(F)** cisplatin (CDDP). All values are presented as group mean ± s.d. and *p<0.05, **p<0.01, ***p<0.001, ****p<0.0001. Statistical significance was assessed using N = 3 and then by one-way ANOVA. In the case of CFAs, comparison was made between 10 µM ATQ and 30 µM ATQ.

5.2.5 Preloading Glutathione using n-Acetyl-Cysteine Abolishes Atovaquone-Mediated Platinum Sensitisation *in vitro*

To further probe the role of GSH in mediating the observed chemosensitisation, we acquired the stable and well-characterised GSH precursor molecule, n-Acetyl-Cysteine (NAC) [214]. We probed whether pre-loading cells prior to combination treatment abrogates ATQ-mediated platinum sensitisation. Using PI-exclusion, sensitisation was observed using ATQ and carboplatin but was not present when cells were preloaded with NAC 2 - 10 mM (Figure 5.6a), implicating GSH levels as key mediators. Clonogenic assays were performed using FaDu or H460 cells with 2 hr of NAC preloading following by 30 μM ATQ combination treatment, which revealed a reduction in synergy with increasing NAC (Figure 5.6b-d).

5.2.6 Atovaquone Safely Potentiates the Efficacy of Carboplatin *in vivo*

To explore the translational viability and evaluate the potential clinical efficacy of using ATQ to sensitise tumours to platinum-class chemotherapies, we completed an *in vivo* xenograft tumour growth delay experiment using human H460 cells in immunocompromised BALB/c *nu/nu* mice (Figure 5.7a). We opted to use carboplatin as a representative platinum-agent rather than cisplatin since it is better tolerated *in vivo*. The combination carboplatin + ATQ arm resulted in significantly inhibited tumour growth compared to carboplatin or ATQ alone groups. During the experiment, tolerability was evaluated using weight loss as a surrogate marker (Figure 5.7b). No significant difference between carboplatin or carboplatin + ATQ groups was recorded. Evaluating the number of days before surpassing the volumetric limit of 1000 mm^3 (legal tumour volume endpoint) revealed supra-additive effectiveness according to a mean growth delay of 3.1 days compared to carboplatin-alone (Figure 5.7c).

We then further probed the tolerability of ATQ + carboplatin *in vitro*. Tumour bearing mice treated as before but this time their bloods processed

for electrolyte concentrations, creatinine levels, acid-base balance indicators, anion gap, glucose concentrations, haemoglobin (Hb), and haematocrit (Hct) levels (Figure 5.8). No statistical difference between carboplatin and carboplatin + ATQ groups was found, but all animals having received carboplatin had a discernible reduction in Hct.

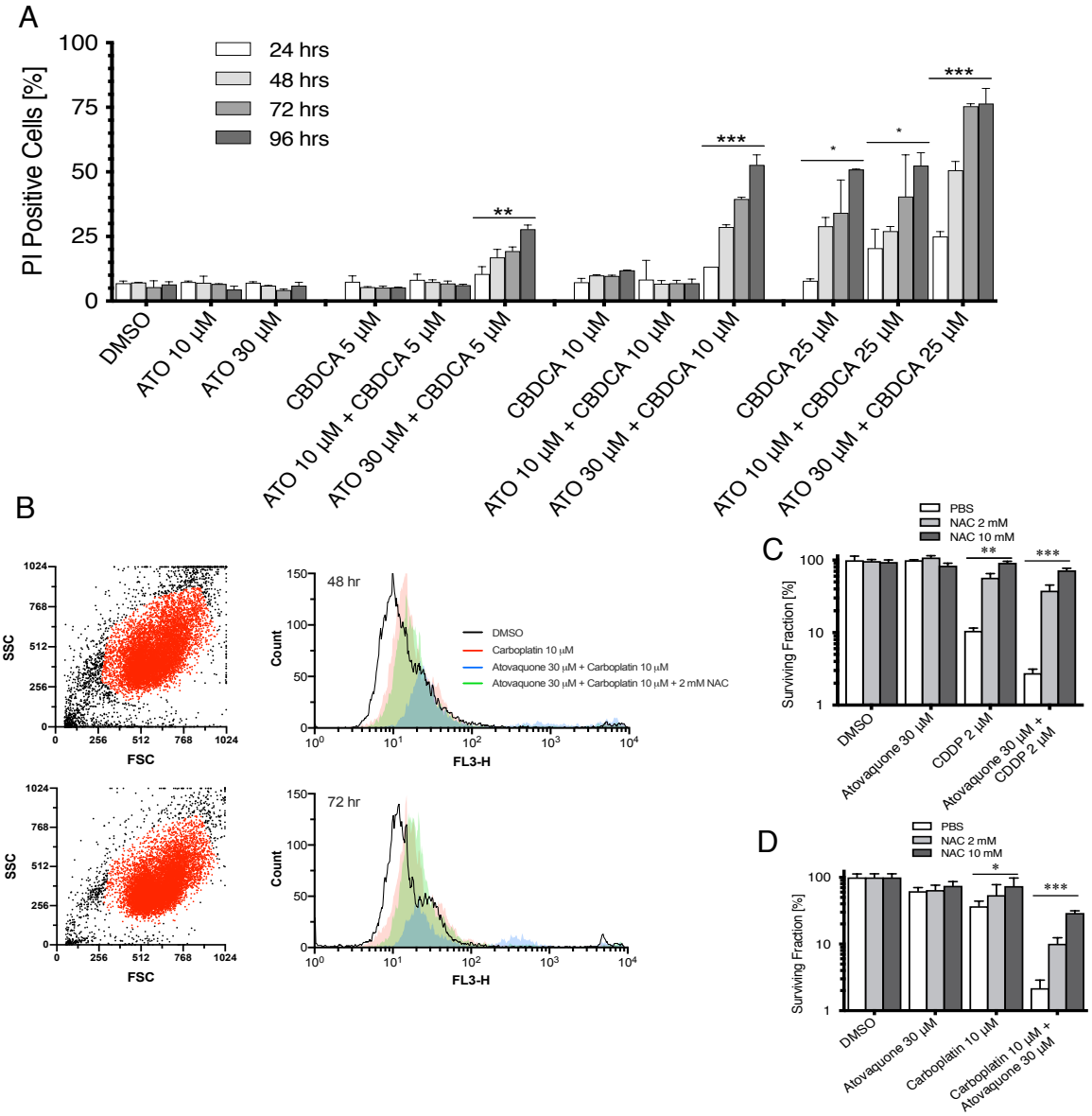


Figure 5.6 – Pre-Loading Cells with the GSH Precursor NAC Abrogates Atovaquone-Platinum Cell Death Synergy **(A)** Time course PI-exclusion assays of 1 x 10^5 H460 cells plated and allowed to attach overnight before 2 hr preincubation with 0 – 10 mM NAC, followed by 2 hr co-incubation with 0 – 30 μM ATQ or DMSO, and then 24 hr concomitant incubation with carboplatin (CBDCA). (B) Histograms of (A) for ATQ 30 μM and carboplatin 10 μM with NAC 2 mM. H460 cells were lifted, stained with 50 μg/mL PI, and processed by flow cytometry at 24, 48, 72, or 96 hr after treatment. **(C, D)** H460 cells were plated for colony forming assays (CFAs) and pre-treated with 0 – 10 mM NAC for 2 hr, followed by 2 hr co-incubation with 0 – 30 μM ATQ or DMSO, and then 24 hr concomitant incubation with carboplatin or cisplatin, as indicated. All values are presented as *N* = 3 group mean ± s.d from three biological replicates.

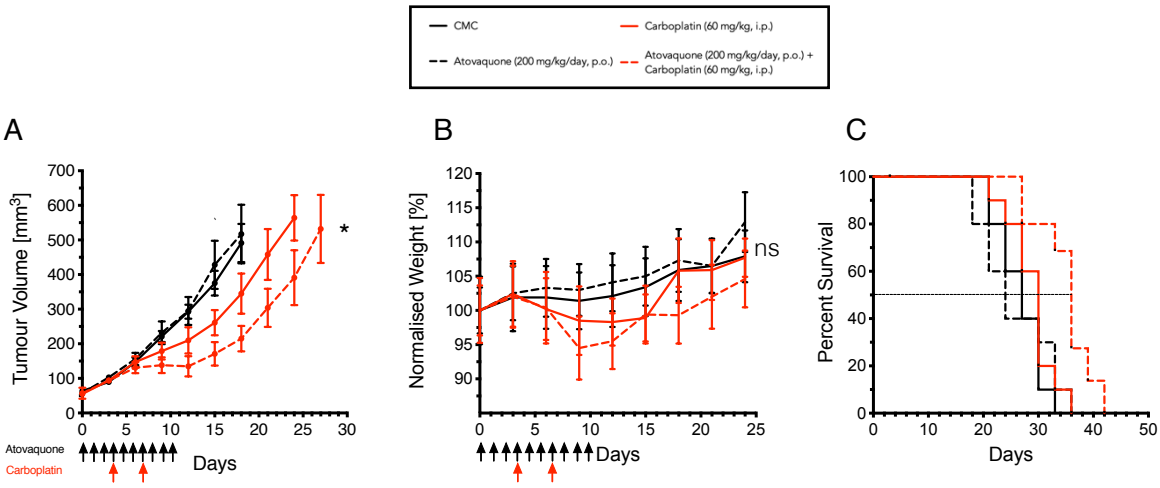


Figure 5.7 – Atovaquone Potentiates the Anti-Tumour Effect of Carboplatin **(A)** Mice bearing H460 xenograft tumours of 75-100 mm^3 were treated as indicated (N = 8, each; see floating legend): with 200 mg/kg/day Atovaquone (ATQ) or MC via oral gavage (p.o.) for 9 days, and were injected intraperitoneally (i.p.) with (–) saline or (---) 60 mg/kg carboplatin on days 4 & 7. Tumour growth was assessed via callipers averaging measurements from two independent operators. **(B)** Subject weights were recorded for each measurement. At least eight mice were used for each treatment group and all animals were culled by a Schedule 1 method. **(C)** Days to reach threshold tumour burden (1000 mm^3) plotted as percent survival. Survival curve significance was computed using Mantel-Cox test (median survival of carboplatin vs. combination: 30 vs. 36 days, p=0.0076).

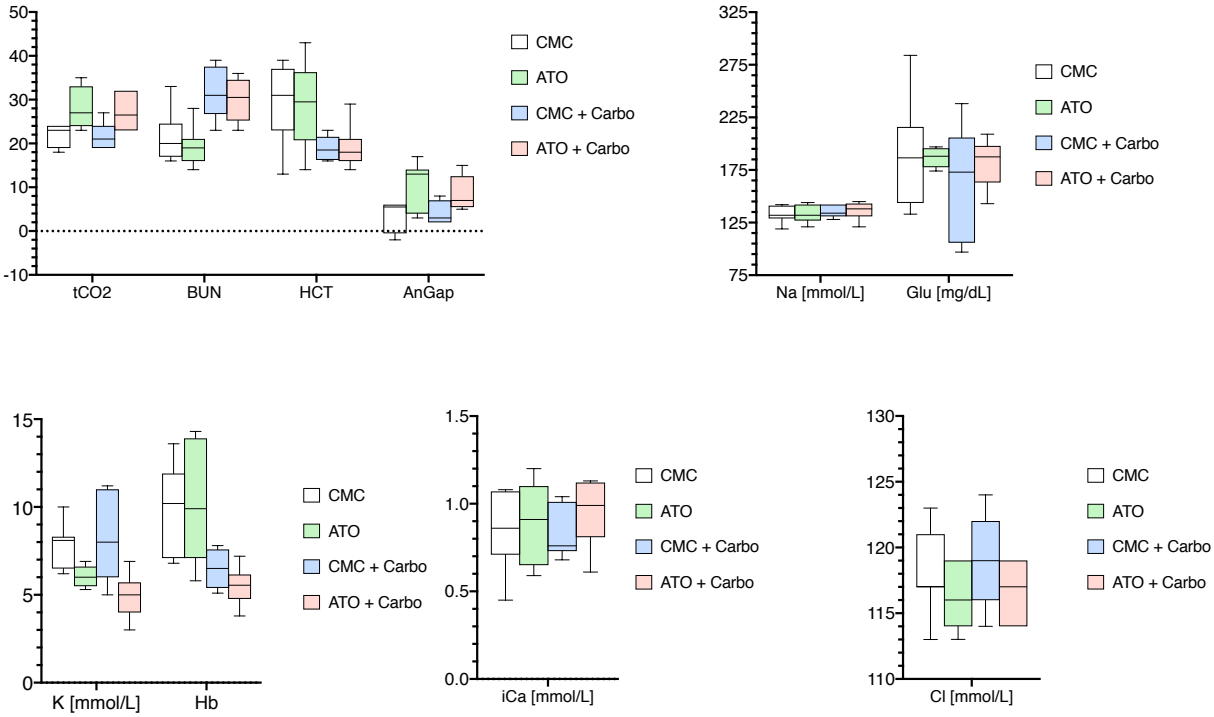


Figure 5.8 – Atovaquone Does Not Induce Systemic Toxicities in Combination with Carboplatin *in vivo* Mice (N = 8, each treatment) bearing H460 xenograft tumours of 75-100 mm^3 were treated with 200 mg/kg/day Atovaquone (ATQ) or CMC via oral gavage (p.o.) for 9 days, and were injected intraperitoneally (i.p.) with (–) saline or (---) 60 mg/kg carboplatin on days 4 & 7. Three days after completion of treatment, subjects were sacrificed using a Schedule 1 method and blood samples (~100 L) were collected via cardiac puncture and placed in Heparin-containing tubes on ice before immediate processing using a VetScan i-STAT device (Ablaxis, UK) with CHEM 8+ tip configuration. The i-STAT provides measurements (as indicated) on blood gas, electrolyte, chemistry and haematology factors.

5.3 Discussion

Tumour hypoxia has long been known to induce resistance to chemotherapy-based treatment regimens. Given the efficacy of ATQ in alleviating tumour hypoxia, we studied whether ATQ might combine well with commonly used chemotherapies. We first tested combinations using a three-dimensional spheroid-based assay, which used ATQ to alleviate spheroid hypoxia before chemotherapy treatment to reflect the potential use of ATQ as a hypoxia modifier.

When combined with ATQ, we identified that carboplatin potentiated the inhibition of spheroid growth, while other agents, such as 5FU, demonstrate only an additive effect (sensitisation enhancement ratio [SER] ≈ 1). To confirm that the synergy is dependent upon the reversal of spheroid hypoxia, clonogenic assays were completed. To our surprise, we found that ATQ potentiates the efficacy of both carboplatin and cisplatin in clonogenics under normoxia, indicating an underlying mechanism that is hypoxia-independent. We then confirmed that the observed platinum synergy is independent of $pSTAT3^{Y705}$ and HIF-1α.

We theorised that the underpinning mechanism for sensitisation was related to ROS given previous reports in literature on platinum-agent induced damage to mtDNA [11], and a report detailing increased H_2O_2 levels after cancer cell exposure to ATQ [216]. To explore whether ROS mediated the platinum potentiation, we used MitoSOX to evaluate mitochondrially-generated superoxide using the same treatment protocol as was employed in our clonogenic and spheroid experiments. Using flow cytometry, we confirmed that ATQ reliably increased ROS at 2 hr and then proceeded to investigate downstream ROS-induced changes. We also used resazurin as a redox indicator for proliferation and cell growth since it does not affect ETC function [215]. Finally, using NAC as a GSH precursor that is well tolerated,

we demonstrated that pre-loading cells with NAC mitigates ATQ-induced platinum potentiation.

Under normal physiological conditions, cells control ROS levels by balancing the generation of ROS with elimination by scavengers (reduced-GSH and SOD) [217,218]. But under oxidative stress conditions, excessive ROS can damage cells and contribute to oncogenesis. Cancer cells exhibit greater ROS stress than normal cells do, partly due to oncogene activation and increased metabolic activity, but also mitochondrial dysregulation [219]. Oxidative stress is also one of the most important mechanisms involved in cisplatin toxicity [13]. Chiefly, cisplatin induces ROS depending on concentration and length of exposure, triggering cell death by perturbing intracellular redox homeostasis. Thiol group (-SH) molecules, such as GSH, become depleted upon cisplatin-mediated ROS saturation, which leads to the formation of thiol-based radicals that in turn generate more ROS [220].

We used H460 xenografts to confirm the efficacy of combination therapy as well as its tolerability and safety. To this end, we completed a tumour growth delay using a moderate dosing regimen of ATQ and two doses of carboplatin, which was selected over cisplatin due to reduced nephrotoxicity and overall better tolerability. Our findings demonstrate a notable increase in tumour growth delay, modest changes in animal weights, and no significantly changes in any factors relating to renal function, electrolytes, acid-base balance, or hematopoietic performance. Survival times of all subjects were also plotted using time-to-tumour volume as survival endpoint. According to survival curves, the tumour growth delay is more modest but statistically significant and could theoretically be improved by further dose-optimisation experiments. One limitation in our work is the use of a single cell line *in vivo* with a single platinum agent, which should be extended to reflect *in vitro* findings. Despite *in vivo* experiments generally being lower throughput than *in vitro* assays, replicating ATQ-platinum potentiation in more than one model

evidences the robustness of findings and is critical for advancing beyond pre-clinical studies.

Interestingly, there is some evidence that OXPHOS is an important downstream pathway in mediating platinum chemoresistance [221–223]. For instance, tumour necrosis factor receptor-associated protein 1 (TRAP1) is a mitochondrial chaperone from the Hsp90 family known to upregulate glycolysis in many cancer cell lines. Lower expression of TRAP1 increases OCR, decreases ECAR, and is associated with resistance to platinum agents. If validated, TRAP1-mediated OXPHOS inhibition would be one of possibly many nuclear targets, which, when inhibited, abrogates platinum resistance through metabolic reprogramming.

Future clinical studies could evaluate how cancer cell metabolism evolves throughout treatment in patients receiving a platinum agent. This would help to shed light on whether enduring and resistant cancer cells tend to have more reliance on OXPHOS *in situ*. The limiting factor for such work is likely to be the acquisition of post-treatment biopsies but would provide significant, clinically actionable evidence for combining OXPHOS inhibitors with platinum agents.

CHAPTER 6

GENERAL DISCUSSION

6.1 Summary of Findings

The first experimental chapter of this thesis (Chapter 3) explored the broader effects of ATQ for use as a hypoxia-modifying agent. We demonstrated that ATQ is well-tolerated in animal experiments at high doses or for long-term treatment. The effects of ATQ on cellular OCR and ECAR *in vitro* at pharmacologically relevant concentrations were found to be readily reversible. Experiments using 143B isogenic cybrids demonstrated that ATQ-mediated cytotoxicity is independent of its ability to reduce OCR. We confirmed that ATQ can alleviate spheroid hypoxia using the hypoxia marker EF5 and confirmed this by a reduction in CAIX, which is upregulated by cancer cells under hypoxia. A reduction in CAIX staining demonstrates that ATQ is not unexpectedly attenuating the formation of EF5 adducts vis-à-vis inhibition of nitroreductases. ATQ has also been recently shown to be an excellent inhibitor of $pSTAT3^{Y705}$. We used OCR and ECAR measurements, cytotoxicity assays, and proliferation assays to demonstrate that ATQ can reduce OCR independently of $pSTAT3^{Y705}$. We then generated spheroids using HCT116 cells isogenic for HIF-1α to demonstrate that ATQ alleviates spheroid hypoxia OCR independently of HIF-1α.

ATQ has been shown to alleviate tumour hypoxia, but it also reliably upregulates glycolysis, evidenced by increased ECAR. Increased glycolysis is considered a hallmark of ECM degradation, which itself is linked to the metastatic cascade. As such, Chapter 4 of this thesis explored whether ATQ significantly modulates cellular migration *in vitro*, or metastatic potential *in vivo*, as part of evaluating its translational viability. We firstly presented a series of *in vitro* experiments that were done using xCELLigence technology. We demonstrated that ATQ does not significantly increase migration using this method and did so using a variety of cell lines. As is the case with many

in vitro experiments, xCELLigence assays are not able to replicate all aspects of the metastatic cascade that occurs *in situ*.

To further probe what effect ATQ may have on metastatic potential, we used a BALB/c mammary gland-derived 4T1 orthotopic model to investigate what effect ATQ-mediated reversal of tumour hypoxia might have on spontaneous, distant metastasis. Reoxygenation of hypoxic tumours has been suggested to modulate metastatic potential *in vivo* and so we sought to reverse hypoxia in animals with established tumours [224]. To this end, we characterised 4T1 cells *in vitro* and evaluated whether BALB/c mice could tolerate ATQ without changes in weight or 4T1 tumour volume. With assistance from the NVS and NACWO at our institution and a pathologist, we then confirmed that s.c. injected 4T1 cells into the lower right inguinal mammary fat pad (i.m.m. injections) spontaneously metastasise to the lungs. We repeated the experiment using cardiorespiratory-gated 3 T MRI to visualise lung metastases and concurrent *ex vivo* flow cytometry of lungs, liver, spleen, and tumour – no increase in GFP-positive cell populations were observed in treated vs. control animals, indicating that ATQ does not increase metastatic potential in the 4T1 orthotopic model.

Chapter 5 demonstrated a striking and reproducible sensitisation effect *in vitro* using ATQ with cisplatin or carboplatin in CFAs and PI-exclusion assays. The effect was apparent using concentrations of ATQ that are physiologically relevant and achievable in a clinical setting. Similarly, the concentrations of platinum agents employed are at or below peak concentrations of those seen in patients [225]. These findings were reproduced in spheroid models whereby a striking increase in spheroid regrowth delay effect was noted using the combination, exceeding the additive effect of ATQ and platinum treatment individually. We extended these findings by completing a tumour growth delay study *in vivo*, which demonstrated synergy between ATQ and carboplatin at physiologically

relevant doses. We accomplished this using a treatment regimen reflecting how ATQ might be used clinically alongside platinum agents. Normal tissue side effects are often dose-limiting, albeit in the case of one or multiple agents used in combination. Preliminary toxicology data presented in Chapter 5 indicate that the combination of ATQ with carboplatin may be tolerable and efficacious. No significant differences in animal weights, haematological factors, or other parameters were identified between platinum-alone and combination treatment groups.

6.2 Significance of Findings

Tumour hypoxia is an important impediment to effective cancer therapy and is present in the majority of solid tumours. It occurs due to inadequate oxygen delivery by abnormal vasculature coupled with the increased metabolic demand of rapidly proliferating cancer cells. Oxygenation throughout a tumour is heterogeneous but can also vary significantly between patients and tissue types. Oxygen is also a key mediator of XRT efficacy since hypoxic tumours are known to be radiation resistant. Given its recognition as an important impediment to anti-cancer therapies, many approaches have been tried to overcome tumour hypoxia, but none are in widespread clinical use. Indeed, there exists a need to identify novel strategies to reverse or even exploit tumour hypoxia.

Historical strategies focused on increasing the supply of oxygen to tumour cells or delivering hypoxia-activated pro-drugs to tumours have not demonstrated clinical efficacy –oxygen is unable to reach hypoxic areas, albeit due to leaky vasculature or other reasons, and so perhaps it is unsurprising that small molecules also have difficulty doing so. Instead, our team proposed that inhibitors of oxygen consumption might increase the concentration of unmetabolised oxygen and allow it to diffuse into hypoxic areas. In such a case, well-perfused and peri-hypoxic regions could be targeted rather than hypoxic areas directly. In doing so, we identified that Atovaquone (ATQ) safely reduces oxygen consumption *in vitro* and alleviates tumour hypoxia *in vivo*.

The findings presented in Chapter 3 support ATQ as a translationally viable candidate hypoxia modifying agent deserving of further study. Our team is now conducting a Phase 0 proof-of-principle clinical trial to study ATQ in a clinical context (‘ATQM’, NCT02628080) and are designing a Phase 2b study (‘ARCADIAN’) to evaluate its suitability for use with concurrent

chemoradiotherapy. The ATQM study is investigating the effect of ATQ on tumour hypoxia in patients with NSCLC, but also aims to validate research techniques for stratifying tumour hypoxia using a combination of PET, perfusion CT, DCE-DWI MRI, IHC, and bioinformatics analysis. The full potential of any anti-hypoxia strategy, including ATQ, depends on the development of robust biomarkers. Precision targeting of hypoxic tumours may require multiple biomarker assessments over time for each patient, with individualised treatments based on how the tumour evolves, for instance, in response to chemotherapy.

A recent publication studying the effects of the FDA-approved anti-diabetic biguanide metformin in breast cancer patients has revealed that metformin therapy can lead to a clinically detectable [^{18}F]-FDG flux in tumours [226]. Moreover, the authors identify two distinct metabolic responses to metformin according to OXPHOS-induced transcriptional changes, FDG uptake, and proliferation markers. These findings indeed demonstrate the potential to identify biomarkers of metformin response but may also be widely applicable to other OXPHOS inhibitors and so are deserving of further study and validation.

Platinum-based chemotherapies are an effective treatment for many cancers despite severe side effects and the development of resistance that is often associated with their use [13]. Cisplatin has clinical activity against a wide array of solid cancers. Despite consistent initial responses, cisplatin treatment often results in the development of chemo-resistance, leading to therapeutic failure. The use of cisplatin is also limited by dose associated toxicity and side effects. To mitigate the side effects and resistance resulting from platinum-based chemotherapy, it is essential to investigate new drugs or combinations which are non-toxic and work in alternative/similar pathways to cisplatin alone, thus providing additional therapeutic options. In recent years, several compounds for use in combination with platinum agents have

been explored; however, none of these combinations were successful for clinical application.

We found that ATQ potentiates the anti-cancer effects of cisplatin and carboplatin, an effect mediated by increased oxidative stress and GSH pool depletion (Chapter 5). Our findings demonstrate that the combination of ATQ with a platinum agent does not induce aberrant toxicities *in vivo* but does increase the delay of tumour growth. As such, ATQ with a platinum agent may be a viable and effective combination to consider for clinical use but further study is required using more diverse models, immunocompetent mice, and a broader range of dose regimens. Given the potential use of ATQ as a hypoxia modifier, future work should also consider what effect the combination has when used alongside XRT (chemoradiation). Historical patient records might help to evaluate the efficacy of the combination therapy but would require information on individuals' that received platinum-based chemotherapies alongside ATQ and XRT. This will likely be difficult to ascertain given that patients will often receive several therapies alongside platinum and are probably unlikely to concurrently have been administered ATQ as an anti-malarial before and during therapy. Investigating other known ETC inhibitors and probing whether they also combine well with platinum agents could be of interest to future studies.

Metformin has been reported to synergise with cisplatin, but the extent of these findings is preliminary and many reports are predicated on the use of supra-physiological concentrations of metformin [227–229]. We await the results of ongoing late-phase clinical studies investigating metformin in an anti-cancer setting but also its combination with platinum agents (such as NCT03833466, NCT02949700, NCT02065687). At the time of writing, a search on *ClinicalTrials.gov* lists 126 clinical studies using metformin in an anti-cancer setting that are active, recruiting, or opening soon for recruitment and will undoubtedly provide further insight into metformins' efficacy.

Downstream effects of agents that modulate oxidative stress appear to be complex and diverse. ROS has not only been implicated in mediating XRT efficacy through *the oxygen effect* but also epigenetic modifications [230,231], MAPK/ERK signalling [232], metastatic progression [233], transcriptional regulation of proliferation [234], cellular adhesion [235], the inflammatory response [236], and angiogenesis [237]. Incomplete knowledge of the role that oxidative stress plays in promoting or limiting disease progression has likely limited the success of redox-based treatments to-date. The many roles in which oxidative stress has been implicated furthermore suggests its effects can be compartmentalised, having pro-tumourigenic effects under certain conditions or within certain intracellular compartments, but anti-tumourigenic effects in others.

Therapies that significantly modulate pathways associated with metastatic progression should be carefully probed. ATQ has been shown to alleviate tumour hypoxia, however, our team has also demonstrated that ATQ reliably upregulates glycolysis. Increased glycolysis is considered a hallmark of ECM degradation, itself a key step of the metastatic cascade [238,239]. Though *in vivo* models for metastasis are unable to replicate every aspect of *in situ* metastatic spread, our findings indicate that ATQ does not increase metastatic spread in the models we tested. At the same time, however, increased glycolysis may increase the risk of acidosis, which can affect therapeutic interventions in other ways.

Immunotherapy has recently emerged as arguably the most exciting and potentially effective means of anti-cancer treatment. Both hypoxia and cancer cell metabolism can play important roles in determining the effectiveness of immunotherapies [240]. Anaerobic glycolysis upregulated by tumour cells can result in over-production of adenosine, which is excreted by the tumour cells into the ECM, preventing lymphocyte proliferation [241]. Moreover, the mTOR pathway has been shown to regulate the metabolic

reprogramming of certain immune cell populations [242,243]. Furthermore, HIF-1α expression has been shown to impede the effectiveness of the adaptive immune system [244,245]. It remains for the most part unclear whether OXPHOS inhibitors more generally improve or hinder immunotherapy-based treatment regimens and so further work on this new area of study is needed. An excellent review article by Buck et al. can be found on the *metabolic instruction of immunity* for many insightful discussions on the subject [246].

As the molecular and biochemical mechanisms underlying OXPHOS inhibition emerge, their effects should be investigated in cancer cells but also in non-malignant components of the TME. The use of immunocompetent models and patient-derived data during pre-clinical validation of candidate OXPHOS inhibitors is vital. At this time, it is reasonable to conclude that OXPHOS inhibitors have the potential to trigger both anti-tumourigenic as well as pro-tumourigenic effects. In certain clinical contexts, the advantages associated with the use of OXPHOS inhibitors may outweigh any drawbacks, but further investigation and careful trial patient selection is very much required. Clinically-relevant and potent combinatorial approaches with OXPHOS inhibitors may also exist but need to be carefully evaluated in order to mitigate aberrant toxicities.

6.3 Concluding Remarks

This thesis explored the use of the FDA-approved, anti-malarial drug Atovaquone (ATQ) in anti-cancer therapy. We probed the tolerability of ATQ *in vitro* and *in vivo*, the mechanistic dependencies for its use in reducing oxygen consumption and alleviating spheroid hypoxia, the potential effects ATQ may have on cellular migration and invasion, and demonstrated increased cell-killing when combined with platinum-class chemotherapies.

The alleviation of tumour hypoxia through OXPHOS inhibition appears very promising but remains at an early stage of development. Overall, the effects of OXPHOS inhibition appear to be pleiotropic. Whether it be for alleviating hypoxia or other purposes, future clinical studies using OXPHOS inhibitors should incorporate robust biomarkers to identify patients that could benefit from their use while differentiating non-responders and those with increased sensitivity. Used in combination with accurate and clinically feasible patient stratification, OXPHOS inhibitors could very well transition into routine clinical use in the near future.

REFERENCES

[1] The World Health Organization (WHO). Cancer. Glob Status Rep Noncommunicable Dis 2014. https://www.who.int/topics/cancer/en/ (accessed August 12, 2019).

[2] Cancer Research UK. Cancer Risk Statistics 2018. https://www.cancerresearchuk.org/health-professional/cancer-statistics/risk (accessed August 18, 2019).

[3] Institute NC. NCI Dictionary of Cancer Terms. “National Cancer Institute” 2018.

[4] Bertram JS. The molecular biology of cancer. Mol Aspects Med 2000. doi:10.1016/S0098-2997(00)00007-8.

[5] American Cancer Society. Cancer Treatment & Survivorship Facts & Figures 2016-2017. Am Cancer Soc 2016.

[6] Huang CY, Ju DT, Chang CF, Muralidhar Reddy P, Velmurugan BK. A review on the effects of current chemotherapy drugs and natural agents in treating non-small cell lung cancer. Biomed 2017. doi:10.1051/bmdcn/2017070423.

[7] Chabner BA, Roberts TG. Chemotherapy and the war on cancer. Nat Rev Cancer 2005. doi:10.1038/nrc1529.

[8] Alderden RA, Hall MD, Hambley TW. The discovery and development of cisplatin. J Chem Educ 2006.

[9] Kelland L. The resurgence of platinum-based cancer chemotherapy. Nat Rev Cancer 2007. doi:10.1038/nrc2167.

[10] Galanski M, Jakupec M, Keppler B. Update of the Preclinical Situation of Anticancer Platinum Complexes: Novel Design Strategies and Innovative Analytical Approaches. Curr Med Chem 2005. doi:10.2174/0929867054637626.

[11] Dasari S, Bernard Tchounwou P. Cisplatin in cancer therapy: Molecular mechanisms of action. Eur J Pharmacol 2014;740:364–78. doi:10.1016/j.ejphar.2014.07.025.

[12] Bruno PM, Liu Y, Park GY, Murai J, Koch CE, Eisen TJ, et al. A subset of platinum-containing chemotherapeutic agents kills cells by inducing

ribosome biogenesis stress. Nat Med 2017. doi:10.1038/nm.4291.

[13] Galluzzi L, Senovilla L, Vitale I, Michels J, Martins I, Kepp O, et al. Molecular mechanisms of cisplatin resistance. Oncogene 2012;31:1869–83. doi:10.1038/onc.2011.384.

[14] Society AC, Treatment C. Cancer Treatment. Cancer Treat Surviv Facts Fig 2013. doi:10.1002/14651858.CD003475.pub2.Manual.

[15] Moding EJ, Kastan MB, Kirsch DG. Strategies for optimizing the response of cancer and normal tissues to radiation. Nat Rev Drug Discov 2013;12:526–42. doi:10.1038/nrd4003.

[16] Sher DJ. Cost-effectiveness studies in radiation therapy. Expert Rev Pharmacoeconomics Outcomes Res 2010. doi:10.1586/erp.10.51.

[17] Stafford SL. Clinical Radiation Oncology. Mayo Clin Proc 2012. doi:10.4065/76.7.762-a.

[18] Anderson ARA, Quaranta V. Integrative mathematical oncology. Nat Rev Cancer 2008. doi:10.1038/nrc2329.

[19] Withers HR. The Four R's of Radiotherapy, 1975. doi:10.1016/b978-0-12-035405-4.50012-8.

[20] Steel GG, Mcmillan TJ, Peacock JH. The 5rs of radiobiology. Int J Radiat Biol 1989. doi:10.1080/09553008914552491.

[21] Gray LH, Conger AD, Ebert M, Hornsey S, Scott OC. The concentration of oxygen dissolved in tissues at the time of irradiation as a factor in radiotherapy. Br J Radiol 1953;26:638–48. doi:10.1259/0007-1285-26-312-638.

[22] Thoday JM, Read J. Effect of oxygen on the frequency of chromosome aberrations produced by alpha-rays [8]. Nature 1949. doi:10.1038/163133a0.

[23] Ewing D. The oxygen fixation hypothesis: A reevaluation. Am J Clin Oncol Cancer Clin Trials 1998. doi:10.1097/00000421-199808000-00008.

[24] Joiner M, Kogel a Van Der. Basic Clinical Radiobiology Fourth Edition. 2009. doi:10.1201/b13224.

[25] Brown JM. The Hypoxic Cell. Cancer Res 1999;59:5863–70.

[26] Tannock IF, Hill RP, Bristow RG, Harrington L. Basic science of oncology. Basic Sci Oncol 2005.

[27] Brown JM. Tumor hypoxia in cancer therapy. Methods Enzymol 2007;435:297–321. doi:10.1016/S0076-6879(07)35015-5.

[28] Baumann M, Petersen C. TCP and NTCP: A basic introduction. Rays - Int J Radiol Sci 2005.

[29] Baumann M, Krause M, Overgaard J, Debus J, Bentzen SM, Daartz J, et al. Radiation oncology in the era of precision medicine. Nat Rev Cancer 2016. doi:10.1038/nrc.2016.18.

[30] Vander Heiden MG. Targeting cancer metabolism: A therapeutic window opens. Nat Rev Drug Discov 2011. doi:10.1038/nrd3504.

[31] Marks LB, Yorke ED, Jackson A, Ten Haken RK, Constine LS, Eisbruch A, et al. Use of normal tissue complication probability models in the clinic. Int J Radiat Oncol Biol Phys 2010;76:S10-9. doi:10.1016/j.ijrobp.2009.07.1754.

[32] Hanahan D, Weinberg RA. Hallmarks of cancer: The next generation. Cell 2011;144:646–74. doi:10.1016/j.cell.2011.02.013.

[33] Trédan O, Galmarini CM, Patel K, Tannock IF. Drug resistance and the solid tumor microenvironment. J Natl Cancer Inst 2007. doi:10.1093/jnci/djm135.

[34] Qayum N, Im J, Stratford MR, Bernhard EJ, McKenna WG, Muschel RJ. Modulation of the tumor microvasculature by phosphoinositide-3 kinase inhibition increases doxorubicin delivery In Vivo. Clin Cancer Res 2012;18:161–9. doi:10.1158/1078-0432.CCR-11-1413.

[35] McKeown SR. Defining normoxia, physoxia and hypoxia in tumours - Implications for treatment response. Br J Radiol 2014. doi:10.1259/bjr.20130676.

[36] Ramachandran S, Ient J, Göttgen EL, Krieg AJ, Hammond EM. Epigenetic therapy for solid tumors: Highlighting the impact of tumor hypoxia. Genes (Basel) 2015. doi:10.3390/genes6040935.

[37] Bayer C, Shi K, Astner ST, Maftei CA, Vaupel P. Acute versus chronic hypoxia: Why a simplified classification is simply not enough. Int J Radiat Oncol Biol Phys 2011. doi:10.1016/j.ijrobp.2011.02.049.

[38] Martinive P, Defresne F, Quaghebeur E, Daneau G, Crokart N, Grégoire V, et al. Impact of cyclic hypoxia on HIF-1α regulation in endothelial cells - New insights for anti-tumor treatments. FEBS J 2009. doi:10.1111/j.1742-4658.2008.06798.x.

[39] Semenza GL. Targeting HIF-1 for cancer therapy. Nat Rev Cancer 2003;3:721–32. doi:10.1038/nrc1187.

[40] Semenza GL. Targeting HIF-1 for cancer therapy. Nat Rev Cancer 2003. doi:10.1038/nrc1187.

[41] Semenza GL. Regulation of metabolism by hypoxia-inducible factor 1. Cold Spring Harb Symp Quant Biol 2011. doi:10.1101/sqb.2011.76.010678.

[42] Pouysségur J, Dayan F, Mazure NM. Hypoxia signalling in cancer and approaches to enforce tumour regression. Nature 2006;441:437–43. doi:10.1038/nature04871.

[43] Olcina MM, Hammond EM. Hypoxia and the DNA Damage Response, 2014. doi:10.1007/978-1-4614-9167-5_2.

[44] Lakin ND, Jackson SP. Regulation of p53 in response to DNA damage. Oncogene 1999. doi:10.1038/sj.onc.1203015.

[45] Bindra RS, Crosby ME, Glazer PM. Regulation of DNA repair in hypoxic cancer cells. Cancer Metastasis Rev 2007. doi:10.1007/s10555-007-9061-3.

[46] Bindra RS, Schaffer PJ, Meng A, Woo J, Maseide K, Roth ME, et al. Down-Regulation of Rad51 and Decreased Homologous Recombination in Hypoxic Cancer Cells. Mol Cell Biol 2004. doi:10.1128/mcb.24.19.8504-8518.2004.

[47] Meng AX, Jalali F, Cuddihy A, Chan N, Bindra RS, Glazer PM, et al. Hypoxia down-regulates DNA double strand break repair gene expression in prostate cancer cells. Radiother. Oncol., 2005. doi:10.1016/j.radonc.2005.06.025.

[48] Vaupel P, Höckel M. Tumor Hypoxia : Definitions and Current Clinical , Biologic, and Molecular Aspects. J Natl Cancer Inst 2001.

[49] Zeman EM. The Biological Basis of Radiation Oncology. Clin. Radiat. Oncol., 2015. doi:10.1016/b978-0-323-24098-7.00001-0.

[50] Wilson WR, Hay MP. Targeting hypoxia in cancer therapy. Nat Rev Cancer 2011;11:393–410. doi:10.1038/nrc3064.

[51] Sørensen BS, Hao J, Overgaard J, Vorum H, Honoré B, Alsner J, et al. Influence of oxygen concentration and pH on expression of hypoxia induced genes. Radiother. Oncol., 2005. doi:10.1016/j.radonc.2005.06.037.

[52] Potter C, Harris AL. Hypoxia inducible carbonic anhydrase IX, marker of tumor hypoxia, survival pathway and therapy target. Cell Cycle 2004.

[53] Hodgkiss RJ. Use of 2-nitroimidazoles as bioreductive markers for tumour hypoxia. Anticancer Drug Des 1998.

[54] Nunn A, Linder K, Strauss HW. Nitroimidazoles and imaging hypoxia. Eur J Nucl Med 1995. doi:10.1007/BF01081524.

[55] Bergeron M, Evans SM, Sharp FR, Koch CJ, Lord EM, Ferriero DM. Detection of hypoxic cells with the 2-nitroimidazole, EF5, correlates with early redox changes in rat brain after perinatal hypoxia-ischemia. Neuroscience 1999. doi:10.1016/S0306-4522(98)00377-7.

[56] Osinsky S, Zavelevich M, Vaupel P. Tumor hypoxia and malignant progression. Exp. Oncol., 2009.

[57] Dhani N, Fyles A, Hedley D, Milosevic M. The clinical significance of hypoxia in human cancers. Semin Nucl Med 2015;45:110–21. doi:10.1053/j.semnuclmed.2014.11.002.

[58] Melillo G. Targeting hypoxia cell signaling for cancer therapy. Cancer Metastasis Rev 2007;26:341–52. doi:10.1007/s10555-007-9059-x.

[59] Bergsjø P, Kolstad P. Clinical trial with atmospheric oxygen breathing during radiotherapy of cancer of the cervix. Scand J Clin Lab Invest 1968. doi:10.1080/00365516809168212.

[60] Schwarz G. über Desensibiliserung gegen Röntgen- und Radiumstrahlen. Munchener Medizinische Wochenschrift 1909;24:1–2.

[61] Yu H, Kortylewski M, Pardoll D. Crosstalk between cancer and immune cells: Role of STAT3 in the tumour microenvironment. Nat Rev Immunol 2007;7:41–51. doi:10.1038/nri1995.

[62] Carpenter RL, Lo HW. STAT3 target genes relevant to human cancers. Cancers (Basel) 2014;6:897–925. doi:10.3390/cancers6020897.

[63] Bourgeais J, Gouilleux-Gruart V, Gouilleux F. Oxidative metabolism in cancer: A STAT affair? JAK-STAT 2013. doi:10.4161/jkst.25764.

[64] Avalle L, Camporeale A, Camperi A, Poli V. STAT3 in cancer: A double edged sword. Cytokine 2017. doi:10.1016/j.cyto.2017.03.018.

[65] Johnson DE, O'Keefe RA, Grandis JR. Targeting the IL-6/JAK/STAT3 signalling axis in cancer. Nat Rev Clin Oncol 2018. doi:10.1038/nrclinonc.2018.8.

[66] Xiang M, Kim H, Ho VT, Walker SR, Bar-Natan M, Anahtar M, et al. Gene expression-based discovery of atovaquone as a STAT3 inhibitor and anticancer agent. Blood 2016;128:1845–53. doi:10.1182/blood-2015-07-660506.

[67] Wang ZY, Zhang JA, Wu XJ, Liang YF, Lu Y Bin, Gao YC, et al. IL-6 Inhibition Reduces STAT3 Activation and Enhances the Antitumor Effect of Carboplatin. Mediators Inflamm 2016. doi:10.1155/2016/8026494.

[68] Han Z, Feng J, Hong Z, Chen L, Li W, Liao S, et al. Silencing of the STAT3 signaling pathway reverses the inherent and induced chemoresistance of human ovarian cancer cells. Biochem Biophys Res Commun 2013. doi:10.1016/j.bbrc.2013.04.087.

[69] Abyaneh HS, Gupta N, Radziwon-Balicka A, Jurasz P, Seubert J, Lai R, et al. STAT3 but not HIF-1α is important in mediating hypoxia-induced chemoresistance in MDA-MB-231, a triple negative breast cancer cell line. Cancers (Basel) 2017. doi:10.3390/cancers9100137.

[70] Ferreira LMR. Cancer metabolism: The Warburg effect today. Exp Mol Pathol 2010. doi:10.1016/j.yexmp.2010.08.006.

[71] Dang C V., Gao P, Kim J. Warburg Effect. Encycl. Cancer, 2017. doi:10.1007/978-3-662-46875-3_6229.

[72] Ashton TM, McKenna WG, Kunz-Schughart LA, Higgins GS. Oxidative Phosphorylation as an Emerging Target in Cancer Therapy. Clin Cancer Res 2018. doi:10.1158/1078-0432.CCR-17-3070.

[73] Cairns RA, Harris IS, Mak TW. Regulation of cancer cell metabolism. Nat Rev Cancer 2011. doi:10.1038/nrc2981.

[74] Cox SE. Energy Metabolism. Encycl. Hum. Nutr., 2012. doi:10.1016/B978-0-12-375083-9.00091-X.

[75] Cairns RA, Harris IS, Mak TW. Regulation of cancer cell metabolism. Nat Rev Cancer 2011;11:85–95. doi:10.1038/nrc2981.

[76] Whalley NA, Walters S, Hammond K. Molecular Cell Biology. Mol. Med. Clin., 2018. doi:10.18772/22008014655.9.

[77] Polyzos AA, McMurray CT. The chicken or the egg: mitochondrial dysfunction as a cause or consequence of toxicity in Huntington's disease. Mech Ageing Dev 2017. doi:10.1016/j.mad.2016.09.003.

[78] Warburg O. Über den Stoffwechsel der Carcinomzelle. Naturwissenschaften 1924. doi:10.1007/BF01504608.

[79] Lu J, Tan M, Cai Q. The Warburg effect in tumor progression: Mitochondrial oxidative metabolism as an anti-metastasis mechanism. Cancer Lett 2015. doi:10.1016/j.canlet.2014.04.001.

[80] Danhier P, Bański P, Payen VL, Grasso D, Ippolito L, Sonveaux P, et al. Cancer metabolism in space and time: Beyond the Warburg effect. Biochim Biophys Acta - Bioenerg 2017. doi:10.1016/j.bbabio.2017.02.001.

[81] Kalyanaraman B, Cheng G, Hardy M, Ouari O, Lopez M, Joseph J, et al. A review of the basics of mitochondrial bioenergetics, metabolism, and related signaling pathways in cancer cells: Therapeutic targeting of tumor mitochondria with lipophilic cationic compounds. Redox Biol 2018. doi:10.1016/j.redox.2017.09.020.

[82] Shaw RJ. Glucose metabolism and cancer. Curr Opin Cell Biol 2006.

doi:10.1016/j.ceb.2006.10.005.

[83] Jastroch M, Divakaruni AS, Mookerjee S, Treberg JR, Brand MD. Mitochondrial proton and electron leaks. Essays Biochem 2010. doi:10.1042/BSE0470053.

[84] Brookes PS. Mitochondrial H + leak and ROS generation: An odd couple. Free Radic Biol Med 2005. doi:10.1016/j.freeradbiomed.2004.10.016.

[85] McLennan HR, Esposti MD. The contribution of mitochondrial respiratory complexes to the production of reactive oxygen species. J Bioenerg Biomembr 2000;32:153–62. doi:10.1023/A:1005507913372.

[86] Hirst J. Mitochondrial Complex I. Annu Rev Biochem 2013. doi:10.1146/annurev-biochem-070511-103700.

[87] Mailloux RJ, McBride SL, Harper ME. Unearthing the secrets of mitochondrial ROS and glutathione in bioenergetics. Trends Biochem Sci 2013. doi:10.1016/j.tibs.2013.09.001.

[88] Turrens JF. Mitochondrial formation of reactive oxygen species. J Physiol 2003. doi:10.1113/jphysiol.2003.049478.

[89] Marí M, Morales A, Colell A, García-Ruiz C, Fernández-Checa JC. Mitochondrial glutathione, a key survival antioxidant. Antioxidants Redox Signal 2009. doi:10.1089/ars.2009.2695.

[90] Lee KS, Kim HK, Moon HS, Hong YS, Kang JH, Kim DJ, et al. Effects of buthionine sulfoximine treatment on cellular glutathione levels and cytotoxicities of cisplatin, carboplatin and radiation in human stomach and ovarian cancer cell lines. Korean J Intern Med 1992;7:111–7. doi:10.3904/kjim.1992.7.2.111.

[91] Lan D, Wang L, He R, Ma J, Bin Y, Chi X, et al. Exogenous glutathione contributes to cisplatin resistance in lung cancer A549 cells. Am J Transl Res 2018.

[92] Rocha CRR, Garcia CCM, Vieira DB, Quinet A, De Andrade-Lima LC, Munford V, et al. Glutathione depletion sensitizes cisplatin- and temozolomide-resistant glioma cells in vitro and in vivo. Cell Death Dis 2014. doi:10.1038/cddis.2014.465.

[93] Board PG, Menon D. Glutathione transferases, regulators of cellular metabolism and physiology. Biochim Biophys Acta - Gen Subj 2013. doi:10.1016/j.bbagen.2012.11.019.

[94] Whalen R, Boyer TD. Human glutathione S-transferases. Semin Liver Dis 1998. doi:10.1055/s-2007-1007169.

[95] De Luca A, Parker LJ, Ang WH, Rodolfo C, Gabbarini V, Hancock NC, et al. A structure-based mechanism of cisplatin resistance mediated by glutathione transferase P1-1. Proc Natl Acad Sci U S A 2019. doi:10.1073/pnas.1903297116.

[96] Candas D, Li JJ. MnSOD in oxidative stress response-potential regulation via mitochondrial protein influx. Antioxidants Redox Signal 2014. doi:10.1089/ars.2013.5305.

[97] Hart PC, Mao M, De Abreu ALP, Ansenberger-Fricano K, Ekoue DN, Ganini D, et al. MnSOD upregulation sustains the Warburg effect via mitochondrial ROS and AMPK-dependent signalling in cancer. Nat Commun 2015. doi:10.1038/ncomms7053.

[98] Nguyen T, Nioi P, Pickett CB. The Nrf2-antioxidant response element signaling pathway and its activation by oxidative stress. J Biol Chem 2009. doi:10.1074/jbc.R900010200.

[99] Denicola GM, Karreth FA, Humpton TJ, Gopinathan A, Wei C, Frese K, et al. Oncogene-induced Nrf2 transcription promotes ROS detoxification and tumorigenesis. Nature 2011. doi:10.1038/nature10189.

[100] Lu J, Holmgren A. The thioredoxin antioxidant system. Free Radic Biol Med 2014. doi:10.1016/j.freeradbiomed.2013.07.036.

[101] Weydert CJ, Cullen JJ. Measurement of superoxide dismutase, catalase and glutathione peroxidase in cultured cells and tissue. Nat Protoc 2010. doi:10.1038/nprot.2009.197.

[102] Cox AG, Winterbourn CC, Hampton MB. Mitochondrial peroxiredoxin involvement in antioxidant defence and redox signalling. Biochem J 2010. doi:10.1042/BJ20091541.

[103] Harrington KJ. The biology of cancer. Med (United Kingdom) 2016.

doi:10.1016/j.mpmed.2015.10.005.

[104] Friedl P, Alexander S. Cancer invasion and the microenvironment: Plasticity and reciprocity. Cell 2011. doi:10.1016/j.cell.2011.11.016.

[105] Estrella V, Chen T, Lloyd M, Wojtkowiak J, Cornnell HH, Ibrahim-Hashim A, et al. Acidity generated by the tumor microenvironment drives local invasion. Cancer Res 2013;73:1524–35. doi:10.1158/0008-5472.CAN-12-2796.

[106] Kato Y, Ozawa S, Miyamoto C, Maehata Y, Suzuki A, Maeda T, et al. Acidic extracellular microenvironment and cancer. Cancer Cell Int 2013. doi:10.1186/1475-2867-13-89.

[107] Chiang SPH, Cabrera RM, Segall JE. Tumor cell intravasation. Am J Physiol Physiol 2016. doi:10.1152/ajpcell.00238.2015.

[108] Wong SY, Hynes RO. Lymphatic or hematogenous dissemination: How does a metastatic tumor cell decide? Cell Cycle 2006. doi:10.4161/cc.5.8.2646.

[109] Yu M, Stott S, Toner M, Maheswaran S, Haber DA. Circulating tumor cells: Approaches to isolation and characterization. J Cell Biol 2011. doi:10.1083/jcb.201010021.

[110] Gómez-Cuadrado L, Tracey N, Ma R, Qian B, Brunton VG. Mouse models of metastasis: progress and prospects. Dis Model Mech 2017. doi:10.1242/dmm.030403.

[111] De Berardinis RJ, Chandel NS. Fundamentals of cancer metabolism. Sci Adv 2016. doi:10.1126/sciadv.1600200.

[112] Chiche J, Brahimi-Horn MC, Pouysségur J. Tumour hypoxia induces a metabolic shift causing acidosis: A common feature in cancer. J Cell Mol Med 2010. doi:10.1111/j.1582-4934.2009.00994.x.

[113] Peppicelli S, Bianchini F, Calorini L. Extracellular acidity, a “reappreciated” trait of tumor environment driving malignancy: Perspectives in diagnosis and therapy. Cancer Metastasis Rev 2014;33:823–32. doi:10.1007/s10555-014-9506-4.

[114] An OXPHOS Inhibitor Has Antitumor Activity in Multiple Tumor Models.

Cancer Discov 2018;8:OF13–OF13. doi:10.1158/2159-8290.CD-RW2018-106.

[115] Klimova T, Chandel NS. Mitochondrial complex III regulates hypoxic activation of HIF. Cell Death Differ 2008;15:660–6. doi:10.1038/sj.cdd.4402307.

[116] Dewhirst MW, Cao Y, Li CY, Moeller B. Exploring the role of HIF-1 in early angiogenesis and response to radiotherapy. Radiother Oncol 2007. doi:10.1016/j.radonc.2007.05.016.

[117] Bayer C, Vaupel P. Acute versus chronic hypoxia in tumors : Controversial data concerning time frames and biological consequences. Strahlentherapie Und Onkol 2012. doi:10.1007/s00066-012-0085-4.

[118] Zhou J, Wu SG, Sun JY, Li FY, Lin HX, Chen QH, et al. Comparison of clinical outcomes of squamous cell carcinoma, adenocarcinoma, and adenosquamous carcinoma of the uterine cervix after definitive radiotherapy: a population-based analysis. J Cancer Res Clin Oncol 2017. doi:10.1007/s00432-016-2246-9.

[119] Micalizzi DS, Maheswaran S, Haber DA. A conduit to metastasis: Circulating tumor cell biology. Genes Dev 2017. doi:10.1101/gad.305805.117.

[120] Graham K, Unger E. Overcoming tumor hypoxia as a barrier to radiotherapy, chemotherapy and immunotherapy in cancer treatment. Int J Nanomedicine 2018. doi:10.2147/IJN.S140462.

[121] Overgaard J. Hypoxic modification of radiotherapy in squamous cell carcinoma of the head and neck - A systematic review and meta-analysis. Radiother Oncol 2011;100:22–32. doi:10.1016/j.radonc.2011.03.004.

[122] Janssens GO, Rademakers SE, Terhaard CH, Doornaert PA, Bijl HP, van den Ende P, et al. Accelerated Radiotherapy With Carbogen and Nicotinamide for Laryngeal Cancer: Results of a Phase III Randomized Trial. J Clin Oncol 2012;30:1777–83. doi:10.1200/JCO.2011.35.9315.

[123] Marcu L, Olver I. Tirapazamine: From Bench to Clinical Trials. Curr Clin Pharmacol 2006;1:71–9. doi:10.2174/157488406775268192.

[124] DiSilvestro PA, Ali S, Craighead PS, Lucci JA, Lee YC, Cohn DE, et al. Phase III randomized trial of weekly cisplatin and irradiation versus cisplatin and tirapazamine and irradiation in stages IB2, IIA, IIB, IIIB, and IVA cervical carcinoma limited to the pelvis: A gynecologic oncology group study. J Clin Oncol 2014;32:458–64. doi:10.1200/JCO.2013.51.4265.

[125] Naughton DP. Drug targeting to hypoxic tissue using self-inactivating bioreductive delivery systems. Adv Drug Deliv Rev 2001. doi:10.1016/S0169-409X(01)00229-0.

[126] Held KD. Radiobiology for the Radiologist, 6th ed., by Eric J. Hall and Amato J. Giaccia. Radiat Res 2006;166:816–7. doi:10.1667/RR0771.1.

[127] Cerecetto H, Gonzalez M, Lavaggi M. Development of Hypoxia Selective Cytotoxins for Cancer Treatment: An Update. Med Chem (Los Angeles) 2006. doi:10.2174/157340606776930808.

[128] Overgaard J. Hypoxic radiosensitization: Adored and ignored. J Clin Oncol 2007;25:4066–74. doi:10.1200/JCO.2007.12.7878.

[129] Overgaard J, Overgaard M, Nielsen OS, Pedersen AK, Timothy AR. A comparative investigation of nimorazole and misonidazole as hypoxic radiosensitizers in a C3H mammary carcinoma in vivo. Br J Cancer 1982;46:904–11. doi:10.1038/bjc.1982.300.

[130] Thomson D, Yang H, Baines H, Miles E, Bolton S, West C, et al. NIMRAD - A phase III trial to investigate the use of nimorazole hypoxia modification with intensity-modulated radiotherapy in head and neck cancer. Clin Oncol 2014;26:344–7. doi:10.1016/j.clon.2014.03.003.

[131] Overgaard J, Hansen HS, Overgaard M, Bastholt L, Berthelsen A, Specht L, et al. A randomized double-blind phase III study of nimorazole as a hypoxic radiosensitizer of primary radiotherapy in supraglottic larynx and pharynx carcinoma. Results of the Danish Head and Neck Cancer Study (DAHANCA) Protocol 5-85. Radiother Oncol 1998;46:135–46. doi:10.1016/S0167-8140(97)00220-X.

[132] Overgaard J, Eriksen JG, Nordsmark M, Alsner J, Horsman MR. Plasma osteopontin, hypoxia, and response to the hypoxia sensitiser nimorazole in radiotherapy of head and neck cancer: Results from the

DAHANCA 5 randomised double-blind placebo-controlled trial. Lancet Oncol 2005. doi:10.1016/S1470-2045(05)70292-8.

[133] J.G. E, C. M, J. J, H. P, J. E, C.A. K, et al. DAHANCA19: A randomized phase III study of primary (chemo-) radiotherapy and zalutumumab in head and neck carcinomas. Radiother Oncol 2014;111:S143–4.

[134] Sugie C, Shibamoto Y, Ito M, Ogino H, Suzuki H, Uto Y, et al. Reevaluation of the radiosensitizing effects of sanazole and nimorazole in vitro and in vivo. J Radiat Res 2005;46:453–9. doi:10.1269/jrr.46.453.

[135] Secondary CA, Author C, Coates J, Skwarski M, Higgins GS, Coates J. The British Journal of Radiology Targeting tumour hypoxia : shifting focus from oxygen supply to demand n.d.

[136] Grimes DR, Kelly C, Bloch K, Partridge M. A method for estimating the oxygen consumption rate in multicellular tumour spheroids. J R Soc Interface 2014;11:20131124. doi:10.1098/rsif.2013.1124.

[137] Helbig L, Koi L, Brüchner K, Gurtner K, Hess-Stumpp H, Unterschemmann K, et al. BAY 87-2243, a novel inhibitor of hypoxia-induced gene activation, improves local tumor control after fractionated irradiation in a schedule-dependent manner in head and neck human xenografts. Radiat Oncol 2014;9:1–10. doi:10.1186/1748-717X-9-207.

[138] Ellinghaus P, Heisler I, Unterschemmann K, Haerter M, Beck H, Greschat S, et al. BAY 87-2243, a highly potent and selective inhibitor of hypoxia-induced gene activation has antitumor activities by inhibition of mitochondrial complex I. Cancer Med 2013;2:611–24. doi:10.1002/cam4.112.

[139] Zannella VE, Pra AD, Muaddi H, McKee TD, Stapleton S, Sykes J, et al. Reprogramming metabolism with metformin improves tumor oxygenation and radiotherapy response. Clin Cancer Res 2013;19:6741–50. doi:10.1158/1078-0432.CCR-13-1787.

[140] Koritzinsky M. Metformin: A novel biological modifier of tumor response to radiation therapy. Int J Radiat Oncol Biol Phys 2015;93:454–64. doi:10.1016/j.ijrobp.2015.06.003.

[141] Bridges HR, Jones AJY, Pollak MN, Hirst J. Effects of metformin and other biguanides on oxidative phosphorylation in mitochondria. Biochem J 2014. doi:10.1042/BJ20140620.

[142] Wheaton WW, Weinberg SE, Hamanaka RB, Soberanes S, Sullivan LB, Anso E, et al. Metformin inhibits mitochondrial complex I of cancer cells to reduce tumorigenesis. Elife 2014;2014. doi:10.7554/eLife.02242.

[143] Bailey CJ. Biguanides and NIDDM. Diabetes Care 1992. doi:10.2337/diacare.15.6.755.

[144] Iommarini L, Ghelli A, Gasparre G, Porcelli AM. Mitochondrial metabolism and energy sensing in tumor progression. Biochim Biophys Acta - Bioenerg 2017. doi:10.1016/j.bbabio.2017.02.006.

[145] Andrzejewski S, Gravel S-P, Pollak M, St-Pierre J. Metformin directly acts on mitochondria to alter cellular bioenergetics. Cancer Metab 2014. doi:10.1186/2049-3002-2-12.

[146] Sullivan LB, Luengo A, Danai L V., Bush LN, Diehl FF, Hosios AM, et al. Aspartate is an endogenous metabolic limitation for tumour growth. Nat Cell Biol 2018. doi:10.1038/s41556-018-0125-0.

[147] Griss T, Vincent EE, Egnatchik R, Chen J, Ma EH, Faubert B, et al. Metformin Antagonizes Cancer Cell Proliferation by Suppressing Mitochondrial-Dependent Biosynthesis. PLoS Biol 2015. doi:10.1371/journal.pbio.1002309.

[148] Kurelac I, Umesh Ganesh N, Iorio M, Porcelli AM, Gasparre G. The multifaceted effects of metformin on tumor microenvironment. Semin Cell Dev Biol 2019. doi:10.1016/j.semcdb.2019.05.010.

[149] Spiering MJ. The mystery of metformin. J Biol Chem 2019. doi:10.1074/jbc.CL119.008628.

[150] Dowling RJO, Lam S, Bassi C, Mouaaz S, Aman A, Kiyota T, et al. Metformin Pharmacokinetics in Mouse Tumors: Implications for Human Therapy. Cell Metab 2016. doi:10.1016/j.cmet.2016.03.006.

[151] Ashton TM, Fokas E, Kunz-Schughart LA, Folkes LK, Anbalagan S, Huether M, et al. The anti-malarial atovaquone increases

radiosensitivity by alleviating tumour hypoxia. Nat Commun 2016;7:1–13. doi:10.1038/ncomms12308.

[152] Cheng G, Zielonka J, Ouari O, Lopez M, McAllister D, Boyle K, et al. Mitochondria-targeted analogues of metformin exhibit enhanced antiproliferative and radiosensitizing effects in pancreatic cancer cells. Cancer Res 2016. doi:10.1158/0008-5472.CAN-15-2534.

[153] De Bruycker S, Vangestel C, Staelens S, wyffels L, Detrez J, Verschuuren M, et al. Effects of metformin on tumor hypoxia and radiotherapy efficacy: a [18F]HX4 PET imaging study in colorectal cancer xenografts. EJNMMI Res 2019. doi:10.1186/s13550-019-0543-4.

[154] Chandel NS, Avizonis D, Reczek CR, Weinberg SE, Menz S, Neuhaus R, et al. Are Metformin Doses Used in Murine Cancer Models Clinically Relevant? Cell Metab 2016. doi:10.1016/j.cmet.2016.03.010.

[155] Baggish AL, Hill DR. Antiparasitic agent atovaquone. Antimicrob Agents Chemother 2002. doi:10.1128/AAC.46.5.1163-1173.2002.

[156] Capper MJ, O'Neill PM, Fisher N, Strange RW, Moss D, Ward SA, et al. Antimalarial 4(1H)-pyridones bind to the Qi site of cytochrome bc1. Proc Natl Acad Sci U S A 2015. doi:10.1073/pnas.1416611112.

[157] Biagini GA, Fisher N, Berry N, Stocks PA, Meunier B, Williams DP, et al. Acridinediones: Selective and potent inhibitors of the malaria parasite mitochondrial bc1 complex. Mol Pharmacol 2008. doi:10.1124/mol.108.045120.

[158] Owen MR, Doran E, Halestrap AP. Evidence that metformin exerts its anti-diabetic effects through inhibition of complex 1 of the mitochondrial respiratory chain. Biochem J 2000. doi:10.1042/0264-6021:3480607.

[159] Dixon R, Pozniak AL, Watt HM, Rolan P, Posner J. Single-dose and steady-state pharmacokinetics of a novel microfluidized suspension of atovaquone in human immunodeficiency virus-seropositive patients. Antimicrob Agents Chemother 1996;40:556–60.

[160] Nixon GL, Moss DM, Shone AE, Lalloo DG, Fisher N, O'neill PM, et al. Antimalarial pharmacology and therapeutics of atovaquone. J

Antimicrob Chemother 2013;68:977–85. doi:10.1093/jac/dks504.

[161] PUCK TT, MARCUS PI. Action of x-rays on mammalian cells. J Exp Med 1956. doi:10.1084/jem.103.5.653.

[162] Rafehi H, Orlowski C, Georgiadis GT, Ververis K, El-Osta A, Karagiannis TC. Clonogenic assay: Adherent cells. J Vis Exp 2011. doi:10.3791/2573.

[163] Nixon GL, Moss DM, Shone AE, Lalloo DG, Fisher N, O'neill PM, et al. Antimalarial pharmacology and therapeutics of atovaquone. J Antimicrob Chemother 2013;68:977–85. doi:10.1093/jac/dks504.

[164] Bleby J. Animals (Scientific Procedures) Act 1986. Vet Rec 1986. doi:10.1136/vr.119.1.22-a.

[165] DuPré SA, Redelman D, Hunter KW. The mouse mammary carcinoma 4T1: Characterization of the cellular landscape of primary tumours and metastatic tumour foci. Int J Exp Pathol 2007;88:351–60. doi:10.1111/j.1365-2613.2007.00539.x.

[166] Kinchesh P, Gilchrist S, Beech JS, Gomes AL, Kersemans V, Newman RG, et al. Prospective gating control for highly efficient cardio-respiratory synchronised short and constant TR MRI in the mouse. Magn Reson Imaging 2018. doi:10.1016/j.mri.2018.06.017.

[167] Ray KJ, Simard MA, Larkin JR, Coates J, Kinchesh P, Smart SC, et al. Tumor pH and protein concentration contribute to the signal of amide proton transfer magnetic resonance imaging. Cancer Res 2019. doi:10.1158/0008-5472.CAN-18-2168.

[168] Harston GWJ, Tee YK, Blockley N, Okell TW, Thandeswaran S, Shaya G, et al. Identifying the ischaemic penumbra using pH-weighted magnetic resonance imaging. Brain 2015. doi:10.1093/brain/awu374.

[169] Zhao X, Wen Z, Zhang G, Huang F, Lu S, Wang X, et al. Three-dimensional turbo-spin-echo amide proton transfer MR imaging at 3-tesla and its application to high-grade human brain tumors. Mol Imaging Biol 2013. doi:10.1007/s11307-012-0563-1.

[170] Park JE, Kim HS, Park KJ, Choi CG, Kim SJ. Histogram analysis of amide proton transfer imaging to identify contrast-enhancing low-

grade brain tumor that mimics high-grade tumor: Increased accuracy of MR perfusion[1]. Radiology 2015. doi:10.1148/radiol.2015142347.

[171] McDonald JC. Quantitative concepts and dosimetry in radiobiology, ICRU report 30. Int J Appl Radiat Isot 1980. doi:10.1016/0020-708x(80)90134-9.

[172] Scharping NE, Menk A V., Whetstone RD, Zeng X, Delgoffe GM. Efficacy of PD-1 Blockade Is Potentiated by Metformin-Induced Reduction of Tumor Hypoxia. Cancer Immunol Res 2017;5:9–16. doi:10.1158/2326-6066.CIR-16-0103.

[173] Brown JM, Wilson WR. Exploiting tumour hypoxia in cancer treatment. Nat Rev Cancer 2004;4:437–47. doi:10.1038/nrc1367.

[174] Aleksandrova A V., Pulkova NP, Gerasimenko TN, Anisimov NY, Tonevitskaya SA, Sakharov DA. Mathematical and Experimental Model of Oxygen Diffusion for HepaRG Cell Spheroids. Bull Exp Biol Med 2016. doi:10.1007/s10517-016-3326-1.

[175] Grimes DR, Kelly C, Bloch K, Partridge M. A method for estimating the oxygen consumption rate in multicellular tumour spheroids. J R Soc Interface 2014. doi:10.1098/rsif.2013.1124.

[176] Diepart C, Karroum O, Magat J, Feron O, Verrax J, Calderon PB, et al. Arsenic trioxide treatment decreases the oxygen consumption rate of tumor cells and radiosensitizes solid tumors. Cancer Res 2012;72:482–90. doi:10.1158/0008-5472.CAN-11-1755.

[177] Tafreshi NK, Lloyd MC, Proemsey JB, Bui MM, Kim J, Gillies RJ, et al. Evaluation of CAIX and CAXII Expression in Breast Cancer at Varied O2 Levels: CAIX is the Superior Surrogate Imaging Biomarker of Tumor Hypoxia. Mol Imaging Biol 2016. doi:10.1007/s11307-015-0885-x.

[178] Hazan-Halevy I, Harris D, Liu Z, Liu J, Li P, Chen X, et al. STAT3 is constitutively phosphorylated on serine 727 residues, binds DNA, and activates transcription in CLL cells. Blood 2010. doi:10.1182/blood-2009-10-230060.

[179] Berishaj M, Gao SP, Ahmed S, Leslie K, Al-Ahmadie H, Gerald WL, et al. Stat3 is tyrosine-phosphorylated through the interleukin-

6/glycoprotein 130/Janus kinase pathway in breast cancer. Breast Cancer Res 2007. doi:10.1186/bcr1680.

[180] Semenza GL. HIF-1: upstream and downstream of cancer metabolism. Curr Opin Genet Dev 2010;20:51–6. doi:10.1016/j.gde.2009.10.009.

[181] Laughlin KM, Evans SM, Jenkins WT, Tracy M, Chan CY, Lord EM, et al. Biodistribution of the nitroimidazole EF5 (2-[2-nitro-1H-imidazol-1-yl]-N-(2,2,3,3,3-pentafluoropropyl) acetamide) in mice bearing subcutaneous EMT6 tumors. J Pharmacol Exp Ther 1996.

[182] Dewhirst MW, Cao Y, Moeller B. Cycling hypoxia and free radicals regulate angiogenesis and radiotherapy response. Nat Rev Cancer 2008. doi:10.1038/nrc2397.

[183] Louie E, Nik S, Chen J suei, Schmidt M, Song B, Pacson C, et al. Identification of a stem-like cell population by exposing metastatic breast cancer cell lines to repetitive cycles of hypoxia and reoxygenation. Breast Cancer Res 2010. doi:10.1186/bcr2773.

[184] Liu H, Jiang F, Jia X, Lan J, Guo H, Li E, et al. Cycling hypoxia affects cell invasion and proliferation through direct regulation of claudin 1/claudin7 expression, and indirect regulation of P18 through claudin7. Oncotarget 2017. doi:10.18632/oncotarget.14397.

[185] Li C, Jackson RM. Reactive species mechanisms of cellular hypoxia-reoxygenation injury. Am J Physiol - Cell Physiol 2002.

[186] Koch CJ, Evans SM. Optimizing hypoxia detection and treatment strategies. Semin Nucl Med 2015. doi:10.1053/j.semnuclmed.2014.10.004.

[187] Wilson WR, Hay MP. Targeting hypoxia in cancer therapy. Nat Rev Cancer 2011. doi:10.1038/nrc3064.

[188] Cheung TW. Overdose of atovaquone in a patient with AIDS. AIDS 1999;13.

[189] Gilkes DM, Semenza GL, Wirtz D. Hypoxia and the extracellular matrix: Drivers of tumour metastasis. Nat Rev Cancer 2014;14:430–9. doi:10.1038/nrc3726.

[190] Heiden MG Vander, Cantley LC, Thompson CB. Understanding the warburg effect: The metabolic requirements of cell proliferation. Science (80-) 2009. doi:10.1126/science.1160809.

[191] Jose C, Bellance N, Rossignol R. Choosing between glycolysis and oxidative phosphorylation: A tumor's dilemma? Biochim Biophys Acta - Bioenerg 2011. doi:10.1016/j.bbabio.2010.10.012.

[192] Zheng J. Energy metabolism of cancer: Glycolysis versus oxidative phosphorylation (review). Oncol Lett 2012;4:1151–7. doi:10.3892/ol.2012.928.

[193] Jakóbisiak M, Lasek W, Gołąb J. Natural mechanisms protecting against cancer. Immunol Lett 2003. doi:10.1016/j.imlet.2003.08.005.

[194] Doherty JR, Cleveland JL. Targeting lactate metabolism for cancer therapeutics. J Clin Invest 2013. doi:10.1172/JCI69741.

[195] Pulaski B a, Ostrand-Rosenberg S. Mouse 4T1 breast tumor model. Curr Protoc Immunol 2001;Chapter 20:Unit 20.2. doi:10.1002/0471142735.im2002s39.

[196] London School of Hygiene and Tropical Medicine. Cancer Research UK Cancer Survival Group Statistics. Pers Commun 2014.

[197] Francia G, Cruz-Munoz W, Man S, Xu P, Kerbel RS. Mouse models of advanced spontaneous metastasis for experimental therapeutics. Nat Rev Cancer 2011. doi:10.1038/nrc3001.

[198] Birsoy K, Possemato R, Lorbeer FK, Bayraktar EC, Thiru P, Yucel B, et al. Metabolic determinants of cancer cell sensitivity to glucose limitation and biguanides. Nature 2014. doi:10.1038/nature13110.

[199] Pascual G, Domínguez D, Benitah SA. The contributions of cancer cell metabolism to metastasis. Dis Model Mech 2018. doi:10.1242/dmm.032920.

[200] Lebleu VS, O'Connell JT, Gonzalez Herrera KN, Wikman H, Pantel K, Haigis MC, et al. PGC-1α mediates mitochondrial biogenesis and oxidative phosphorylation in cancer cells to promote metastasis. Nat Cell Biol 2014. doi:10.1038/ncb3039.

[201] Torrano V, Valcarcel-Jimenez L, Cortazar AR, Liu X, Urosevic J, Castillo-Martin M, et al. The metabolic co-regulator PGC1α suppresses prostate cancer metastasis. Nat Cell Biol 2016. doi:10.1038/ncb3357.

[202] Dupuy F, Tabariès S, Andrzejewski S, Dong Z, Blagih J, Annis MG, et al. PDK1-dependent metabolic reprogramming dictates metastatic potential in breast cancer. Cell Metab 2015. doi:10.1016/j.cmet.2015.08.007.

[203] Christen S, Lorendeau D, Schmieder R, Broekaert D, Metzger K, Veys K, et al. Breast Cancer-Derived Lung Metastases Show Increased Pyruvate Carboxylase-Dependent Anaplerosis. Cell Rep 2016. doi:10.1016/j.celrep.2016.09.042.

[204] Elia I, Broekaert D, Christen S, Boon R, Radaelli E, Orth MF, et al. Proline metabolism supports metastasis formation and could be inhibited to selectively target metastasizing cancer cells. Nat Commun 2017. doi:10.1038/ncomms15267.

[205] J. Adams D, R. Morgan L. Tumor Physiology and Charge Dynamics of Anticancer Drugs: Implications for Camptothecin-based Drug Development. Curr Med Chem 2011. doi:10.2174/092986711795029609.

[206] Kobayashi H. Cancer chemotherapy specific to acidic nests. Cancers (Basel) 2017. doi:10.3390/cancers9040036.

[207] Cosse J-P, Michiels C. Tumour Hypoxia Affects the Responsiveness of Cancer Cells to Chemotherapy and Promotes Cancer Progression. Anticancer Agents Med Chem 2012. doi:10.2174/187152008785914798.

[208] Bruno PM, Liu Y, Park GY, Murai J, Koch CE, Eisen TJ, et al. A subset of platinum-containing chemotherapeutic agents kills cells by inducing ribosome biogenesis stress. Nat Med 2017;23:461–71. doi:10.1038/nm.4291.

[209] Siddik ZH. Cisplatin: Mode of cytotoxic action and molecular basis of resistance. Oncogene 2003;22:7265–79. doi:10.1038/sj.onc.1206933.

[210] Peng M, Darko KO, Tao T, Huang Y, Su Q, He C, et al. Combination of

metformin with chemotherapeutic drugs via different molecular mechanisms. Cancer Treat Rev 2017;54:24–33. doi:10.1016/j.ctrv.2017.01.005.

[211] Ahmad S. Kinetic aspects of platinum anticancer agents. Polyhedron 2017. doi:10.1016/j.poly.2017.09.016.

[212] Xiang M, Kim H, Ho VT, Walker SR, Bar-Natan M, Anahtar M, et al. Gene expression-based discovery of atovaquone as a STAT3 inhibitor and anti-cancer agent. Blood 2016;128:blood-2015-07-660506. doi:10.1182/blood-2015-07-660506.

[213] Schust J, Sperl B, Hollis A, Mayer TU, Berg T. Stattic: A Small-Molecule Inhibitor of STAT3 Activation and Dimerization. Chem Biol 2006. doi:10.1016/j.chembiol.2006.09.018.

[214] Sun SY. N-acetylcysteine, reactive oxygen species and beyond. Cancer Biol Ther 2010. doi:10.4161/cbt.9.2.10583.

[215] Rasmussen ES. Use of fluorescent redox indicators to evaluate cell proliferation and viability. Vitr Mol Toxicol J Basic Appl Res 1999.

[216] Fiorillo M, Lamb R, Tanowitz HB, Mutti L, Krstic-Demonacos M, Cappello AR, et al. Repurposing atovaquone: Targeting mitochondrial complex III and OXPHOS to eradicate cancer stem cells. Oncotarget 2016;7:34084–99. doi:10.18632/oncotarget.9122.

[217] Van Houten B, Woshner V, Santos JH. Role of mitochondrial DNA in toxic responses to oxidative stress. DNA Repair (Amst) 2006;5:145–52. doi:10.1016/j.dnarep.2005.03.002.

[218] Vyas S, Zaganjor E, Haigis MC. Mitochondria and Cancer. Cell 2016. doi:10.1016/j.cell.2016.07.002.

[219] Ishikawa K, Takenaga K, Akimoto M, Koshikawa N, Yamaguchi A, Imanishi H, et al. ROS-Generating Mitochondrial DNA Mutations Can Regulate Tumor Cell Metastasis. Science (80-) 2008;320:661–4. doi:10.1126/science.1156906.

[220] Chatterjee A. Reduced glutathione: A radioprotector or a modulator of DNA-repair activity? Nutrients 2013;5:525–42. doi:10.3390/nu5020525.

[221] Matassa DS, Amoroso MR, Lu H, Avolio R, Arzeni D, Procaccini C, et al. Oxidative metabolism drives inflammation-induced platinum resistance in human ovarian cancer. Cell Death Differ 2016. doi:10.1038/cdd.2016.39.

[222] Yoshida S, Tsutsumi S, Muhlebach G, Sourbier C, Lee MJ, Lee S, et al. Molecular chaperone TRAP1 regulates a metabolic switch between mitochondrial respiration and aerobic glycolysis. Proc Natl Acad Sci U S A 2013. doi:10.1073/pnas.1220659110.

[223] Amoroso MR, Matassa DS, Agliarulo I, Avolio R, Lu H, Sisinni L, et al. TRAP1 downregulation in human ovarian cancer enhances invasion and epithelial-mesenchymal transition. Cell Death Dis 2016. doi:10.1038/cddis.2016.

[224] Brahimi-Horn MC, Chiche J, Pouysségur J. Hypoxia and cancer. J Mol Med 2007;85:1301–7. doi:10.1007/s00109-007-0281-3.

[225] Di Pasqua AJ, Goodisman J, Dabrowiak JC. Understanding how the platinum anticancer drug carboplatin works: From the bottle to the cell. Inorganica Chim Acta 2012. doi:10.1016/j.ica.2012.01.028.

[226] Lord SR, Cheng WC, Liu D, Gaude E, Haider S, Metcalf T, et al. Integrated Pharmacodynamic Analysis Identifies Two Metabolic Adaption Pathways to Metformin in Breast Cancer. Cell Metab 2018. doi:10.1016/j.cmet.2018.08.021.

[227] Dang JH, Jin ZJ, Liu XJ, Hu D, Wang J, Luo Y, et al. Metformin in combination with cisplatin inhibits cell viability and induces apoptosis of human ovarian cancer cells by inactivating ERK 1/2. Oncol Lett 2017. doi:10.3892/ol.2017.7176.

[228] dos Santos Guimarães I, Ladislau-Magescky T, Tessarollo NG, dos Santos DZ, Gimba ERP, Sternberg C, et al. Chemosensitizing effects of metformin on cisplatin- and paclitaxel-resistant ovarian cancer cell lines. Pharmacol Reports 2018. doi:10.1016/j.pharep.2017.11.007.

[229] Zhu HQ, Ma J Ben, Song X, Gao HJ, Ma CQ, Chang H, et al. Metformin potentiates the anticancer activities of gemcitabine and cisplatin against cholangiocarcinoma cells in vitro and in vivo. Oncol Rep 2016;36:3488–96. doi:10.3892/or.2016.5187.

[230] Lim SO, Gu JM, Kim MS, Kim HS, Park YN, Park CK, et al. Epigenetic Changes Induced by Reactive Oxygen Species in Hepatocellular Carcinoma: Methylation of the E-cadherin Promoter. Gastroenterology 2008. doi:10.1053/j.gastro.2008.07.027.

[231] Wu Q, Ni X. ROS-Mediated DNA Methylation Pattern Alterations in Carcinogenesis. Curr Drug Targets 2015. doi:10.2174/1389450116666150113121054.

[232] Weinberg F, Hamanaka R, Wheaton WW, Weinberg S, Joseph J, Lopez M, et al. Mitochondrial metabolism and ROS generation are essential for Kras-mediated tumorigenicity. Proc Natl Acad Sci 2010;107:8788–93. doi:10.1073/pnas.1003428107.

[233] Wu WS. The signaling mechanism of ROS in tumor progression. Cancer Metastasis Rev 2006. doi:10.1007/s10555-006-9037-8.

[234] Tsukagoshi H, Busch W, Benfey PN. Transcriptional regulation of ROS controls transition from proliferation to differentiation in the root. Cell 2010. doi:10.1016/j.cell.2010.10.020.

[235] Hurd TR, DeGennaro M, Lehmann R. Redox regulation of cell migration and adhesion. Trends Cell Biol 2012. doi:10.1016/j.tcb.2011.11.002.

[236] Blaser H, Dostert C, Mak TW, Brenner D. TNF and ROS Crosstalk in Inflammation. Trends Cell Biol 2016. doi:10.1016/j.tcb.2015.12.002.

[237] Ushio-Fukai M, Nakamura Y. Reactive oxygen species and angiogenesis: NADPH oxidase as target for cancer therapy. Cancer Lett 2008. doi:10.1016/j.canlet.2008.02.044.

[238] Gilkes DM, Semenza GL, Wirtz D. Hypoxia and the extracellular matrix: Drivers of tumour metastasis. Nat Rev Cancer 2014. doi:10.1038/nrc3726.

[239] Lu P, Weaver VM, Werb Z. The extracellular matrix: A dynamic niche in cancer progression. J Cell Biol 2012. doi:10.1083/jcb.201102147.

[240] Chouaib S, Noman MZ, Kosmatopoulos K, Curran MA. Hypoxic stress: Obstacles and opportunities for innovative immunotherapy of cancer. Oncogene 2017. doi:10.1038/onc.2016.225.

[241] Klein Geltink RI, Kyle RL, Pearce EL. Unraveling the Complex Interplay Between T Cell Metabolism and Function. Annu Rev Immunol 2018. doi:10.1146/annurev-immunol-042617-053019.

[242] Weichhart T, Hengstschläger M, Linke M. Regulation of innate immune cell function by mTOR. Nat Rev Immunol 2015. doi:10.1038/nri3901.

[243] Zeng H. mTOR signaling in immune cells and its implications for cancer immunotherapy. Cancer Lett 2017. doi:10.1016/j.canlet.2017.08.038.

[244] Sitkovsky M, Lukashev D. Regulation of immune cells by local-tissue oxygen tension: HIF1α and adenosine receptors. Nat Rev Immunol 2005. doi:10.1038/nri1685.

[245] Mascanfroni ID, Takenaka MC, Yeste A, Patel B, Wu Y, Kenison JE, et al. Metabolic control of type 1 regulatory T cell differentiation by AHR and HIF1-α. Nat Med 2015. doi:10.1038/nm.3868.

[246] Buck MD, Sowell RT, Kaech SM, Pearce EL. Metabolic Instruction of Immunity. Cell 2017. doi:10.1016/j.cell.2017.04.004.

Appendix A

Transfer & Confirmation of Status

* Wrong form Sent by Dept. - See email confirmation this was for DPhil

MEDICAL SCIENCES DIVISION

Transfer from P.R.S. to ~~MSc~~ DPhil by Research Status (1st Attempt)

Student: James Coates **Programme:**

Supervisor(s): Geoffrey Higgins & G McKenna **Interview date:** 25 Jan 2017

Please consult the *Guidelines for Transfer of Status Assessors in the Medical Sciences* before completing this form.

On the basis of the student's transfer report and the transfer interview, please indicate your assessment of the following, circling as appropriate: (Note: The average student is *Adequate*).

Please tick to confirm that you, the assessors, have received and reviewed the candidate's GSO.2 MSD Application for Transfer of Status form and that it was signed by the DGS: ☑

Familiarity with and knowledge of background literature:	Inadequate	Adequate	Good		
Amount of work completed:	Inadequate	Adequate	Good		
Quality of work completed:	Inadequate	Adequate	Good		
Novelty and originality of work:	Inadequate	Adequate	Good		
Ideas and plans for future work:	Inadequate	Adequate	Good		
Ability to work independently:	Inadequate	Adequate	Good		
Compared to other students at this stage, this student's competency appears to be:	Inadequate	Adequate	Good		
Student's competence in written and spoken English:	Inadequate	Adequate	Good		
Prospect of the student submitting by their current maximum submission date:	None	Unlikely	Possible	Probably	Highly likely

Would the student benefit from additional supervision to facilitate his/her studies? Yes / No

Overall Recommendation:

☑ **Transfer to ~~MSc~~ DPhil status without reservations**

☐ **Transfer to ~~MSc~~ status if a satisfactory written response to this report is obtained**

☐ **Student should make a 2nd attempt to transfer to MSc status in 1 term**

The Board requires assessors to provide a separate written report on the student's work and interview for review by the Graduate School Committee. Assessors should particularly comment on any area that they have assessed as inadequate. *Assessors are also invited to comment on the student's acquisition of transferable skills (and plans to develop such skills) as outlined in the GSO.2MSD form.*

Signed: (Assessor 1) Ruth Musch	**Signed:** (Assessor 2)
Print Name: Ruth Muschel	**Print Name:** A L HARRIS
Date: 25 Jan 2017	**Date** 25.1.17

Please return this assessment form, along with your written report, within 7 days of the interview, to: Graduate School Assistants, Medical Sciences Graduate School Office, Level 3, John Radcliffe Hospital, Oxford OX3 9DU

Assessment form for Transfer to MSc Status – 1st Attempt (Updated August 2015)

MEDICAL SCIENCES OFFICE
Level 3, John Radcliffe Hospital, Headley Way, Oxford OX3 9DU

UNIVERSITY OF OXFORD

Mr James Coates
St. Hughs College
St. Margarets Road
Oxford
OX2 6LE

Ref: GSO2

Student No.: 759627

09 May 2017

Dear Mr Coates,

Transfer of Status

I am pleased to inform you that permission has been granted for you to transfer from:

Probationer Research Student Status
Department of Oncology
Medical Sciences Division

to:

D.Phil. Student Status
Department of Oncology
Medical Sciences Division

Your approved supervision arrangements are: Prof William Mckenna and Dr Geoffrey Higgins.

Thesis Title: Investigation of the influence of atovaquone on metastatic potential chemosensitisation.

If you wish to change your thesis title between now and applying for appointment of examiners, you can do so by completing and submitting a GSO6 form (application for change of thesis title). Please note that you will have the opportunity to change your thesis title when submitting the GSO3 form for appointment of examiners but until that time your thesis title will be officially recorded as above unless a GSO6 application is submitted and approved.

You may continue to hold this new status, subject to the relevant decrees, until Trinity Term, 2019 this being the term by which your thesis must be submitted.

Please note that you will be required to submit your application for confirmation of D.Phil. status before the end of your ninth term as a graduate student, in your case this will be Trinity Term 2018 – 5th October 2018.

Your maximum submission date is Friday 11 October 2019 this is the final date by when your thesis should be submitted to the Examination Schools.

Please note that expected completion date found on your University Card and Enrolment Certificate is your maximum submission date plus a further six months. This is to allow adequate time for your *viva voce* examination, and if requested by the examiners, to submit any minor corrections required. During this period you will be classed as being 'under examination'

Direct Line Tel: +44 (0)1865 851094 / 851061
Fax: +44 (0)1865 750750 Email: graduate.studies@medsci.ox.ac.uk

MEDICAL SCIENCES DIVISION

Confirmation of D.Phil. status (1st Attempt)

Assessment form for: James Coates **Dept:** Oncology

Principal supervisor(s): Geoff Higgins / Gillies McKenna **Presentation date:** 8/10/18

On the basis of the graduate student's presentation of their DPhil project, their full thesis contents list and their GSO.14 form, please indicate your assessment of the following, circling as appropriate. (Note. The average student is *Adequate*).

Ability to present a coherent account of the project and its significance:	Inadequate	Adequate	Good		
Amount of work completed:	Inadequate	Adequate	Good		
Quality of work completed:	Inadequate	Adequate	Good		
Novelty and originality of work:	Inadequate	Adequate	Good		
Proposed structure of the final thesis:	Inadequate	Adequate	Good		
Timetable for writing:	Inadequate	Adequate	Good		
Training undertaken:	Inadequate	Adequate	Good		
Graduate student's competence in written and spoken English:	Inadequate	Adequate	Good		
Prospect of the student submitting within 4 years from their programme start date:	None	Unlikely	Possible	Probably	Highly likely

Would the student benefit from additional supervision to facilitate his/her studies? Yes / No

Overall recommendation:

☑ **Confirmation of DPhil status without reservations**

☐ **Student should make a 2nd attempt to confirm DPhil status in 1 term**

☐ **Confirmation of DPhil status if a satisfactory written response to this report is obtained**

NB **The Board requires assessor(s)[1] to comment on any area that they have assessed as inadequate, detailing any additional requirements where applicable. Please continue overleaf or attach separate sheet**

Signed: [signature] **Signed:** [signature]

Print: P. McHugh **(Supervisor/Assessor)** Vincenzo Di Nicola Piccardo **(Assessor)**

Date:

Please return this assessment form along with the timetable and GSO.14 form within 7 days of the presentation to:
Graduate Studies Assistant, Medical Sciences Office, Level 3 John Radcliffe Hospital, Oxford, OX3 9DU

MEDICAL SCIENCES OFFICE
Level 3, John Radcliffe Hospital, Headley Way, Oxford OX3 9DU

Mr James Coates
St. Hughs College
St. Margarets Road
Oxford
OX2 6LE
United Kingdom

Ref: GSO14

Student No.: 759627

05 November 2018

Dear Mr Coates,

Confirmation of D.Phil. Status

I am pleased to inform you that your application for confirmation of D.Phil. status has been approved.

Please note that your final term remains as **TrinityTerm 2019** which gives you a final submission date of **Friday 11th October 2019.** Your thesis should be submitted to the Examination Schools no later than this date.

Please note that the expected completion date found on your University Card and Enrolment Certificate is your maximum submission date plus a further six months. This is to allow adequate time for your *viva voce* examination, and if requested by the examiners, to submit any minor corrections required. During this period you will be classed as being 'under examination' until you are granted leave to supplicate. *Note:* The extra six months is not additional time for you to complete your research as your maximum submission date remains the same (see above).

For information concerning fees, residence and other matters you are advised to refer to the Examination Decrees and Regulations of the University and the Medical Sciences Division's Notes of Guidance.

Please do not hesitate to contact me if you have any queries regarding this.

Yours sincerely,

Claire Oerton
Graduate School Assistant

CC: Supervisors: Prof Gillies McKenna and Dr Geoffrey Higgins
Tutor for Graduates, St Hugh's College

Direct Line Tel: +44 (0)1865 289547 / 289553 / 289549
Email: graduate.studies@medsci.ox.ac.uk

Appendix B

Summary of Publications

The following is a list of works published by the author during the doctorate. Some of these works are cited in the text and therefore also appear in the full bibliography.

Tumor pH and Protein Concentration Contribute to the Signal of Amide Proton Transfer Magnetic Resonance Imaging
Kevin J Ray, Manon A Simard, James R Larkin, James T Coates, Paul Kinchesh, Sean C Smart, Geoff S Higgins, Michael A Chappell, Nicola R Sibson
Cancer Research
2019/4

Targeting Tumour Hypoxia: Shifting Focus from Oxygen Supply to Demand
James T Coates, Michael Skwarski, Geoff S Higgins
The British Journal of Radiology
2019/1

Radiogenomics Models in Precision Radiotherapy: from Mechanistic to Machine Learning
John Kang, James T Coates, Robert L Strawderman, Barry S Rosenstein, Sarah L Kerns
Medical Physics (arXiv:1904.09662)
2018/8

Biological Data: The use of-omics in Outcome Models
Issam El Naqa, Sarah L Kerns, James T Coates, Yi Luo, Corey Speers, Randall K Ten Haken, Catharine ML West, Barry S Rosenstein
Book: A Guide to Outcome Modeling In Radiotherapy and Oncology
2018/4

Radiogenomics and Radiotherapy Response Modeling
Issam El Naqa, Sarah L Kerns, James T Coates, Yi Luo, Corey Speers, Catharine ML West, Barry S Rosenstein, Randall K Ten Haken
Physics in Medicine & Biology
2017/8

Motivation for the Inclusion of Genetic Risk Factors of Radiosensitivity Alongside Dosimetric and Clinical Parameters in Predicting Normal Tissue Effects
James T Coates
Acta Oncologica
2015/9

THIS PAGE INTENTIONALLY BLANK